Nanoscale Clay Minerals for Functional Ecomaterials: Fabrication, Applications, and Future Trends

Wenbo Wang and Aiqin Wang

Contents

Abstract

As the "from nature, for nature, and into nature" idea increasingly becomes popular, the naturally available nanomaterials have been especially concerned due to being safe, low-cost, sustainable, and harmless to human health and the

W. Wang · A. Wang (✉)
Key Laboratory of Clay Mineral Applied Research of Gansu Province, Center of Eco-materials and Green Chemistry, Lanzhou Institute of Chemical Physics, Chinese Adcademy of Sciences, Lanzhou, China

R&D Center of Xuyi Palygorskite Applied Technology, Lanzhou Institute of Chemical Physics, Chinese Academy of Sciences, Xuyi, China
e-mail: aqwang@licp.cas.cn

L.M.T. Martínez et al. (eds.), *Handbook of Ecomaterials*,
https://doi.org/10.1007/978-3-319-48281-1_125-1

ecological environment. Nanoscale clay minerals composed of safe Si, O, Al, and Mg elements are the broad class of naturally abundant inorganic materials, which have unique structure and diverse morphologies such as nanorods, nanofiber, nanotubes and nanosheets, special physicochemical properties, and ecofriendly advantages. The application of modern nanotechnology can disassociate or strip the clay minerals as nanosize units to produce silicate nanomaterials that have been honored as the materials of "greening twenty-first-century material world." Compared with the artificial nanomaterials, natural nanomateirals are enjoying a surge in interest as the "building blocks" of high-performance functional materials, and they help improve the quality of the product, economize on the cost, and repair the polluted environment.

This chapter comprehensively expounds the structure, morphology, and physicochemical features of different types of clay minerals including palygorskite, sepiolite, halloysite, imogolite, kaolinite, montmorillonite, mica, vermiculite, chlorite, rectorite, and illite/smectite clay, as well as their applications as "green" components to fabricate functional ecomaterials. In addition, this chapter reports recent advances in the nanoscale dispersion, modifications, and nanocomposite techniques for the development of new functional materials. The future development trends of clay mineral-based functional materials and their potential applications in advanced functional materials were discussed in general by drawing from the scientific literatures. This chapter would arouse more attention for their applications in greening functional materials.

Keywords

Clay minerals · Eco-materials · Adsorbent · Composites · Nanomaterial · Hydrothermal treatrment · Acid activation · Base treatment · Surfactant modification · Adsorption · Pollutants · Catalysis · Superabsorbent · Intercalation

Abbreviations

AA	Acrylic acid
AAm-AMPS/MMT	Poly(acrylamide(AAm)-2-acrylamido-2-methylpropane sulfonic acid)/montmorillonite
Alginate-g-PAMPS/MMT	Alginate-*g*-2-acrylamido-2-methyl-1-propanesulfonic acid/Na^+ montmorillonite(MMT)
AMPS	2-Acryloylamino-2-methyl-1-propanesulfonic acid)
APT	Attapulgite
ATP/P(AA-co-AM)	Attapulgite/poly(acrylic acid-co-acrylamide)
ATP/PAA	Attapulgite/poly(acrylic acid)
BCB	Brilliant cresyl blue
CMC-g-PAA/APT	Carboxymethyl cellulose-g-poly(acrylic acid)/attapulgite
CMC-g-PAA/MS	Carboxymethylcellulose-g-poly(sodium acrylate)/medical stone

CMC-g-PAA/REC	Carboxymethyl cellulose-graft-poly(acrylic acid)/rectorite
CMC-*g*–PNaA/APT	Carboxymethyl cellulose-g-poly(sodium acrylate)/attapulgite
CMC-g-poly(AA-co-AM-co-AMPS)/MMT	Carboxymethyl cellulose-graft-poly(acrylic acid-co-acrylamide(AM)/2-acrylamido-2-methyl-1-propanesulfonic acid/montmorillonite
CMWS-g-PAA/APT	Wheat straw-g-poly(acrylic acid)/attapulgite
COBDS	Cyclo(4, 4-oxybis(benzene)disulfide) oligomers
COL-g-PAA-co-AM/MMT	Collagen-g-poly(sodium acrylate-co-acrylamide)/sodium montmorillonite
CTS-g-AA–IA/APT	Chitosan–graft-poly(acrylic acid–co-itaconic acid/attapulgite
CTS-g-PAA/APT	Chitosan-g-poly(acrylic acid)/attapulgite
CTS-g-PAA/BT	Chitosan-g-poly(acrylic acid)/biotite
CTS-g-PAA/kaolin	Chitosan-g-poly(acrylic acid)/kaolin
CTS-g-PAA/MMT	Chitosan-g-poly(acrylic acid)/montmorillonite
CTS-g-PAA/NONT	Chitosan-graft-poly(acrylic acid)/nontronite
CTS-g-PAA/OREC	Chitosan-g-poly(acrylic acid)/organo-Rectorite
CTS-g-PAA/REC	Chitosan-g-poly(acrylic acid)/rectorite
CTS-g-PAA/UVMT	Chitosan-graf-poly(acrylic acid)/unexpanded vermiculite
CTS-g-PAA/VMT	Chitosan-g-poly(acrylic acid)/vermiculite
CTS-g-PAAm/MMT	Chitosan-g-poly(acrylamide)/montmorillonite
CTS-g-PMAA/Bent	Poly(methacrylic acid)-grafted chitosan/bentonite
CV	Crystal violet
Dextrin-graft-AA/Na-MMT	Dextrin-graft-acrylic acid/montmorillonite
GG-g-P(NaA-co-St)/APT	Guar gum-graftpoly(sodium acrylate-co-styrene)/attapulgite
GG-g-P(NaA-co-St)/MVT	Guar gum-g-poly(sodium acrylate-co-styrene)/muscovite
GG-g-PAA/cloisite	Guar gum-g-poly(sodiu macrylate)/cloisite
GG-g-PAA/MS	Guar gum-g-poly(sodium acrylate)/medicinal stone
GG-g-PNaA/CTA^+-REC	Guar gum-graft-poly(sodium acrylate)/organified rectorite
HEC-g-PAA/diatomite	Hydroxyethyl cellulose-g-poly(acrylic acid)/diatomite
HEC-g-PAA/MS	Hydroxyethyl cellulose-graft-poly(sodium acrylate)/medicinal stone
HEC-g-PAA/VMT	Hydroxyethyl cellulose-g-poly(acrylic acid)/vermiculite
HVMT	HCl-modified VMT
kC-g-PAA/Celite	κ-Carrageenan-g-poly(acrylic acid)/celite

LCL-g-PAA/MMT	Lignocellulose-g-poly(acrylic acid)/montmorillonite
MB	Methylene blue
MBA	N, N′-Methylenebisacrylamide
MG	Malachite green
MV	Methyl violet
NaAlg-g-p(AA-co-St)/I/S	Sodium alginate-g-poly(sodium acrylate-costyrene)/illite/smectite mixed-layer clays
NaAlg-g-p(AA-co-St)/organo-I/S	Sodium alginate-g-poly(sodium acrylate-co-styrene)/ illite/smectite clay
NaAlg-g-PAA/KAO	Alginate-g-poly(sodium acrylate)/kaolin
NaAlg-g-PAA/O-loess	Sodium alginate-g-poly(acrylic acid)/organo-loess
NaAlg-g-PNaA/APT	Sodium alginate-g-poly(sodium acrylate)/attapulgite
NaAlg-g-poly(AA-co-AAm)/MMT	Sodium alginate-g-poly(acrylic acid-co-acrylamide)/montmorillonite
NaAlg-g-poly(NaA-co-NaSS)/APT	Sodium alginate-g-poly(sodium acrylate-co-sodium p-styrenesulfonate)/attapulgite
NaAlg-g-poly(NaA-co-St)/APT	Sodium alginate-g-poly(sodium acrylate-co-styrene/attapulgite
NH_4^+-N	Ammonium nitrogen
NVMT	Na-exchangeable vermiculite
OB-Fe_3O_4 PSA	Organo-bentonite-Fe_3O_4 poly(sodiumacrylate)
Org-ATP/PAA	Organified attapulgite/poly(acrylic acid)
OVMT	Organo-vermiculite
P(AA-*co*-AM)/MMT/SH	poly(acrylic acid-co-acrylamide)/montmorillonite/sodium humate
P(AA-co-AMPS)/APT	Poly(acrylic acid-co-2-acryloylamino-2-methyl-1-propanesulfonic acid)/APT
PAA/APT	Poly(acrylic acid)/attapulgite
PAA/APT/SH	Poly(acrylic acid)/attapulgite/sodium humate
PAA/BT	Poly(acrylic acid)/biotite
PAA/BT	Poly(sodium acrylate)/bentonite
PAA/CMC-mMMT	Polyacrylate/(carboxymethylcellulose modified montmorillonite)
PAA/DTM	Poly(acrylic acid)/diatomite
PAA/IMMT	Poly(acrylic acid)/intercalated montmorillonite
PAA/MMT	Poly(acrylic acid)/montmorillonite
PAA/ST	Poly(sodium acrylate)/sepiolite
PAA/TM/PVA	Poly(acrylic acid)/tourmaline/polyvinyl alconol
PAA-AAm–HNT–GO	Poly(sodium acrylate-acrylamide)/graphene oxide/halloysite

PAA-AM/Al-MMT/SH	Poly(acrylic acid-acrylamide)/Al-montmorillonite/sodium humate
PAA-AM/BT	Poly(acrylate-co-acrylamide)/bentonite
PAA-AM/Ca-MMT/SH	Poly(acrylic acid-acrylamide)/Ca-montmorillonite/sodium humate
PAA-Am/EVMT	Poly(acrylate-co-acrylamide)/expanded vermiculite
PAA-AM/Li-MMT/SH	Poly(acrylic acid-acrylamide)/Li-montmorillonite/sodium humate
PAA-AM/Na-MMT/SH	Poly(acrylic acid-acrylamide)/Na-montmorillonite/sodium humate
PAA-AM/O-APT/SH	Poly(acrylamic acid-acrylamide)/organified attapulgite/sodium humate
PAA-AM/O-MMT/SH	Poly(acrylic acid-co-acrylamide)/organomontmorillonite/sodium humate
PAA-AM/SH/APT	Poly(acrylic acid-acrylamide)/sodium humate/attapulgite
PAA-AM-IA/MT	Poly(acrylic acid–co-acrylamide-co-itaconic acid/muscovite
PAA-co-2-DRAEMA/MMT	Poly(acrylic acid-co-2-(diethylamino)ethyl methacrylate)/montmorillonite
PAA-co-AM/KAO	Poly(acrylic acid-co-acrylamide)/kaolinite
PAA-co-PAM/CloisiteVR30B	Poly(acrylic acid-co-acrylamide)/cloisiteVR30B
PAA-co-VP/Lap	Poly(acrylic acid-co-N-vinyl-2-pyrrolodone)/laponite RDS
PAAm/Lap	Poly(acrylamide)/laponite
PAA-MAA/MMT	Poly(acrylic acid–methacrylic acid)/montmorillonite
PAAM-IANa/MMT	Poly(acrylamide–co-itaconic sodium)/montmorillonite
PAM/AAPT	Poly(acrylamide)/acid-treated attapulgite
PAM/APT	poly(acrylamide)/attapulgite
PAM/HAPT	Poly(acrylamide)/heat-treated attapulgite
PAM/Lap/SH	Poly(acrylamide)/laponite/sodium humate
PAM/PA	Polyacrylamide/palygorskite
PAM/SH/LAP	Poly(acrylamide)/sodium humate/laponite RD
PAM/SH/Lap	Poly(acrylamide)/sodium humate/Laponite RD
PAM-AA/MMT	Poly(acrylamide-co-acrylate/montmorillonite
PAM-IA/Mica	Poly(Acrylamide–itaconic acid)/mica
PAM-PVA/Cloisite	Poly(acrylamide-co-vinyl alcohol)/cloisite30B
PE-g-PAA/KAO	Polyethylene-g-poly(acrylic acid)/kaolin
PE-g-PAA-co-starch/OMMT	Polyethylene-g-poly(acrylic acid)-co-starch/organo-montmorillonite

PL-g-P(AA-AM)/OMMT	Potato leaves-g-poly(acrylic acid-co-acrylamide)/organified montmorillonite
PMAA-g-Cell/Bent	Poly(methacrylic acid)-grafted-cellulose/bentonite
PNaA/MMT	Poly(sodium acrylate)/montmorillonite
POBDS/VMT	Poly(4, 4-oxybis(benzene)disulfide)/vermiculite
poly(AA–AM/CTAB–MMT	Poly(acrylic acid-co-acrylamide)/ cetyl trimethyl ammonium bromide-modified montmorillonite
poly(AA–AM/DMAEA–DB–MMT	Poly(acrylic acid-co-acrylamide)/N,N′-dimethyl-N-dodecyl methacryloxylethyl ammonium bromide-modified montmorillonite
Poly(AA-co-AM)/APT	Poly(acrylic acid-co-acrylamide)/attapulgite
Poly(AA-co-AM)/HNTs	Poly(acrylic acid-co-acrylamide)/halloysite
PSSNa/MMT	Poly(sodium4-styrene sulfonate)/montmorillonite
P-St-AM/APT	Starch phosphate-graft-acrylamide/attapulgite
PSY-g-PAA/APT	Psyllium-g-Poly(acrylic acid)/attapulgite
PULL/PVA/MMT	Polysaccharide pullulan/polyvinyl alcohol/montmorillonite
SA/Na^+REC	Sodium alginate/Na^+-rectorite
SA/Na^+-REC-g-PAA	Sodium alginate/Na^+-rectorite-graft-poly acrylic acid
SA-g-AA/Na^+REC	Sodium alginate-graft-acrylic acid/Na^+rectorite
SA-g-P(AA-co-AMPS)/APT	Sodium alginate graft poly(acrylic acid-co-2-acrylamido-2-methyl-1-propane sulfonic acid)/attapulgite
S-g-AA/MMT	Starch-graft-acrylic acid/montmorillonite
SS-g-PAA/APT	Silk sericin-g-poly(acrylic acid)/attapulgite
St-g-PAA/O-zeolite	Starch-g-poly(acrylic acid)/organo-Zeolite4A
St-g-PAA/zeolite	starch-g-poly(acrylic acid)/zeolite4A
St-g-PAM/APT	Starch-graft-poly(acrylamide)/attapulgite
St-g-PAM/KAO	Starch-graft-acrylamide/kaolinite
St-g-PAM/KAO	Starch-graft-polyacrylamide/kaolinite
St-g-PAM-AA/MMT	Starch-graft-poly-[acrylamide(AM)–acrylic acid(AA)]/montmorillonite
VMT	Vermiculite

Introduction

Nanomaterials have been focused intensively over the past few decades due to their huge potential applications in many fields such as chemical industry, medicine, environment, energy, and new materials [1–3]. The frequently used nanomaterials include one-dimensional nanorods, nanofibers and nanotubes, and two-dimensional nanosheets. They are mainly artificially synthesized by various approaches, e.g.,

hydrothermal, solvothermal, soft/hard template, chemical vapor deposition (CVD), and electrochemistry [4–6]. Currently, the research on the synthesis of various nanomaterials has made great progress, but their industrial applications are still challenging because the synthesized nanomaterials and/or "building bricks" of nanomaterials are very expensive, and the synthesis process is complex, energy-intensive, and even not environment-friendly. What's more, some synthesized nanomaterials are proving to be potentially toxic, which greatly limited their applications in many fields.

With the increasing concerns on the issues of global environmental safety and health, the design and development of ecomaterials as a substitution of traditional hazardous materials becomes the subject of great interests [7, 8]. It has been expected that the applications of new ecomaterials can reduce the environmental burden, remedy the polluted environment, and minimize the secondary pollution caused by the usage of materials. Especially in recent years, the "from nature, for nature, into nature" idea increasingly becomes popular, and the naturally available nanomaterials received more attention due to their excellent performance, low cost, as well as ecofriendly and sustainable advantages [9, 10]. Currently, the development of ecomaterials from natural nanomaterials deeps to many areas, such as chemical engineering, environment protection, and composites, and great progress on this subject has been made [11, 12]. Nanoscale clay minerals are a broad class of naturally occurring inorganic nonmetallic minerals, which are available in nature, and have unique structure, diverse morphologies from one- to three-dimensions, special physicochemical properties, and ecofriendly advantages [13]. They are industrially valuable in many application fields because of their greater surface area, high surface reactivity, stronger adsorptive properties, and excellent cation exchange capacities. Their surface properties such as hydrophilic, hydrophobic, and acidity can be easily adjusted by simple modification, so that they are more easily to be dispersed in more matrixes such as a polymer with better compatibility [14, 15]. Natural nanoscale clay minerals are the "gift" of nature to human. They have been applied in ancient times, for producing chinaware, and pigments such as Maya blue [16]. However, due to the technical limitation, the clay minerals for these applications have not been dispersed as nanoscale units. With the rapid development of nanoscience and nanotechnology, the microscopic structure of clay minerals has been recognized, and their versatile functionalities have also been applied. The framework composed of Si, O, Al, and Mg elements exhibits multiple morphologies, e.g., nanorods, nanofiber, nanotubes, and nanosheets [17–20].

The modern nanotechnology can disassociate or strip clay minerals as nanosize blocks, and transform clay minerals into nanomaterials [21]. The nanometerization of clay minerals endow them with the greater specific surface area, plentiful surface groups, and good interface compatibility, and have been honored as the materials in "greening twenty-first-century material world" [22]. As the filler, nanoscale clay mineral can be well dispersed in polymer matrix, and improve the flexibility, thermal stability, and mechanical strength at low content, but does not affect the optical properties of polymer [23]. As a carrier, nanoscale clay mineral makes it possible to fabricate ultrasmall size nanoparticles on its surface, and thus greatly enhance the

activity of the catalyst [24]. As an adsorbent, the unique pore structure and surface charge of nanoscale clay mineral make it able to strongly adsorb various matters such as heavy metal ions, dyes, antibiotic, and color matters [25–28]. Compared with the artificial nanomaterials, the advantages of natural nanomateirals, as the new favorite in fabricating high-performance functional materials, are inimitable, and they are potential to play more and more roles for developing new functional materials [29, 30]. Nanoscale clays help to improve the quality of product, economize on the cost, and save the environment.

Nanoclays have found applications in many fields, which have attracted both academic and industrial attention because they exhibit dramatic improvement of properties. The development trends of clay mineral-based functional materials and their future potential applications in advanced functional materials were discussed in general by drawing from the scientific literatures. This chapter would provide a "key" to open a new avenue to recognize diverse natural nanomaterials and arouse more attention for their application in greening functional materials.

Natural Nanoscale Clay Minerals

Nanoclays are natural nanomaterials that occur in the clay fraction of soil, among which montmorillonite and allophane are the most important species. Nanoclays are easily available, environment-friendly, low-cost chemical substances, and a large volume of literatures have accumulated on various perspectives of nanoclay's research over the past few decades.

Natural Nanorods

Nanorods have been widely applied in many areas such as functional carriers, polymer composites, colloidal agents, adsorbents, and others due to the particular one-dimensional nanosize effect. The conventionally used nanorods (i.e., noble metal, metal oxides, and silica) were usually synthesized by various methods such as hydrothermal, CVD, soft or hard template methods, electrochemistry, and others. However, the synthesis process is usually costly and energy-consuming, and it is inevitable to use large amounts of chemical reagents or solvents, which has the risk of causing environmental pollution. With the increasing emphasis on the safety of materials, natural one-dimensional nanoscale clay minerals with nanorod-shape morphology have received more and more attention.

Palygorskite (also called as attapulgite) is a representative natural nanorod with the main composition of Si, Mg, and Al; nanoscale pores; and active surface groups. Palygorskite is assigned as the family of sepiolite in mineralogy because they have similar microscopic structure and morphology [31]. It could be found in many countries in the world such as China, United States, Spain, Turkey, India, Mexicanos, and others. It has a 2:1 ribbon-layer structure with the theoretical formula of $Si_8Mg_8O_{20}(OH)_2(H_2O)_4{\cdot}4H_2O$ [32–35]. The ribbons are connected

with each other by the inversion of SiO_4 tetrahedrons through Si-O-Si bonds, which formed zeolite-like channels with the dimensions of 0.37 nm × 0.64 nm [36–40] (Fig. 1a–d). The perfect palygorskite crystal should be a trioctahedral mineral in which the octahedral sites are all occupied by Mg^{2+} ions. However, some trivalent cations, e.g., Al^{3+} and Fe^{3+} ions, may replace the Mg^{2+} ions in octahedral sites due to the isomorphism substitution effect, which leads to the formation of dioctahedral or intermediate structure [33, 41–43]. As a result, the crystallographic defects could be found in the octahedral sheets of natural palygorskite, and the structural negative charges are usually compensated by considerable amounts of exchangeable cations [44]. About the definition of the main microcosmic building units in natural palygorskite, there is still no uniform statement. García-Romero and Suárez [45, 46] demonstrate that natural palygorskite is mainly composed of the laths (the smallest structure units), the rods (the oriented association of laths), and the bundles (the association of rods). In many other researches, fibers [47–50] or rods [51–53] have been frequently adopted to describe the smallest crystal units (Fig. 1e).

The special crystal structure, stacking mode, and nanometric dimension of the rod crystals of palygorskite endow it with plentiful pores, higher aspect ratio, better ion-exchange capacity (about 30–40 meq/100 g), and affluent surface groups [54–56]. So, palygorskite shows excellent colloidal, adsorption, reinforcing properties, and thermal/mechanical stability, and so it has been applied as ideal candidates in many fields such as colloidal or stabilizing agents [57, 58], adsorbents [59, 60], carrier of catalysts [61–63], polymer composites [64, 65], organic-inorganic hybrid pigments [66], drug delivery carriers [67], biosensing materials [68], antibacterial material [69], health care and therapeutic products [70], pharmaceutical product [71], electro-rheological materials [72], sealing materials [73], and animal feeding [74].

Natural Nanofiber

Nanofibers as reinforcing fillers have plaid extremely important roles in fabricating various nanocomposites for potential applications in aerospace, food packaging, and biomedical to engineering sectors such as automotive. The well-known reinforcing fillers such as carbon fibers, glass fibers, and cellulose fibers have been widely applied in modern industrial or national defense fields. With the increasing attention on environment and safety of materials, natural nanofibers such as sepiolite are increasingly attracting attention. Sepiolite [ideal formula: $Mg_8Si_{12}O_{30}(OH)_4(OH_2)_4{\bullet}8H_2O$] is a natural fibrous Mg-rich silicate clay mineral, with the fiber length up to several micrometer. It is an end-member to the palygorskite-sepiolite group and has a similar structure with palygorskite. For example, both of them have nanoscale pores and plentiful surface functional groups. In the structure of sepiolite, the octahedral (O) sheet is discontinuous, which splits into z-elongated ribbons; whereas the tetrahedral (T) sheet remains continuous, and the apical oxygen atoms in tetrahedral sheet inversed regularly and alternately bond to the upper or lower O strip (Fig. 2a) [75]. So, the structure of sepiolite can be described as modulated TOT silicate layers showing a continuous T and a discontinuous O sheet [76] or as a framework of

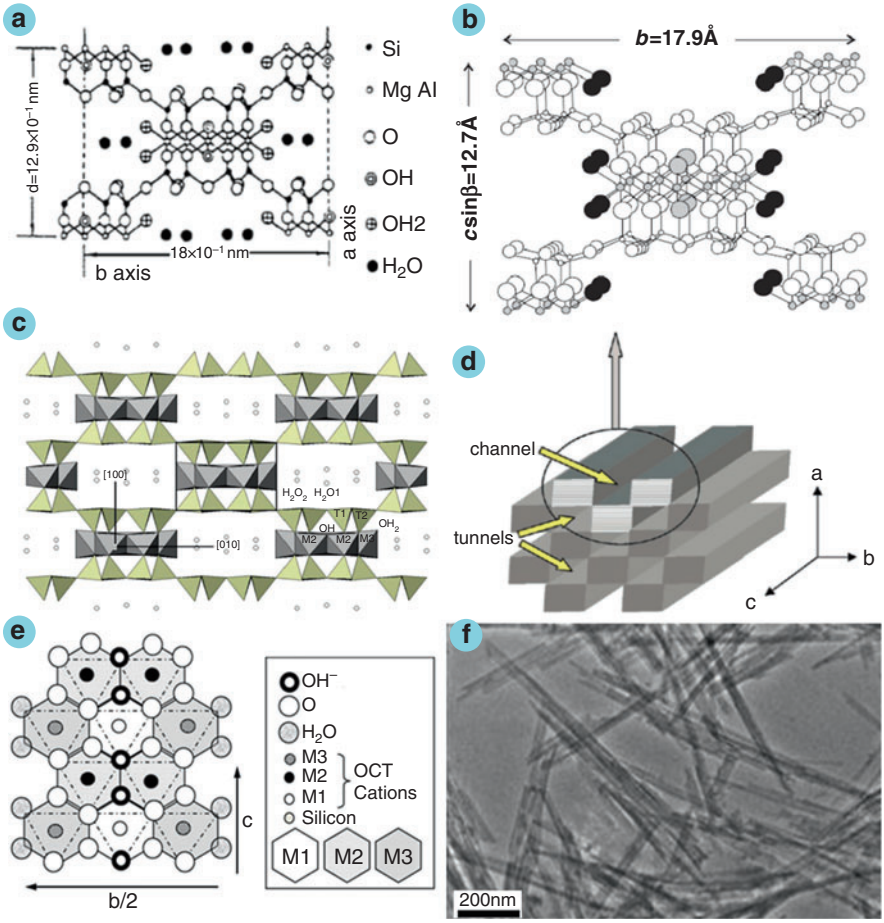

Fig. 1 (**a**) The crystal structure (001 plane projection), (**b**) crystal structure parameters, and (**c**, **d**) the pore distribution of palygorskite; (**e**) the (100) plane of palygorskite, showing the M1, M2, and M3 sites in the octahedral layer as well as the structural hydroxyl groups, coordination water, and zeolite water (Reproduced with permission from Ref. [32, 36–38]); (**f**) the TEM image of palygorskite (Reproduced with permission from Ref. [53])

chessboard connected TOT ribbons [77]. The nanotunnels with the size of 1.06 nm × 0.37 nm elongated along [001], filled by weakly bound zeolitic H_2O molecules (H_2O hereafter) and exchangeable cations [78] (Fig. 3). Tightly bound, structural OH_2 [79] (OH_2 hereafter) protrudes in the channels completing the coordination of octahedral cations at the borders of the TOT ribbons. The biggest difference between sepiolite and palygorskite is that sepiolite has relatively larger tunnel size (1.06 nm × 0.37 nm) than palygorskite (0.64 nm × 0.37 nm), and the tetrahedral sheet of sepiolite in each polysome is composed of five SiO_4 units (only four SiO_4 units for palygorskite).

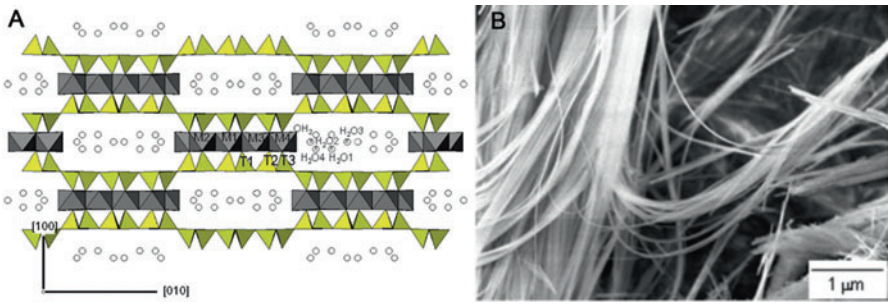

Fig. 2 Structure Scheme (**a**) (Reproduced with permission from Ref. [75]) and SEM image (**b**) of sepiolite (Reproduced with permission from Ref. [80])

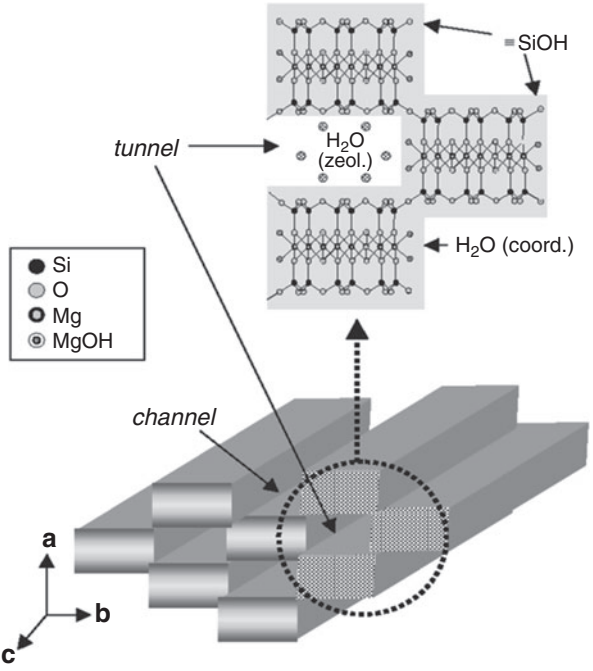

Fig. 3 Structural model of sepiolite showing the arrangement of tunnels and channels in a cross-section of a microfiber (Reproduced with permission from Ref. [78])

Sepiolite has fibrous crystal morphology [80] (Fig. 3), great specific surface areas, and rich surface active groups, so it shows excellent adsorption, reinforcing, and carrier properties; and has been widely applied in many fields such as adsorbents [81–83], polymer composite [84], catalysts [85–87], antibacterial agent [88], pigment [89], flame retardant [90], drug-delivery carrier [91], and others. Due to the special structure and properties of sepiolite as a fibrous nanomaterial, sepiolite has been widely applied for the preparation of ecomaterials, such as superabsorbent composite [92], environmental repair materials [93], and flame-retardant materials [94].

Natural Nanotubes

The nanotubes have been widely used in many fields because of their special one-dimensional nanomaterial properties and special cavity structure. Silica-oxygen tetrahedrons and aluminum-oxide octahedrons that make up the clay minerals can form tubular forms by means of special combination styles. The most common nanotubes in the nature are halloysite and imogolite [95].

Halloysite is a type of naturally available multiwalled aluminosilicates. The layer structure of halloysite consists of Al^{3+} with octahedral coordination and Si^{4+} with tetrahedral coordination in a 1:1 arrangement, and the water molecules are present between the layers, as shown in Fig. 4 [96]. Halloysite was in the same families of kaolin, which was discovered first by Berthier in 1826. It was named "halloysite" after Omalius d'Halloy who analyzed the mineral at first time. The halloysite can be found from the deposits that distributed in many countries such as China, Spain, Australia, Brazil, France, Belgium, New Zealand, Mexico, America, and others [97, 98]. Halloysite has similar morphology with multiwalled carbon nanotubes, in which the aluminosilicate sheets are rolled into nanosized tubes (called as halloysite nanotube (HNT)). The geometric dimensions of HNT are source dependent and range 0.2–2 μm

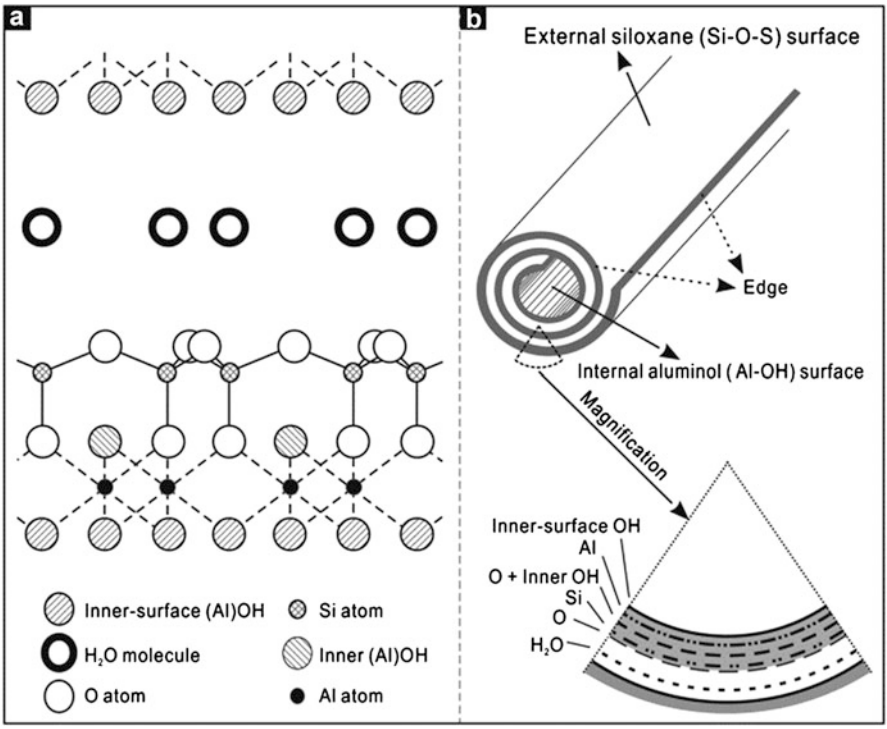

Fig. 4 Schematic diagrams of (**a**) the crystalline structure of halloysite-(10 Å), and (**b**) the structure of a halloysite nanotube (Reproduced with permission from Ref. [96])

in length, 40–100 nm in outer diameter, and 10–40 nm in lumen diameter. The wall-length, wall thickness, and spiral structures (power spiral, logarithmic spiral) of HNT are different because in the formation process of HNT the crystallization conditions and geological occurrences are different [99–101].

In comparison with other morphologies, the tubular structure of halloysite is the dominant, so that the application of halloysite as natural nanotubes has been widely concerned in different scientific or industrial fields, such as high-quality ceramics, polymer nanocomposite [102, 103], adsorption and separation [104], catalysis [105], encapsulation vessel for drug delivery [106], tissue engineering [107], flame retardant [108], hydrogen storage [109], and supercapacitor [110, 111]. The structural formula of halloysite is $Al_2(OH)_4Si_2O_5 \bullet nH_2O$. n represents the number of water molecules and could be 2 or 0, which corresponds to hydrated or dehydrated halloysite. The *n* value for the naturally occurred halloysite is 2, which is called as HNTs-10 Å (the "10 Å" designation indicates the d_{001}-value of the layers). The halloysite with $n = 0$ is called as HNT-7 Å), which was usually obtained by removing the interlayer water molecules *via* heating and/or a vacuum treatment. It is encouraging that the morphology of halloysite remains unchanged after dehydration, and only the lattice parameters slightly changed after removal of interlayer water. The chemical composition of halloysite is close to platy clay kaolinite with water molecules, and the unit layers in halloysites are separated by a monolayer of water molecules, so that the halloysites and kaolinite could be distinguished by the difference in interlayer water. Also, there are difference in lattice parameters of alumina and silica in both *a* and *b* directions ($a = 0.502$ nm, $b = 0.916$ nm for silica; and $a = 0.507$ nm, $b = 0.866$ nm for alumina), which lead to a dimensional mismatch of the sheets. In addition to lessen the electrostatic force between the adjacent layers, the presence of interlayer water facilitates the curvature of the layers to accommodate the dimensional mismatch of the octahedral and tetrahedral sheets. As a result, halloysite crystallizes with the Al–OH sheet forming the inside and the Si–O sheet forming the outside of a unit layer [112, 113]. In dehydrated halloysite structure, the aluminosilicate sheets are rolled over and over; and the structure resembles multiwalled carbon nanotubes. The halloysite nanotubes can be prepared by the rolling of kaolinite sheet in moderate synthesis condition [114].

Imogolite is also a naturally occurring aluminum silicate with nanotube morphology, which is often found in soil originating from a volcanic material such as pumice and volcanic ash. It is classified as a clay mineral, with tube dimensions of about 2 nm in outside diameter, 1 nm in inside diameter, and lengths ranging from tens of nanometers to several micrometers (Fig. 5) [115–117]. In recent years, imogolite has also received attention as a naturally occurring nanomaterial, and can be expected to find a wide range of applications in such diverse areas as fuel storage media for natural gases [118], catalyst support [119], nanocomposites [120, 121], a humidity-controlling material [115], adsorbents [122, 123], and nanohybrid materials [124, 125]. The amount of naturally occurring imogolite is very small, so it is hoped that large-scale synthesis can be carried out. Many methods such as microwave hydrothermal [126], surfactant template [127], and fluoride route [128]. In the synthesis process of imogolite, the other elements such as Ge [129, 130] and Fe [131, 132] can be simultaneously introduced to control the size, physicochemical properties, and functionality.

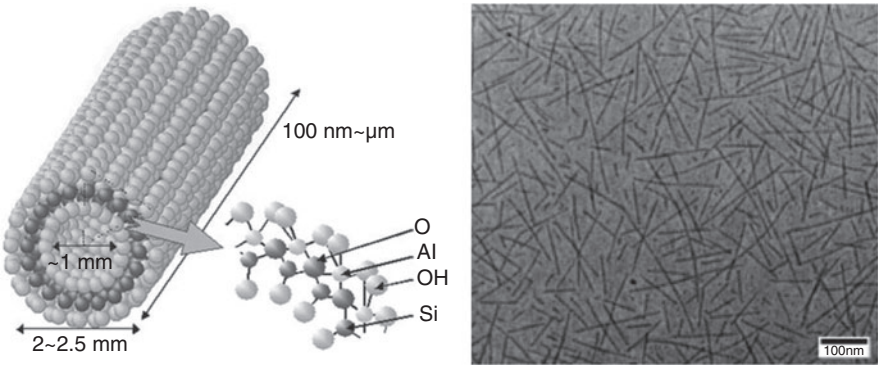

Fig. 5 Structure scheme of imogolite (Reproduced with permission from Ref. [115]) and TEM image (Reproduced with permission from Ref. [116])

Natural Nanosheets

Compared with one-dimensional nanoscale silicate clay minerals, the Al-rich silicate clay minerals with two-dimensional layered structure have more wide distribution, more reserves and species in the nature. The phyllosilicates are commonly divided into three categories (1: 1 type, 2: 1 type, and mixed-layer type) according to their structure and composition. However, due to the difference in structure, the performance and potentional application fields of different two-dimensional clay minerals are also different. The typical 1:1-type sheet-shaped clay minerals are kaoline and serpentine; and the representative 2:1-type sheet-shaped clay minerals are montmorillonite, smectite, vermiculite, illite, muscovite, saponite, and others; and the typical 2:1:1 type clay mineral is chlorite; and the typical mixed-layer clay minerals are rectorite and illite/smectite clay.

Sheets-shaped kaolinite families include kaolinite, dickite, and nacrite, which are formed by the decomposition of orthoclase feldspar (e.g., in granite). Dickite and nacrite are rather rare in the nature and are usually found mixed with kaolinite in deposits of hydrothermal origin [133]. The kaolinite is composed of one silica-oxygen tetrahedral layer and one alumina-oxygen octahedral layer by the 1:1 ratio with the molecular formula of $Al_2Si_2O_5(OH)_4$, as is shown in Fig. 6 [134]. The chemical composition of kaolinite, dickite, and nacrite is similar; and the major components of SiO_2, Al_2O_3, and H_2O, and the minor amounts of Mg, K, Fe, Ti, etc. have the theoretical composition of SiO_2 46.54%, Al_2O_3 39.50%, and H_2O 13.96% expressed in terms of the oxides. The formula indicates that there is no substitution of Si^{4+} with Al^{3+} in the tetrahedral layer and no substitution of Al^{3+} with other ions (e.g., Mg^{2+}, Zn^{2+}, Fe^{2+}, Ca^{2+}, Na^{+}, or K^{+}) in the octahedral layer. Thus, the net layer charge of kaolinite is: $[4\ (+\ 4)] + [4\ (+\ 3)] + [10\ (-\ 2)] + [8\ (-\ 1)] = 0$, but in nature, kaolinite has a small net negative change arising from broken edges on the crystals. This negative charge, although small, is responsible for the surface not being completely inerted. Some workers have also reported substitution of octahedral Al^{3+} with Fe^{2+} and/or Ti^{4+} in kaolinite [135].

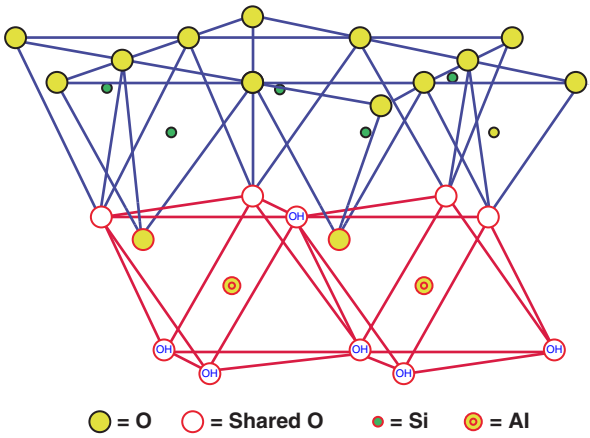

Fig. 6 Structure of Kaolinite (Reproduced with permission from Ref. [134])

Smectite-family clay minerals have been widely used as the reinforcing nano-fillers for the fabrication of nanocomposites because of their larger surface area and large aspect ratio [136, 137]. Among them, montmorillonite (MMT) has been especially concerned in contrast to the other member of nanoclays owing to its advantages such as abundance, environmentally friendliness, and well-studied chemistry. MMT is a dioctahedral clay mineral with the 2:1 layer linkage. The individual layers of MMT have the lateral dimensions of 200–600 nm and the thickness of a few nanometers, and each layer is composed of two tetrahedral sheets and an octahedral sheet, with the sandwhich-like structure. The sheets are linked to each other in such a way that the silicon oxide tetrahedron (SiO_4) shares its three out of four oxygen atoms with the central octahedral sheets, as shown in Fig. 7 [138, 139]. The isomorphic substitution of Al^{3+} by Fe^{2+} or Mg^{2+}, and Mg^{2+} by Li^{1+}, in the octahedral sheet induces the overall negative charge on each layer, and the different metal cations such as Na^{1+} and Ca^{2+} are present in the interlayer of the galleries to keep the charge balance, which make MMT having cation exchangeable capability and hydrated capability [139, 140]. The hydration of MMT causes the swelling and expansion of the galleries, and so MMT shows excellent colloidal properties superior to most of the other clay minerals. In addition, the pristine clays are hydrophilic, and so can only be dispersed in hydrophilic solvents or hydrophilic polymers. The metal cations present in the clay galleries can also be exchanged with organic cations, such as alkylammonuim or alkyphosphonium/onium ions to form intercalation or coating structure, which allows the MMT clay to be modified as hydrophobic or partially hydrophobic surface. Murray [141] reported that the charge imbalance called as cation exchange capacity (CEC) in smectite is about 0.66 per unit cell due to the isomorphic substitution. The CEC depends on the nature of isomorphic substitutions and varies from layer to layer; hence an average value on the complete crystal is considered [142]. It is expressed as mequiv/100 g (meq/100 g) and is reported to range from 80 to 150 meq/100 g for smectites.

Vermiculite (VMT) is a mica-type trioctahedral silicate clay mineral with 2:1 layered structure like the well-known montmorillonite. Each layer is composed of

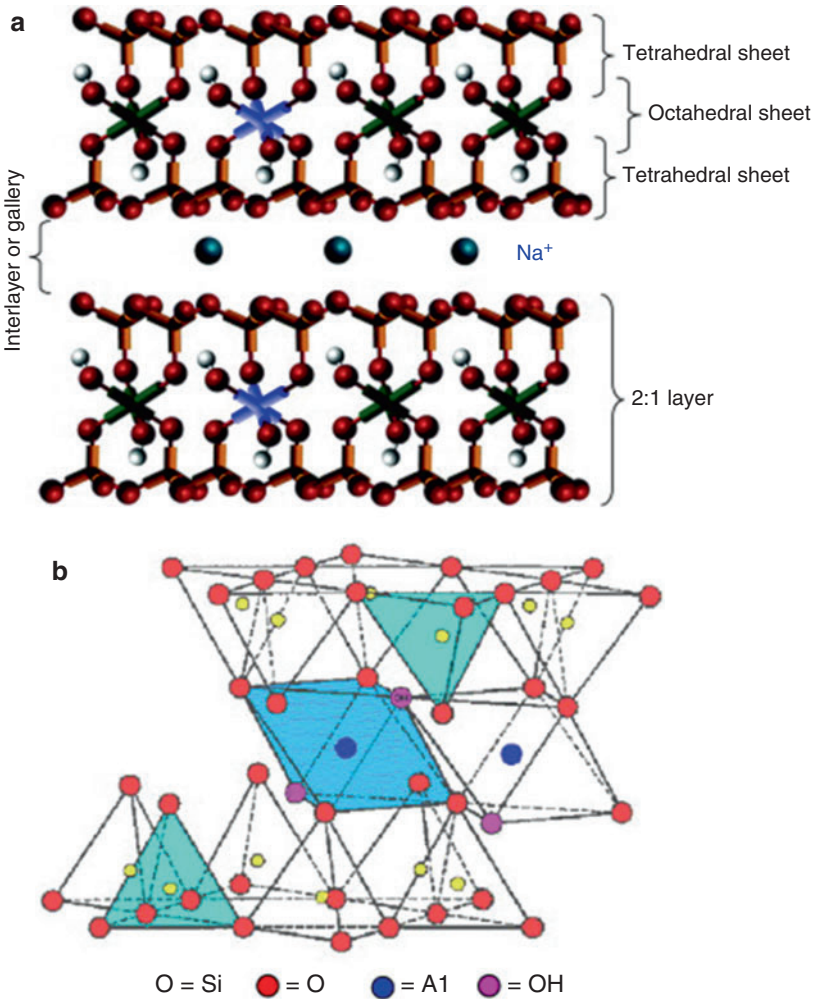

Fig. 7 Structure schemes of sodium montmorillonite (Reproduced with permission from Ref. [138, 139])

octahedrally coordinated cations (typically Mg^{2+}, Al^{3+}, and Fe^{2+} ions) sandwiched by tetrahedrally coordinated cations (typically Si^{4+} and Al^{3+}). The isomorphous substitution of Si^{4+} by Al^{3+} leads to a net negative surface charge (>0.6 per formula unit), that is compensated by an interlayer of exchangeable hydrated cations (Ca^{2+}, Mg^{2+}, Cu^{2+}, Na^{+}, and H^{+}) (Fig. 8) [143]. Compared to montmorillonite, chlorite, kaolinite, and hydrous mica, vermiculite is abundant and has larger cation exchange content (CEC) (100–150 cmol/kg). Therefore, it could be modified with acid, sodium, and long-chain quaternary ammonium, respectively. VMT is usually used as a packaging material for antishocking, abundant, and much cheaper in comparison with MMT, hectorite, and saponite [144, 145]. VMT has been proved to be a

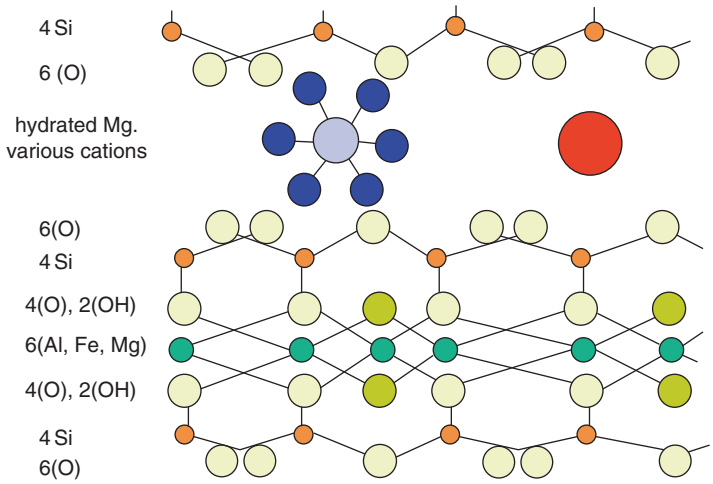

Fig. 8 Structure scheme of vermiculite (Reproduced with permission from Ref. [143])

nice raw material to fabricate adsorbent [146], water-saving material [147], carrier of catalyst [148], and reinforcement for the preparation of nanocomposites [149].

Mica family minerals are mainly biotite and phlogopite, and their chemical composition can be expressed by $K(Mg, Fe)_3[Si_3AlO_{10}](OH)_2$. The space group is $C_{2/m}$, with $a_0 = 0.531$ nm, $b_0 = 0.92$ nm, $c_0 = 1.022$ nm, $\beta = 100°$. In the octahedral structure, Mg^{2+} and Fe^{2+} in the octahedral layer exhibit complete isomorphous. Usually, Mg: Fe > 2: 1 is for the phlogopite, and Mg: Fe <2: 1 is for the biotite. In natural mica, a portion of Mg^{2+} and Fe^{2+} are often replaced by Al^{3+}, Fe^{3+}, Ti^{4+}, and Mn^{2+}. The crystal structure of the mica mineral is composed of octahedral sheets sandwiched between two $[(Si, Al)O_4]$ tetrahedral sheets. The $[(Si, Al)O_4]$ tetrahedrons with a total of three corners connected with each other to form a hexagonal network, and the tetrahedral reactive oxygen is in the same side. The hydroxyl group is located in the center of the hexagonal network and is on the same plane as the active oxygen. The active oxygen in the upper and lower tetrahedrons of the structural layer is opposite and displace $a_0/3$ (about 0.17 nm) along the a-axis direction, so that the two layers of active oxygen and hydroxyl exhibits the most close stack, and Mg^{2+}, Fe^{3+}, and others fill in the pores formed by octahedron, which is called mica structure layer. Since the Si^{4+} in the tetrahedral sheet is replaced by 1/4 of Al^{3+}, the remaining negative charge appears in the structure layer. In order to achieve the balance of the charges, there is a large cation (such as K^+) between the structural layers. The crystal structure of mica mineral is shown in Fig. 9 [150, 151].

Chlorite is a 2: 1 type of aqueous layered aluminosilicate [152]. Chlorite minerals often form in clay-rich sedimentary rocks that are buried in deep sedimentary basins or subjected to regional metamorphism at a convergent plate boundary. Chlorite that forms here is usually associated with biotite, muscovite, garnet, staurolite, andalusite, or cordierite [153]. Metamorphic rocks rich in chlorite might include phyllite and chlorite schist. Another formation environment of chlorite mineral is in oceanic

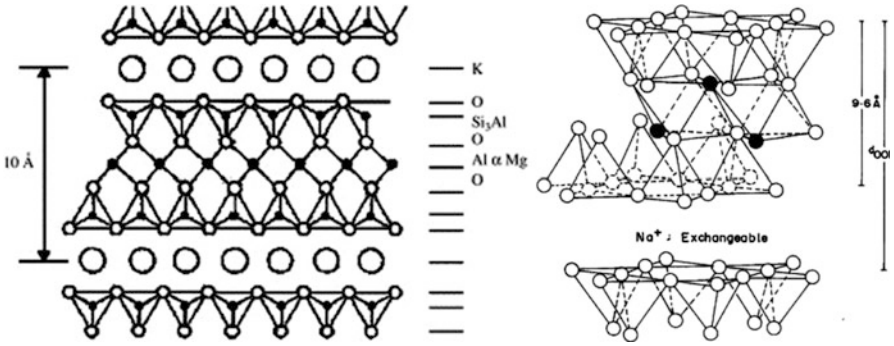

Fig. 9 Scheme of muscovite mica structure (left) (Reproduced with permission from Ref. [150]) and the structure of fluorotetrasilicic mica (Reproduced with permission from Ref. [151])

crust descending into subduction zones. Here, amphiboles, pyroxenes, and micas are altered into chlorite. Chlorite minerals also form during the hydrothermal, metasomatic, or contact metamorphism. These chlorite minerals are often found in fractures, solution cavities, or the vesicles of igneous rocks. Unlike other 2: 1 minerals, the interlayer of the chlorite structure unit layer is filled by positively charged octahedral sheet to form a 1.4 nm basic structural unit that is highly stable at high temperature. Since there are interlayer hydroxyl groups between the upper and lower 2: 1 interlayer, the hydrogen bonding interaction among them is strong, and so the octahedral layer (or hydroxide sheet) has high thermal stability. However, the chlorite formed at low temperature has an incomplete interlayer. Chlorite minerals have a generalized chemical composition of $(X, Y)_{4-6}(Si, Al)_4O_{10}(OH, O)_8$. The "X" and "Y" in the formula represent ions, which might include Fe^{2+}, Mn^{2+}, Fe^{3+}, Mg^{2+}, Ni^{2+}, Zn^{2+}, Al^{3+}, Li^{1+}, or Ti^{4+} [154]. The composition and physical properties of chlorites vary as these ions substitute for one another.

The mixed-layer clay mineral is different from the conventional 1:1 or 2:1 layered clay mineral. It has the transition structure in which two or more layer types are vertically stacked in the direction parallel to c^* [155–157]. The interstratifications can be classified as ordered, random, or partially ordered according to the stacking ordering [158]. Rectorite and illite/smectite are the representative mixed-layer clay minerals in the nature.

Rectorite is a kind of layered silicate, with the structure and characteristics much like those of montmorillonite. It is a regularly interstratified clay mineral with alternate pairs of dioctahedral mica-like layer (nonexpansible) and dioctahedral montmorillonite-like layer (expansible) in a 1:1 ratio [159]. The thickness of a single rectorite layer is about 2 nm, and the width and length vary from a micron to several microns. The interlayer cations of montmorillonite-like layers can be exchanged easily by either organic or inorganic cations, and therefore rectorite has a water-swelling property similar to that of montmorillonite, which makes it possible to prepare nanocomposites by solution-mixing processing technique [160]. Rectorite has been widely applied in many areas such as adsorbent [161, 162], carrier of catalyst [163], drug-delivery carrier [164], and polymer composite [165].

Illite/smectite mixed layer clay (IS) is a mixture of crystallites that contain disproportionate illite and smectite as two distinct, interstratified mineral entitles [166], and is one of the most frequent mineral reactions occurring in deeply buried sedimentary environments. It is formed from the illitization of smectite, so that IS has the dual characteristics of illite and smectite [167]. The formation of IS is dependent on time, temperature, pressure, K^+ content, Al^{3+} for Si^{4+} substitution and interlayer hydration, and the expandable and nonexpandable layers coexist in it. The crystal structure of IS is interpreted in terms of a nonpolar and a polar 2:1 layer. In the nonpolar model, individual 2:1 layers are chemically homogeneous, whereas 2:1 layers in the polar model present a smectite charge on one side and an illite charge on the other [167]. The interstratifications between nonexpandable layers of illite and expandable layers of smectite have attracted the attention of many researchers because of their peculiar properties. IS demonstrates it potential application in many areas such as adsorbent [168], geopolymers [169], and polymer composite [170].

In addition to natural sources, the layered silicate clay minerals such as kaolinite [171], montmorillonite [172], saponite [173], hectorite [174], smectite [175, 176], mica [177], and hydrotalcite [178] can be synthesized by artificial methods, and can also be synthesized by the hydrothermal transformation of other clay minerals such as palygorskite [179, 180].

From Clay Minerals to Nanomaterials

Although the diverse assembly styles of silica-oxygen tetrahedrons and aluminium or magnesium-oxygen octahedrons lead to the formation of a variety of nanostructures, the nanoscale units are usually aggregated together to form bulk aggregates and crystal bundles, or the nanosheets are usually assemble together to form sandwiched structure with the interlayer cations. The advantages of clay minerals as nanomaterial have not been fully developed due to the larger size of their natural existence forms, so that the dispersion of clay minerals into a smaller size is the basic premise of fully utilizing their nanomaterial advantages. For a long-term, the dispersion of clay minerals as nanoscale is the subject of great significance, and has attracted considerable attention. For one-dimensional clay minerals, the rod-, fiber-, or tube-shaped nanoscale crystals can be obtained by disaggregating the crystal bundles or aggregates through various mechanical, physical, and chemical methods; and the sheet-shaped nanoscale crystals could be obtained by exfoliating the sandwich-like mineral or intercalating organic molecules into the interlayer.

Disaggregation of Crystal Bundles or Aggregates

As for the applications of one-dimensional nanoclays, the rod-crystal bundles or fiber bundles need to be dispersed as individual single crystals by an efficient method in order to take full advantage of their nanomaterial properties. In fact, the rods or

fibers of natural one-dimensional nanoclays usually exist as bulk crystal bundles or aggregates [21], which is not readily dispersible in either water or common organic solvents. In this chapter, the smallest crystal units of palygorskite were described as "rod," and correspondingly the aggregation of rods was described as crystal bundles, and the association of crystal bundles was described as aggregates. The single rod crystal of palygorskite is demonstrated to be a nanoscale material, but the crystal bundles or aggregates with bulk size fail to demonstrate the characteristic of one-dimensional nanomaterial. The bulk crystal bundles in natural palygorskite clay are difficult to be dispersed in other medium or matrix, which certainly limited the application of palygorskite in many areas, especial in nanocomposites.

As is known, the palygorskite crystal bundles can be disaggregated well when the electrostatic, hydrogen-bonding, and Van der Waals' forces among rods could be overcome by external forces. Thus far, many physical methods (i.e., ball milling, extrusion, ultrasonication, and high-speed shearing) or chemical modification methods (i.e., acid treatment, salt treatment, and organification) methods have been employed [14, 181–183]. Mechanical treatment is helpful to disperse the bulk bundles as smaller bundles or single rods by the extrusion, shearing, and knead forces. Chemical treatment may alter the surface charges of palygorskite and weaken the interaction among rods. Although these traditional treatment methods have been widely used in industries, the disaggregation efficiency is not satisfactory, and the strong mechanical action may break the rod crystals, which reduced the aspect ratio of palygorskite. So, the disaggregation and dispersion of palygorskite crystal bundles with no expense of reducing aspect ratio have been desired, because of the increasing demand for highly dispersed one-dimensional nanorods.

In order to disaggregate the palygorskite crystal bundles as single nanorods, Wang's groups [53, 184–187] have employed high-pressure homogenization technology to treat palygorskite suspension, and found that the crystal bundles has been dispersed as individual nanorods by the cavity effect generated by high-pressure homogenization process. In addition, the organic solvents have been introduced in this process to prevent the secondary aggregation of dispersed nanorods [188–190]. The high-pressure homogenization treatment of palygorskite at different ethanol/water ratio has a great influence on the swelling properties of the superabsorbent (NaAlg-*g*-P(NaA-*co*-St)/APT). It was found that the crystal bundles were effectively disaggregated in the solution with the *m*(ethanol): *m*(water) = 5: 5 after homogenized at 50 MPa, which clearly improved the gel strength (from 1300 to 1410 Pa, $\omega = 100$ rad/s), swelling capacity (from 442 to 521 g/g), swelling rate (from 3.3303 to 4.5736 g/g/s), and reswelling ability of the resultant superabsorbent nanocomposite. This confirms that the disaggregation of palygorskite crystal bundles is favorable to enhance the properties of the superabsorbent. The highly dispersed palygorskite demonstrates excellent performance that is obviously better than raw one, which paves a solid foundation for the high-value utilization of palygorskite in functional materials [23].

Sepiolite is a fibrous clay mineral and has been widely applied in many areas, but the individual particles of sepiolite with fiber-like morphology usually lying in a

highly aggregated state formed by bundles, so that the disaggregation or dispersion of sepiolite has also been concerned in recent years. Zhou et al. [191] purified sepiolite associated with quartz and calcite *via* sedimentation method and the microwave-assisted acid treatment. The crystal structure of sepiolite shows no change after freezing at −50 °C for 12 h or modification with hexadecyl trimethyl ammonium bromide (HDTMA), but the aggregates were effectively disaggregated. de Lima et al. [192] treated sepiolite with three ionic liquids based on imidazolium cations with different alkyl chains (1-alkyl-3-methylimidazolium); alkyl = butyl (BMIm), octyl (OMIm), and dodecyl (DMIm) and bis(trifluoromethanesulfonyl) imide (Tf2N) as an anion. It has been revealed that sepiolite particles in the Sep/BMImTf2N sample are more disaggregated, forming a 3D network of fibers. The disaggregated sepiolites can be potentially applied as a reinforcing agent for polymers, template for nanostructured materials, and support for catalysts.

Intercalation and Exfoliation of Layered Clay Minerals

The two-dimensional clay minerals (i.e., kaolinite, montmoriollite, illite, and mica) have the "sandwich"-type structure composed of two tetrahedral sheets and one octahedral sheet. The dispersion of two-dimensional clay minerals in composites can be divided into three main categories: microcomposites, intercalated nanocomposites, and exfoliated nanocomposites, so that the intercalation of guest species into the interlayer of clay minerals or the exfoliation of sandwich-type structure as nanosized sheets are essential to fabricate a nanocomposite and fully utilize the advantages of clay minerals as nanomaterials [193].

Sheet-shaped clay minerals have certain cation-exchange capacity and interlayer cations, so the other organic molecules or metal ions may intercalate into the interlayer to form an intercalation complex. The conventional sheet-type clay minerals could be intercalated by cationic species, such as chitosan [194], cationic surfactants [195], positively charged hydroxyl aluminum [196], cationic polyacrylamide [197], the cationic vinyl monomers diallyl dimethyl ammonium chloride [198], and others [199]. The intercalation of cationic species leads to the formation of a nanocomposite, in which the clay mineral was dispersed as nanosize. The preparative intercalation techniques include: (i) intercalation of surfactants, polymers or prepolymers from solution; (ii) in situ intercalative polymerization method; and (iii) melt intercalation method. The intercalative composite materials frequently exhibit improved mechanical properties in comparison with origin polymers or conventional micro- and macrocomposites.

Figure 10 shows the scheme of the pretreatment and intercalation of vermiculite [143]. Three methods have been proposed for the modification of vermiculite. It has been shown that the diffraction peaks of vermiculite at $2\theta = 7.3°$ ($d = 1.2$ nm) shift to $2\theta = 8.1°$ ($d = 1.1$ nm) after acid treatment, remain unchanged after ion-exchange treatment with Na^+, but shift to $2\theta = 8.1°$ ($d = 3.7$ nm) after treatment with cetyltrimethylammonium bromide. It is obvious that the gallery spacing (d value) was significantly larger than that of original VMT and NVMT. The larger gallery

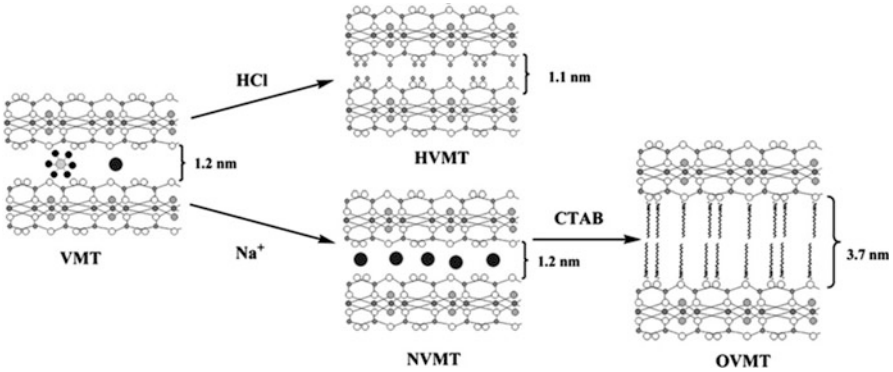

Fig. 10 Schematic drawing of modified VMT in three different ways (Reproduced with permission from Ref. [143])

spacing indicated the intercalation of cetyltrimethylammonium bromide between the silicate layers, and the gallery spacing depends on the packing density and chain length, the intercalating agents radiated away from the surface forming bimolecular tilted arrangement. The intercalation of clay minerals with surfactants is usually the premise of prepare the polymer/clay intercalation composite. The increased gallery spacing resulted from the intercalation of surfactants allow the polymer chains to be easily intercalated into the interlayer.

The intercalation of clay minerals by natural polymer chitosan in solution has been widely studied because such materials are ecofriendly and effective. Monvisade and Siriphannon [200] prepared the chitosan-intercalated montmorillonite and studied its adsorption performance for dyes. In this process, chitosan (4 g) with the deacetylation degree (DD) of 82.5% was dissolved in 196 mL of 2% *v/v* acetic acid, and 2.5 g Na^+-MMT was dispersed in 100 mL of distilled water with the assistance of ultrasonication for 1 h. After that, the chitosan solution was slowly added into the aqueous suspension of Na^+-MMT using the peristaltic pump at the rate of about 50 mL/h with vigorous stirring, and the mixture was treated at 60 °C for 24 h to obtain the chitosan-intercalated montmorillonite. The basal spacing of d_{001} increased from 1.23 nm to ~1.36 nm and ~2.25 nm, respectively, which corresponds to the monolayers (~1.36 nm) and bilayers (~2.25 nm) of chitosan in MMT (Fig. 11).

In situ intercalative polymerization method has also been used to prepare intercalation composites. The poly(methylmetacrylate)/montmorillonite (PMMA)/(MMT) nanocomposites were prepared by one-step in situ intercalative solution polymerization involving simultaneous modification of MMT with quaternary ammonium salts (QAS), polymerization, and polymer intercalation [201]. The largest extent of intercalation was achieved in nanocomposites with the QAS having one long alkyl (C16) chain, and the MMT layers were uniformly dispersed in the polymer matrix (Fig. 12). The obtained PMMA/MMT intercalated nanocomposites exhibited a higher glass transition temperature, better thermal stability, and improved solvent resistance than the neat PMMA.

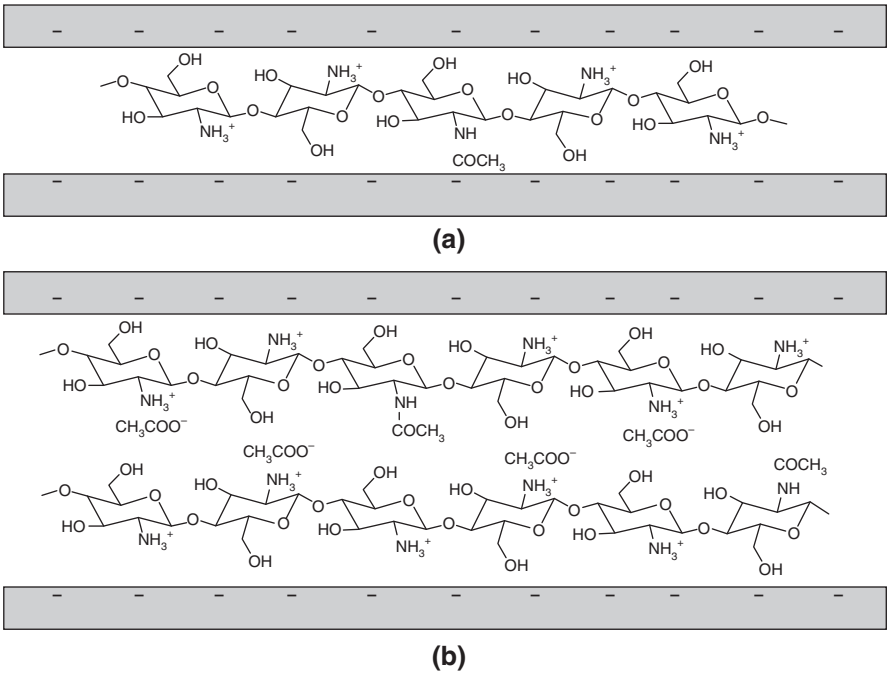

Fig. 11 Intercalation of chitosan into Na^{+}-MMT: (**a**) monolayer and (**b**) bilayer structures (Reproduced with permission from Ref. [200])

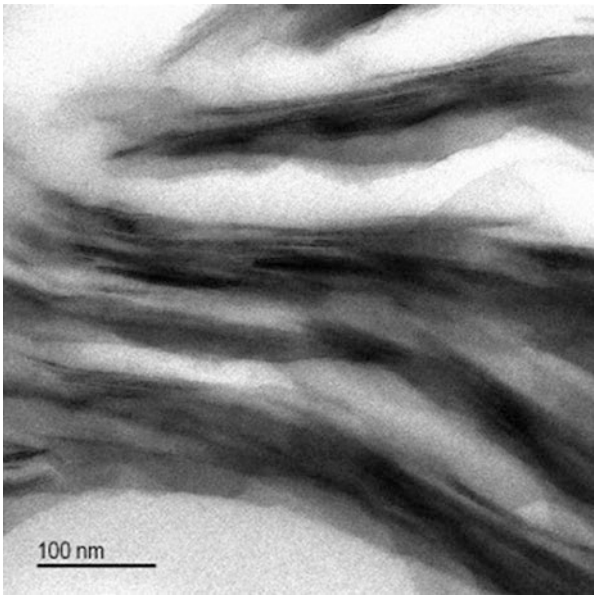

Fig. 12 TEM micrograph of PMMA/MMT–CTMAB nanocomposite with 4.8% MMT (Reproduced with permission from Ref. [201])

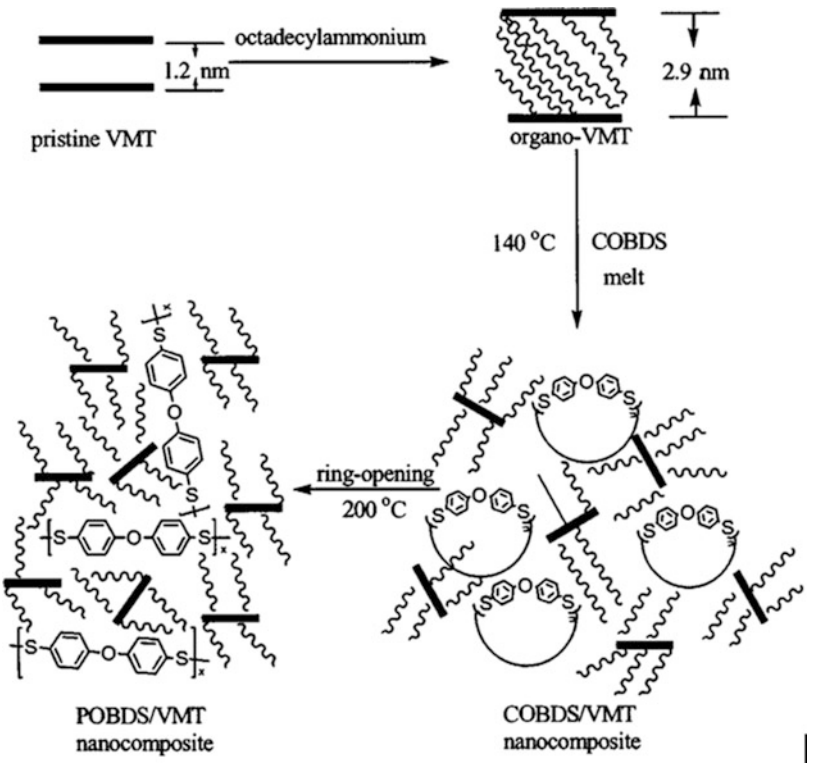

Fig. 13 Schematic representation of the processes for preparation of POBDS–VMT nanocomposite (Reproduced with permission from Ref. [202])

Two approaches have usually been employed to exfoliate the sheet-shaped clay mineral. One is the exfoliation by mechanical shearing action, and another method is the in situ polymerization of monomers in the layers. Figure 13 shows the schematic representation of the preparation processes of POBDS–vermiculite nanocomposite [202]. The pristine vermiculite (VMT) was firstly intercalated with octadecylammonium, which leads to the increase of gallery spacing from 1.2 nm to 2.9 nm. The cyclo(4, 4′-oxybis(benzene)disulfide) oligomers (COBDS) were further intercalated into organo-VMT *via* diffusion of COBDS melt into VMT galleries. It is demonstrated that small molecular COBDS, with relatively lower melt viscosity, facilitates its diffusion into the interlayer of organoclay. This indicates the main merit of utilization of cyclic oligomers as intermediate or precursor for the composite matrix. Generally, the formation of nanocomposite *via* melt intercalation depends upon the mobility of the matrix melt. Hence, this is important in terms of the polymer dynamics and diffusion in the confined environment of polymer/layered clay. By heating the COBDS/VMT nanocomposite precursor at 200 °C, an instant ring-opening polymerization of COBDS occurs (Fig. 13). There is no XRD reflection

Fig. 14 TEM micrograph of POBDS–VMT nanocomposite (Reproduced with permission from Ref. [202])

observed for the resulting material, demonstrating the formation of exfoliated POBDS–VMT nanocomposite. The exfoliated nanosized VMT layers were uniformly dispersed in the polymer matrix (Fig. 14).

The modification methods of clay minerals have also a great influence on the structure of the formed nanocomposites. Wang and Wang [203] prepared a series of superabsorbent composites using modified rectorite as the inorganic components. It was found that the intercalated nanocomposite was obtained using organified rectorite (CTA^+-REC) as the inorganic component, but only exfoliated nanocomposite was obtained using raw rectorite or acid-treated rectorite (H^+-REC) as the inorganic components (Fig. 15). The intercalated nanocomposite shows better water absorption capability than exfoliated nanocomposite.

Functional Ecomaterials Based on Nanoscale Clay Minerals

In addition to the industrial applications mentioned above, nanoclays are also helpful in environmental protection and remediation. Their potential as adsorbents, catalysts, reinforcing agents for volatile organic compounds, and organic/inorganic contaminants

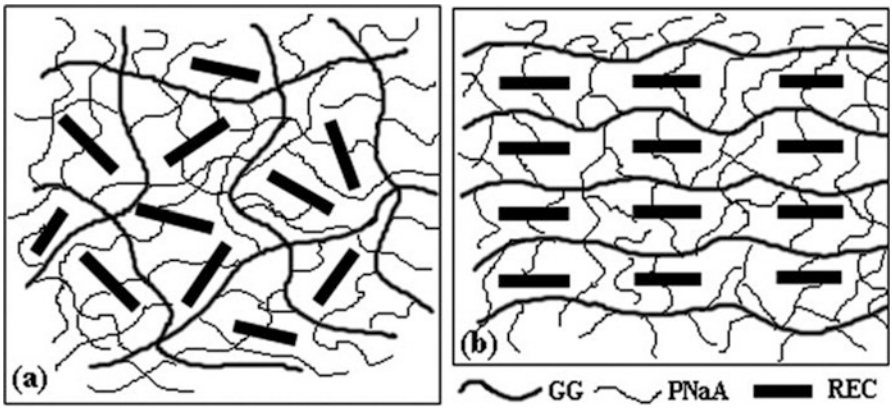

Fig. 15 Illustration of (**a**) exfoliated nanocomposite GG-*g*-PNaA/H^+-REC and (**b**) intercalated nanocomposite GG-*g*-PNaA/CTA^+-REC (Reproduced with permission from Ref. [203])

in wastewater is well documented. In this section, the functional ecomaterials derived from various clay minerals have been summarized systematically.

Adsorption Materials

Modified Clay Minerals

Mechanical-Treated Clay Minerals

Mechanical-chemical treatment is an effective method to alter the structure, surface properties, and performance of natural nanoscale clay minerals [204, 205]. The mechanical treatment may disperse bulk crystal bundles or aggregates as smaller units to increase the specific surface area or break the inert Si-O-Si(or M) bonds to form active $Si\text{-}O^-$ groups, which are greatly helpful to improve the adsorption performance. The mechanical treatment of palygorskite by stone milling may partially disaggregate the crystal bundles, and greatly enhance the specific surface area from 153 to 229 m^2/g, micropore area from 28 to 103 m^2/g, and micropore volume from 0.012 to 0.047 cm^3/g, as well as the adsorption capacity for Methylene blue from 89.21 to 111.78 mg/g [181]. Djukić et al. [206] has evaluated the effect of ball-grinding on the adsorption performance of Serbian natural clay, and found that the grinding treatment greatly enhanced its CEC value from 77 meq/100 g to 95 meq/100 g, as well as the adsorption removal efficiency from 80.8 to 86.6% (for Ni(II)), 80.8 to 87.3% (for Cd(II)), respectively. Maleki et al. [207] have employed a ball-milling process to treat local clay and studied the effect of mechanical treatment on the structure and adsorption performance of the clay. It has been found that the adsorbent prepared at the ball/powder mass ratio of 10:1 and the time of 10 h shows the maximum adsorption capacity of 29.76 mg/g for Ni(II), which enhanced by 71.7% in comparison to the initial unmilled clay. In addition, the mechanical-

chemical treatment may promote the loading of cationic inorganic molecules on clay minerals by intercalation [208], or insertion [209], or grafting [210, 211] approaches.

Acid-Modified Clay Minerals

Acid activation is the frequently used method to improve the structure and physicochemical features of clay minerals [212, 213]. Acid leaching of clays and clay minerals causes the disaggregation of clay particles, elimination of impurities, and dissolution of the external layers. The inorganic acid modification may increase the surface area, pore volume, and number of acid sites, and thereby enhance the adsorption capability of clay minerals. The commercial bleaching earth used for decolorization of vegetable oils is usually produced by the acid (mainly H_2SO_4) treatment of bentonite, because this process led to the increase of specific surface area and pore volume. The chemical compositions of the raw bentonite, acid concentration, temperature, and leaching time play significant roles in the chemical composition and mineralogical properties of the bleaching earth [214]. The acidity of the montmorillonite arises from H^+ in the surface exchange sites (Brønsted acid sites). These acid sites were produced by the exchange of interlamellar cations (Mg^{2+} and Al^{3+}) in the octahedral sheet with H^+ from the sulfuric acid. With increasing acid concentration and impregnation time, considerably greater amounts of octahedral Al^{3+} and Mg^{2+} were removed, leading to a decrease in the Lewis acidity [215].

The influence of acid treatments on the adsorption capacity of sepiolites has been studied by Kilislioglu and Aras [216]. The acid-treated forms of clays show a significant increase in the specific surface area. Even though the acid treatments produced clays with higher specific surface area, the adsorption capacity of acid-sepiolite toward UO_2^{2+} ions was smaller than the untreated sepiolite. This phenomenon occurred likely due to the leaching of most of the interlayer Mg^{2+} ions and the collapse of the octahedral layer. Tunisian smectite-rich clay was modified by Chaari and coworkers [217] using two inorganic acids (HCl and H_2SO_4). The modification using H_2SO_4 gave a better adsorption performance than HCl on the removal of Pb(II) from aqueous solution. Compared to nonactivated clay, both acid-activated clays have a higher number of active surface sites for the binding of lead cations. Panda and coworkers [218] studied the influence of acid concentration on the physicochemical characteristics of kaolin clay. The results indicate that high acid strength treatment provoked amorphization and structural transformation to form an amorphous silica type phase. The improvement of pore characteristics such as specific surface area and pore volume was observed after acid treatment. A similar study of the acid activation of kaolin was also conducted by Alkan et al. [219]. The effect of molar concentrations and acid to solid impregnation ratios was studied and they found that the partial distortion of layer structure and specific adsorption of H^+ ions onto the clay surface reduced the active patches of kaolin.

Combination of acid and thermal treatment process was proven to be favorable to increase the adsorption capacity of montmorillonite further [220, 221]. The carbonates were removed by HCl (1 N) and organic compounds were removed by thermal treatment, which make the modified clay minerals have better adsorption performance than raw ones.

Alkaline-Modified Clay Minerals

Compared to the acid modification, the impregnation of clay minerals using base solutions for environmental purpose is seldom used. Sodium hydroxide solution was used to regenerate a spent bleaching earth from an edible oil refinery by Mana et al. [222]. After alkali treatment, the spent bleaching earth was subsequently treated with thermal treatment at 100 °C. The clay structure was not apparently affected by the treatment and the impregnated organic matter was quantitatively removed. The treated spent bleaching earth exhibited a significantly higher adsorption capacity than virgin bleaching earth as well as fast adsorption kinetics at the same metal concentration [222]. The influence of acid, base, and salt modifications of clay on its adsorption rates for naphthalene was examined by Owabor et al. [223]. The chemical modifiers used in their study include hydrochloric acid (HCl), citric acid ($C_6H_8O_7$), sodium hydroxide (NaOH), ammonium hydroxide (NH_4OH), sodium chloride (NaCl), and zinc chloride ($ZnCl_2$). Sodium hydroxide modified clay showed relatively better adsorption performance for the removal of naphthalene from the bulk solution, while ammonium hydroxide modified clay showed a slow adsorption rate of naphthalene from the bulk solution [224]. Sodium hydroxide was also used for modification of illite by Lakevičs et al. [225]. The experimental results indicate that the adsorption performance of illite toward methylene blue increased after the modification process. Wang et al. [226] modified palygorskite with NaOH solution at ambient temperature, and the effect of alkaline activation on the adsorption performance was studied. It was revealed that the palygorskite rods gradually become shorter with increasing the concentration of NaOH, and the Al and Mg ions in the octahedral sheets could be leached out by alkaline attack, and the rod-like morphology disappears after treated with 5 mol/L NaOH solution. The breakage of inert Si-O-Si and Si-O-M bonds leads to the generation of more $Si\text{-}O^-$ groups, which increased the negative surface potentials of palygorskite and intensified the complexation capability to cationic dyes. After modification, the adsorption capability of palygorskite increased from 65.88 mg/g to 154.56 mg/g. Akpomie et al. [227] modified montmorillonite with 1 mol/L NaOH solution and used for the adsorption removal of Ni(II) and Mn(II) from aqueous solution. It was found that the alkaline modification increased the specific surface area from 23.2 to 30.7 m^2/g and the cation exchange capacity from 90.78 to 94.32 meq/100 g, and the maximum adsorption capacities of the activated montmorillonite reached 200 and 197 mg/g for Ni(II) and Mn(II), respectively. Öztop et al. [228] reported a low-cost adsorbent prepared by an alkaline hydrothermal treatment (reflux method) in NaOH solution using montmorillonite-illite clay as the raw materials. After the reaction, the original mineral was converted to a zeolitic material with spherical morphology, and the SiO_2/Al_2O_3 and Na_2O/Al_2O_3 ratios sharply changed. The adsorption ratio of the modified adsorbent for Cs^+ from 0.1 mmol/L of initial solution reached 97%. The moderate alkaline modification is favorable to the adsorption of clay minerals for dyes or heavy metal ions because this process could improve surface charge and increase the surface $Si\text{-}O^-$ groups, which is potential to be used in industry on a large scale.

Ion-Exchange Modified Clay Minerals

There are large amount of exchangeable cations in the clay minerals for the compensation of charges. These ions affect the compositon and surface properties of clay minerals, and thereby affect their adsorption properties. So, ion-exchange modification is also a commonly used method to tailor the surface chemical feature of clays and clay minerals. In this process, the certain exchangeable cations in the interlayers were exchanged with other cations from the solution. The cation exchange modification of natural clinoptilolite was reported by Lihareva et al. [229], and it has been confirmed that the replacement of Na^+ ion toward the interlayer cations (K^+, Ca^{2+}, and Mg^{2+}) enhances the cation exchange capability of Na-clinoptilolite toward Ag^+ ions because of more monoionic character of the clay. Similar study about ion-exchange modification of clinoptilolite using NaCl and HCl solutions was done by Coruh [230] for the removal of zinc ions, and it was found that sodium-exchanged clinoptilolite shows higher effective ion exchange capacity due to lower Si to Al ratio. Ma et al. [231] reported Cu^{2+}-exchanged montmorillonite (CEM) and evaluated its adsorption performance for methylene blue (MB). The BET specific surface area of montmorillonite increased from 367.7 to 576.3 m^2/g, but the adsorption capacity slightly reduced after Cu^{2+} exchange. However, in some case, ion-exchange is not conducive to improve the adsorption capacity of clay minerals. Huang et al. [232] found that the exchange modification of Ca-montmorillonite (Ca-Mont) with titanium cation might increase the BET surface area due to the pore-opening effects and the increased interlayer spacing. The pore size, pore volume, and pore connectivity of montmorillonite also increased due to the pore-opening effects, but the adsorption capacity decreased because high-valuant ions are more difficult to be exchanged than low-valent ions. Wang et al. [233] modified Ca-Mont by ion-exchange with titanium cations. It was found that the Ti-Mont is less crystalline than the Ca-Mont, the Ti cation-exchange process may exfoliate Mont clay to some extent, which leads to from the large increase of surface area from 80.4 to 215.5 mg/g. The adsorption of the modified montmorillonite for basic dyes decreased because Ti^{4+} is more difficult to displace by basic dyes than Ca^{2+}.

Heat-Activated Clay Minerals

Heat activation is a frequently used method to improve the adsorption properties of clay minerals [234, 235]. Different kinds of water located in intracrystalline tunnels of clay minerals can be removed selectively by heat treatment at different temperature, which correspondingly changes the pore structure and surface properties [236, 237]. In addition, heat activation process can broke some inert Si-O-Si (or M) bonds to increase the ion-exchange capability of clay minerals [238]. So, heat treatment has an influence on the specific surface area and cation-exchange capacity, which are very important to judge the adsorption capacity of adsorbent [239]. Chen et al. [238] treated palygorskite by calcinations and studied the effect of this process on the adsorption properties. It was revealed that the change trend of the adsorption capacity of activated samples for dye adsorption is accordant with that of CEC with increasing the calcinations temperature, and the leaching amount of divalent ions (Mg^{2+}, Ca^{2+}) in all samples are significantly higher than that of univalent (Na^+,

K^+) and trivalent ions (Fe^{3+}, Al^{3+}). With further increasing to 700 °C, the characteristic peaks of palygorskite in XRD patterns almost completely disappear, implying a thorough destruction of its crystal structure. It is observed from the pattern of the sample treated at 800 °C that some new peaks attributed to cristobalite and clinoenstatite minerals appear, which means the change of palygorskite to an amorphous structure. The adsorption capacity increased from 48.39 to 78.11 mg/g after heat activation. Sabah et al. [240] found that the specific surface area of sepiolite increased to specific surface area of 235 m^2/g after heat activation, and more Mg^{2+} could be exchanged from heat-activated sepiolite, which is favorable to enhance the adsorption of sepiolite for surfactants. The increased specific surface area and cation ion exchange capability are the main reason for the enhanced adsorption. The heat- or acid/heat- activation process of clay minerals has been widely used in industry to produce various adsorbent, such as decoloring agents of edible or biodiesel, molecular sieve, catalysts, and others.

Organo-Modified Clay Minerals with Surfactants

Currently, various surfactants have been used for the modification of clay materials in order to improve the adsorption performance. The main purpose of the intercalation or coating of surfactant ions onto the clay mineral is to convert the initially hydrophilic clay mineral particles into hydrophobic organoclays. The cationic surfactants such as linear alkyl amines and alkyl ammoniums substances (fatty amine salts and quaternary ammoniums) have been frequently used for the fabrication of organo-modified clay minerals due to their positive charge. The most commonly used cationic surfactants for modification of clay minerals are quaternary ammonium salts, such as cetyltrimethylammonium bromide [241, 242], octadecyltrimethylammonium [243], tetradecyltrimethylammonium bromide [244], dodecyltrimethylammonium bromide [245], and cetyltrimethylammonium chloride [246]. Quaternary phosphonium surfactants were also used for the modification of clay minerals [247]. The surface modification of clays and clay minerals with cationic surfactants involves both cation exchange process and the bonding of the hydrophobic moiety in the clay layers.

It has been demonstrated that the modification with cationic surfactants can alter the surface charges and hydrophilic/hydrophobic characteristics of clay minerals, which make them able to remove more hazardous pollutants from aqueous environment and landfill liner (to protect soil and groundwater from hydrophobic organic compounds pollution) with satisfactory efficiency. The clay minerals modified with quaternary ammonium surfactant have better affinity toward many hydrophobic organic compounds than unmodified ones [248]. For example, the modification of bentonite with surfactant could improve its adsorption removal capability to hydrophobic organic compounds [249]. The quaternary ammonium salts with different alkyl chain lengths and a benzyl substitute group has been used for the modification of montmorillonite and smectite, and it has been found that the properties (hydrophobicity, oleophilicity, interlayer spacing, particle size, and thermal properties) of organo-montmorillonite or organi-smectite can be tuned by altering the alkyl chain lengths and functional groups of surfactants [250]. The modification with quaternary

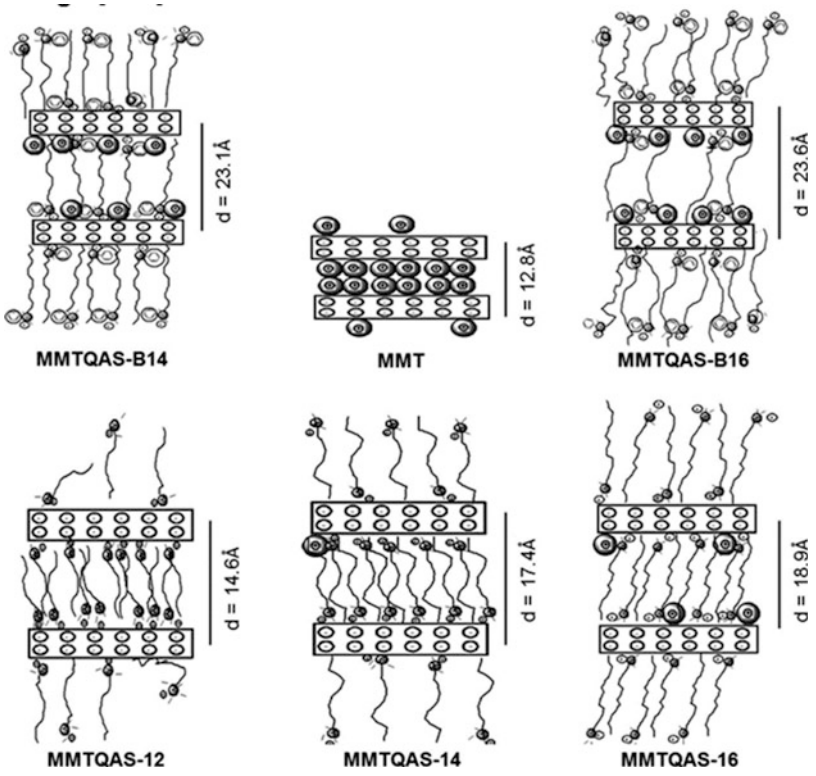

Fig. 16 Schematic illustration of the arrangement of surfactant in interlayer and on surface of clay (Reproduced with permission from Ref. [250])

ammonium surfactants which have benzyl substitute group resulted in water non-wettable and superhydrophobic surface, whereas clays modified with quaternary ammonium surfactants without benzyl substitute group became more water-wettable and hydrophilic than the pristine clay [250]. The arrangement of surfactants on and in clay platelets was estimated and schematically illustrated in Fig. 16. In case of surfactants having benzyl substituent, the adsorption of these surfactants is governed by steric hindrance and stacking interaction of aromatic rings. The larger width of head group (8.29 Å) in this kind of surfactants is larger than the width of alkyl chain (3.65 Å). Then, this type of surfactants creates an array consisting of π–π stacking in the clay, which resists the penetration of water molecules into adsorbed surfactant monolayer. However, nonpolar organic liquids are suitable to this surfactant array because of the affinity of long hydrocarbon chains and aromatic rings toward such liquids like n-octane. The modification of one-dimensional clay mineral such as sepiolite with cationic tetradecytrimethylammonium bromide also altered the negative surface charge to the positive charge [251].

The functionalization of the surface chemistry of clay minerals using an intercalation method with anionic surfactant has been carried out [252, 253]. The

preparation of organo-bentonite using linear alkylbenzene sulfonate (LAS) as the anionic surfactant was carried out by Nathaniel et al. [253]. A similar procedure was also employed by Sandy et al. [254] for the modification of bentonite using an anionic surfactant (linear alkylbenzene sulfonate).

Different conventional cationic or anionic surfactants, gemini surfactants are a class of amphiphilic molecules containing two head groups and two aliphatic chains [255]. In the recent years, gemini surfactants have attracted attention of many researchers for modification of clay and clay minerals [256]. Gemini surfactants have been claimed to have many advantages compared to the conventional surfactants, such as higher efficiency in reducing the oil/water interfacial tension, better wetting, lower critical micellar concentration, foaming, and antibacterial activities [257]. Glycol bis-N-cetylnicotinate dibromide a cationic gemini surfactant has been used for the modification of bentonite [247] and montmorillonites [258]. It has been revealed that the cationic gemini surfactant was intercalated into the bentonite or montmorillonite layer. The gemini surfactant modified bentonite has a better adsorption capacity than CTA-bentonite.

The use of synthetic surfactants to modify clay materials sometimes causes quite serious problems to the environment due to the use of excess surfactants. The surfactants could possess poisonous effects to the aquatic life, especially if these chemical compounds are present in sufficient amounts. Rarasaponin extracted from the berry soap (Sapindus rarak DC) was employed as a modifying agent to improve the adsorption capacity of several clay materials [259, 260]. Several functional groups exist in the structure of rarasaponin such as hydroxyls, ester carbonyls, aromatic rings, and also alkanes group both in aliphatic and alicyclic structure [261]. Suwandi et al. [258] studied the modification of kaolin using a rarasaponin surfactant. Modification of kaolin was conducted by soaking kaolin in rarasaponin solution for 24 h at room temperature. The XRD pattern for kaolin and rarasaponin-kaolin indicate that the alternation of basal spacing of kaolin occurred after intercalation of the rarasaponin molecules into interlamelar spacing of kaolin. In relation to environment protection, Chandra et al. [259] employed rarasaponin surfactant as the modifying agent for the preparation of organo-bentonite.

Organo-Modified Clay Minerals by Surface Coating or Grafting

Organic-inorganic nanocomposites with clay minerals as the main components have been confirmed to be new families of adsorbents because they have better adsorption performance than raw clay minerals. The moderate surface modification of clay minerals by different types of organic molecules may tune their surface hydrophilic-hydrophobic properties, charge characteristics, and/or complexing ability to heavy metal, dyes, and other ions or molecules. The commonly used surface modification methods include chemical grafting or surface coating. The chemical grafting method could introduce organic components or functional groups by forming covalent bonds between the silanol groups of clay minerals and the modifier, for example, the reaction of silane coupling agent with clay minerals (Fig. 17) [104, 261]; whereas the surface coating method may introduce organic species by physical action, such as electrostatic, hydrogen bonding, and Van der Waals forces, such as layer-by-layer assembly (Fig. 18) [262, 263].

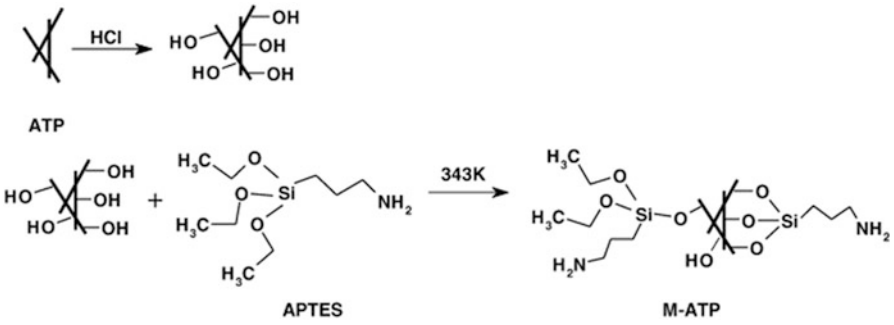

Fig. 17 Schematic illustration of the surface modification of attapulgite (ATP) by 3-aminopropyltriethoxysilane (APTES) (Reproduced with permission from Ref. [261])

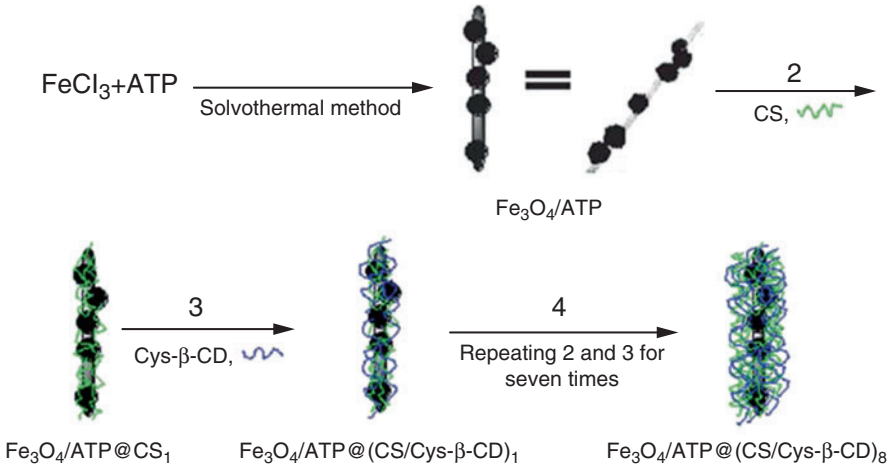

Fig. 18 The mechanism proposed for the preparation of Fe_3O_4/ATP@(CS/Cys-β-CD)$_8$ composite: (1) the synthesis of Fe_3O_4/ATP; (2) the self-assembly of CS on Fe_3O_4/ATP; (3) the self-assembly of Cys-β-CD via electrostatic interactions between CS and Cys-β-CD; (4) the alternate deposition of CS and Cys-β-CD repeated seven times (Reproduced with permission from Ref. [262])

The highly dispersed palygorskite nanorods are obviously advantageous to be used as the ideal carrier of magnetic particles by virtue of the relatively greater surface area and higher surface activity. Wang's group adopted highly dispersed nanoscale palygorskite to fabricate magnetic Fe_3O_4/Pal@(CS/Cys-β-CD)$_8$ [262] and Pal/Fe_3O_4/polyaniline adsorbents [264], which show superior adsorption capability to noble metal ions and dyes. The highly dispersed palygorskite would be potential as an ideal matrix to develop new organic-inorganic composite adsorbents.

The surface modification of clay minerals with natural polymers provided an environment-friendly approach to improve the adsorption properties of clay minerals because of their low production cost and outstanding physicochemical properties.

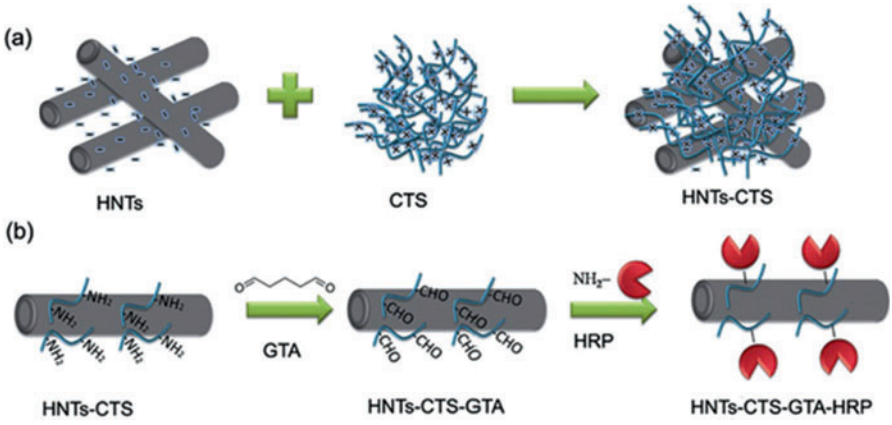

Fig. 19 The assembly process of chitosan onto halloysite nanotube (Reproduced with permission from Ref. [269])

Peng et al. [265] prepared chitosan-modified palygorskite by surface grafting of Pal with chitosan and used for the adsorption of dyes. The maximum adsorption capacity of CTS-modified PA reached 71.38 mg/g, which is greatly higher than that of unmodified palygorskite (6.3 mg/g). In addition, CTS-coated montmorillonite is proved to be an efficient adsorbent for tungsten removal from contaminated sites, reducing the tungsten concentration in product water to below 1 μg/L [266]. CTS/zeolite composites have comparable capacity to other anion exchangers with a nitrate ion exchange capacity of 0.74 mmol NO_3^-/g [267]. CTS/bentonite has been used in removing Pb (II), Cu (II), and Ni (II) from aqueous solution under static conditions, which established inexpensive large-scale barrier filters for the removal of heavy metals contaminations in wastewater [268]. Zhai et al. [269] synthesized chitosan–halloysite nanotubes adsorbent with hierarchically porous structure by the assembly of chitosan onto halloysite nanotube *via* electrostatic interaction (Fig. 19). The as-prepared adsorbent showed excellent immobilization capacity for horseradish peroxidase (HRP), with the maximum enzyme loading amount of 21.5 mg/g (only 3.1 mg/g for raw halloysite). And the immobilized HRP exhibited high removal efficiency for phenol from wastewater. Marrakchi et al. [270] modified sepiolite with chitosan by a combination of surface assembly and crosslinking process. When the ratio of chitosan to sepiolite is 1:1, the resultant adsorbent shows the best adsorption capacities of 40.986 mg/g and 190.965 mg/g for MB and RO 16, respectively.

As described above, the organic molecules containing different functional groups can be attached onto clay minerals with negative charge characteristics by electrostatic or hydrogen bonding interaction, and thereby the adsorption capacity of clay minerals can be enhanced. In addition to the nature of the charge, there are a large number of functional groups on the surface of clay mineral, which can serve as active sites to allow the active organic molecules graft onto it [182, 271, 272]. The functional groups of these molecules may chemically bond to clay minerals, and

thereby the adsorption capacity of the clay mineral was greatly enhanced due to the introduction of functional groups. Celis et al. [273] prepared functionalized sepiolite and montmorillonite by grafting the organic ligands containing thiol (-SH) groups and evaluated their chelating capability to heavy metal ions Hg(II), Pb(II), and Zn (II). The fiber-like sepiolite was modified by chemically grafting of 3-mercapto- propyltrimethoxysilane (MPS) on the surface silanol groups, while the 2:1 sheet-like montmorillonite was modified with 2-mercaptoethylammonium (MEA) by an ion-exchange process. The functionalized sepiolite or montmorillonite are a good adsorbent for Hg(II) ions. The adsorption capacity of sepiolite and montmorillonite for Hg (II) was enhanced from 170 ± 25 mmol/kg to 590 ± 15 mmol/kg, and from 250 ± 30 mmol/kg to 660 ± 25 mmol/kg, respectively, but their adsorption capacities for Pb(II) and Zn(II) are not ideal, which indicate that the adsorbent can selectively adsorb Hg(II). Mercier and Detellier [274] modified montmorillonite with 3-mercaptopropyl trimethoxysilane by a covalent grafting reaction, which shows good adsorption capacities for Pb(II) (70 mg/g) and Hg(II) (65 mg/g), but poor adsorption capacities for Cd(II) and Zn(II). Yuan et al. [96] have modified natural halloysite clay nanotubes with γ-aminopropyltriethoxysilane (APTES). It was found that APTES not only directly graft onto the hydroxyl groups of the internal walls, edges, and external surfaces of the nanotubes, but also condensed with the directly grafted APTES to form a cross-linked structure (Fig. 20). The modification of attapulgite with 3-aminopropyltriethoxysilane (APTES) to introduce

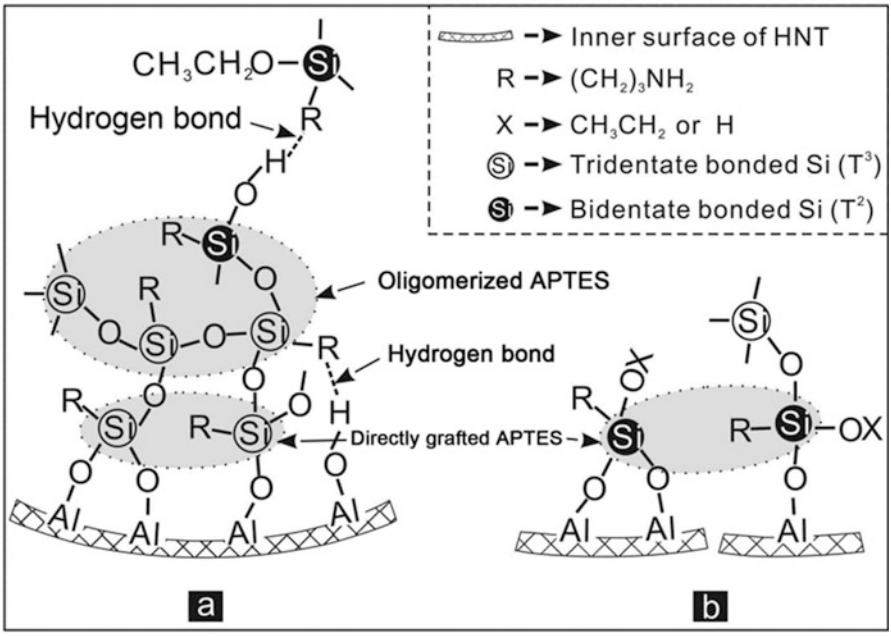

Fig. 20 The proposed mechanism of the formation of cross-linked network (**a**), and of the grafting between bidentate bonded Si and AlOH groups (**b**) (Reproduced with permission from Ref. [96])

–NH_2 groups, and so the NH_2–attapulgite showed better adsorption capability to Hg (II) [261] and high adsorption rates of 99.32%, 99.67%, and 96.42% for Reactive Red 3BS, Reactive Blue KE-R, and Reactive Black GR, respectively [275]. In addition, many other modifiers such as 2-(3-(2-aminoethylthio)propylthio) ethanamine (AEPE) [276], (3-mercaptopropyl)trimethoxysilane [276, 277], and 2,2-bis (hydroxymethyl) propionic acid (bis-MPA) [278].

Organified Modified Clay Minerals by Intercalation Method

As known, most of the clay minerals in nature usually have sandwiched structure, which are composed of the nanoplates constructed by two SiO_4 tetrahedral sheets and one AlO_6 octahedral sheet and interlayer exchangeable cations, such as Ca^{2+}, Na^+, K^+, and Mg^{2+}. These cations can be replaced by other cationic species such as surfactants (i.e., quaternary ammonium salt, quaternary phosphonium salts), positively charged polymers (i.e., chitosan, cationic polyacrylamide) or small molecules (i.e., amino acids, dimethyldiallylammonium chloride), and inorganic polymer (i.e., polyaluminium chloride) [279]. The interlayer spacing tends to increase when the cations were replaced by other larger molecules or polymer, and the intercalated or exfoliated organic/inorganic nanocomposites were formed. The cationic surfactants-intercalated clay minerals such as montmorillonite [280, 281], bentonite [282], rectorite [283, 284], illite [285], muscovite [286], and kaolinite [287] have been widely studied and used for the adsorption of various pollutants. The introduction of surfactants may tune the charges of clay minerals and alter their hydrophilic or hydrophobic features, so that the affinity of clay minerals with different types of pollutants could be controlled by altering the type or structure of surfactants. However, the small surfactant molecules are susceptible to leakage into the environment after use, causing secondary contamination. In addition, the price of the surfactant is relatively expensive. Recently, natural cationic polymer such as chitosan has been used as the organic component to fabricate various intercalated nanocomposites [288]. The nanocomposites of chitosan with different clay minerals including rectorite [289], bentonite [290], and montmorillonite [291, 292] have been prepared and used for the adsorption removal of different pollutants, e.g., dyes, phenol, heavy metals, and others. The intercalation of chitosan into the interlayer spacing of layered clay minerals may increase their interlayer spacing, and simultaneously the –NH_2 functional groups were introduced, which are favorable to improve the chelating capability of the nanocomposite toward dyes or heavy metals (Fig. 21) [293]. Fig. 21 is the schematic illustration of the adsorption mechanism of the chitosan-intercalated montmorillonite. The chitosan polymer chains are presented in the interlayer spacing, whose –NH_2 groups may chelate with Cu(II) to form a stable complex, which is helpful to enhance the adsorption capability of clay minerals.

Solvothermal/Hydrothermal Modified Clay Minerals

Solvothermal and hydrothermal process is a highly effective approach to alter the crystal structure and improve the adsorption properties of clay minerals [294, 295]. In this process, the mineral crystal could be transformed as another crystalline phase

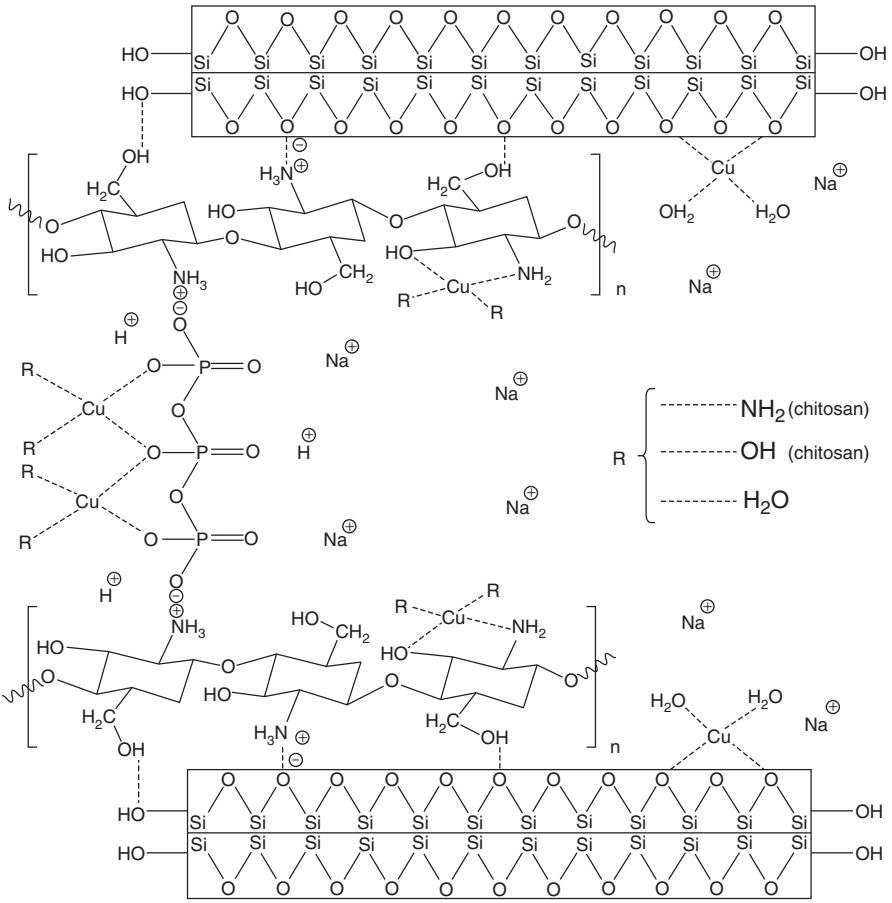

Fig. 21 Proposed binding mechanism for the adsorption of copper ions onto KSF-CTS (The octahedral sheet is not presented in the structure of the silicate) (Reproduced with permission from Ref. [293])

[180], or the inert Si-O-Si or Si-O-M bonds could be broken to form Si-O$^-$ groups with adsorption activity [296]. These groups as adsorption sites may complex with various cationic species such as heavy metal ions, dyes, or antibiotic to enhance the adsorption capacity of the clay minerals. In addition, the structure and adsorption properties of clay minerals could be controlled by altering reaction condition or introducing different organic groups. Tian et al. modified palygorskite by a hydrothermal reaction in the presence of sodium sulfide [297] and ammonium sulfide [298] and studied the effect of hydrothermal process on the structure and adsorption performance of palygorskite. It was found that the modification with ammonium sulfide greatly enhanced the adsorption capacity of palygorskite for Methyl violet from 156.05 to 218.11 mg/g, and the modification with sodium sulfide may enhance the adsorption capacity of palygorskite for methylene blue for MB from 129.71 mg/g

to 187.56 mg/g. It has also been confirmed that the high-pressure homogenization treatment associated with the hydrothermal process could improve the adsorption performance of palygorskite more effectively [299], and the presence of moderate amount of alkaline is favorable to the structure evaluation and performance improvement of palygorskite [300].

In the hydrothermal reaction process, the organic small molecules can be introduced to improve the adsorption performance further. Zhang et al. [301] introduced chloroacetic acid (CA) in the hydrothermal treatment process of palygorskite, and found that the modified palygorskite could almost completely remove MB in the 200 mg/L of MB solution with a removal ratio of 99.8%, while the removal ratio of raw palygorskite for MB is only 59.52%. Similarly, different types of organic acids [302] and glycine [303] have been introduced to enhance the adsorption capability of palygorskite for organic dyes or heavy metal Pb(II) ions.

Clay Minerals-Derived Porous Hybrid Adsorbents

Due to the complex geologic origin, it is difficult to obtain pure clay mineral in the nature. In other word, naturally available clay minerals are usually associated with one more other minerals [304]. The presence of the associated minerals limited the adsorption properties of natural clay minerals. In general, the separation or purification of clay minerals is costly and energy-consuming, which is not suitable for the large-scale industrial application. So, the comprehensive utilization of main minerals and associated minerals is desirable in both of academic or industrial applications. The simultaneous transformation of main mineral and associated minerals as new porous silicate adsorbent is an effective and feasible approach to fully utilize the clay minerals with complex components. It has been reported that palygorskite and associated minerals could be simultaneously transformed as mesoporous hybrid silicate adsorbents by a simple hydrothermal process in the presence of sodium silicate and metal salts. The mesoporous Zn-silicate adsorbent has been prepared by one-step hydrothermal process in the presence of sodium silicate and zinc sulfate [305], which shows the best adsorption capacities of 384 mg/g (only 154 mg/g for raw palygorskite) for aureomycin. Similarly, the mesoporous Mg-silicate adsorbent with spherical morphology and mesopores (Fig. 22) has been also prepared by hydrothermal process using low-grade brick-red palygorskite as the raw materials [306]. It has been confirmed that the palygorskite and associated minerals (Fig. 22a) were transformed as uniform spherical amorphous silicate adsorbent (Fig. 22e), which exhibits a large pore size of 37.74 nm and a high specific surface area of 489.81 m^2/g, and its maximum adsorption capabilities reached 407.95 mg/g and 397.22 mg/g for methylene blue (MB) and crystal violet (CV), respectively. Besides palygorskite, the hydrothermal synthesis method can also be used to prepare mesoporous adsorbent using other clay mineral as raw material, such as illite/smectite clay [307]. The resultant adsorbent shows high specific surface area of 363.52 m^2/g (about 8.7 folds higher than that of illite/smectite clay) and very negative Zeta potential (− 34.5 mV), and the optimal silicate adsorbent can adsorb 408.81 mg/g of chlortetracycline (only 159.7 mg/g for raw illite/smectite clay) and remove 99.3% (only 46.5% for raw illite/smectite clay) of chlortetracycline from 100 mg/L initial

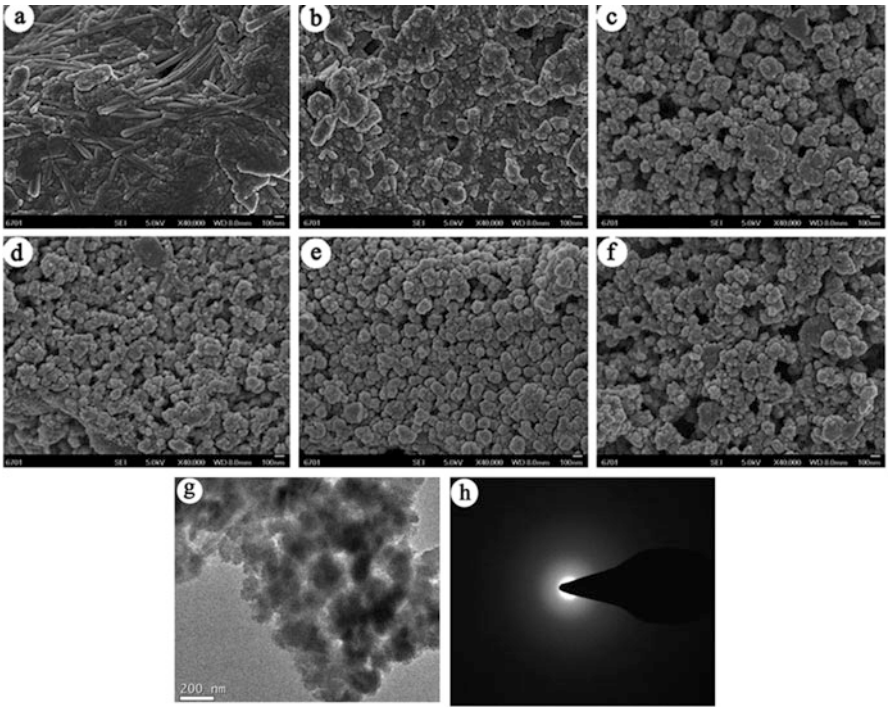

Fig. 22 SEM images of (**a**) RPAL and the adsorbents (**b**) SiMg-21-2, (**c**) SiMg-21-4, (**d**) SiMg-21-8, (**e**) SiMg-21-12, and (**f**) SiMg-21-24; and the (**g**) TEM image of SiMg-21-12 adsorbent, and the respective SAED pattern (**h**) (Reproduced with permission from Ref. [306])

solution (pH 3.51; adsorption temperature 30 °C; adsorbent dosage, 3 g/L). It has been confirmed that the introduction of the organic small molecules with functional groups (i.e., chloroacetic acid, glucine) during hydrothermal reaction process may promote the structure evolution of clay minerals and improve the adsorption performance of the adsorbent. Tian et al. [308] successfully prepared a mesoporous adsorbent by the one-step hydrothermal reaction in the presence of chloroacetic acid and found that the carboxyl groups were introduced onto the adsorbent, and the palygorskite and associated minerals have been converted to new hybrid silicate adsorbent with the specific surface area of 410.61 m^2/g, and the adsorption capacities of 329.84 mg/g for chlortetracycline and 207.47 mg/g for oxytetracycline, respectively. The simultaneous conversion of main mineral and associated minerals has provided an effective approach to utilize comprehensively low-grade clay minerals.

Clay Minerals/Carbon Composites

In recent years, carbon/clay minerals composites as new types of adsorbents have received much attention because they have the advantages of both clay minerals and carbon materials [309]. Many types of clay minerals including one-dimensional nanorods and two-dimensional nanosheets have been used to prepare the carbon/

clay minerals composites. The palygorskite/carbon composites were prepared by a hydrothermal process using different carbon sources, including glucose [310, 311] and cellulose [312], rich hull [313], and it has been confirmed that the composites show good adsorption capacity for cationic dyes and Pb(II) ions, and the generated carboxyl groups during reaction process mainly contribute to the improvement of adsorption capability. In addition, carbon/montmorillonite composites have also been prepared using glucose biomass and *d*-glucose monohydrate. It was found that the composite prepared using glucose biomass as carbon sources shows the maximum adsorption capacity of 194.2 mg/g [314], and the composite derived from *d*-glucose shows the maximum adsorption capacity of 20.76 mg/g at pH 3.95 toward U(VI), and the functional carbonaceous species on the composite improved its sorption capacity [315]. Wu et al. [316] studied the formation mechanism of the carbon/montmorillonite nanocomposite. It has been confirmed that proton-exchanged montmorillonite acted as a catalyst that could promote reactions in the hydrothermal condition, an adsorbent, and an inorganic template for the formation of carbon species. The nanocomposite was formed by two stages: (1) the hydrolysis of cellulose yielding degraded liquid products (e.g., glucose, fructose, and organic acids); second, the formed liquid products were adsorbed by montmorillonite, which catalyzed condensation and aromatization to form carbon particles on the surface of montmorillonite (Fig. 23).

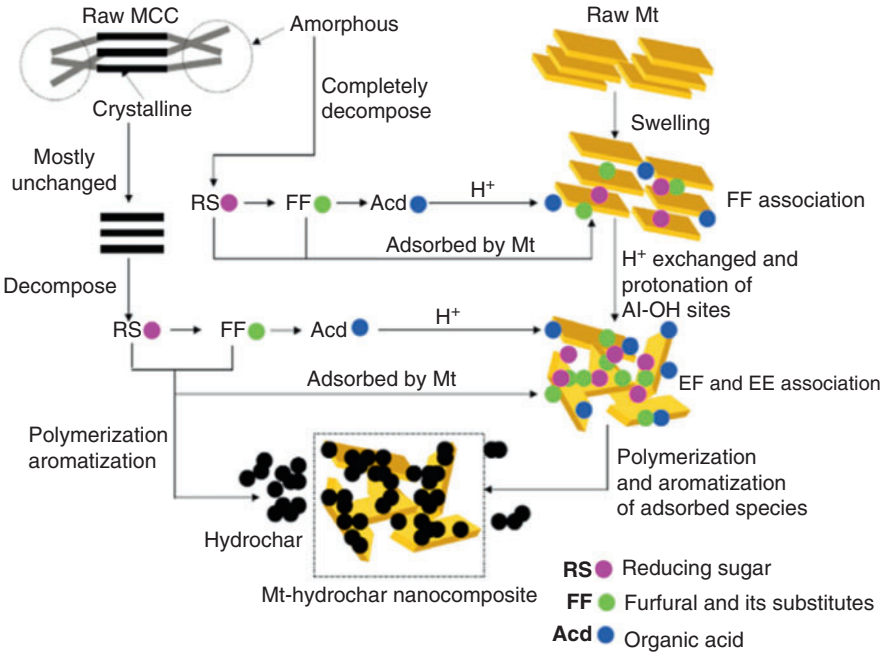

Fig. 23 Evolution of cellulose and mongmorillonite in the reaction of hydrothermal carbonization for formation of carbon/mongmorillonite nanocomposites (Reproduced with permission from Ref. [316])

In addition to small organic molecules, natural polymer has also been used as carbon sources to prepare carbon/clay minerals composite adsorbents. Tian et al. [317] prepared carbon/attapulgite composites using chitosan as carbon sources by a simple one-step calcinations process and used for the bleaching of palm oil. The natural and nontoxic chitosan was firstly self-assembled onto the surface of attapulgite by electrostatic interaction to form a precursor, and then the precursor was calcined at 280 °C to obtain the optimal adsorbent. The bleaching efficiency of the composite for palm oil was greatly improved after the introduction of carbon species. After bleached with the composites, the Red value and the content of peroxide and phospholipid decreased by 57.36%, 76.34%, and 43.11%, respectively; but the commercial bleaching earth can only decrease these values by 38.76%, 71.59%, and 10.15%, respectively.

It has been confirmed that the organic matters can be transformed into carbon species in the presence of clay minerals. This provides a new idea to recycle and reuse the waste clay minerals containing organic matters. Spent bleaching earth (SBE) is a solid waste generated during refining process of the edible oil after bleaching of crude oil, which is usually disposed in a landfill near the factory. SBE usually contains 20–40% by weight of the residual oil, oxidation products, free fatty acids fat, and phosphatides. It was desired that the solid waste can be converted to useful material by a simple approach, and great progress has been made over the past decades. Acid or acid-heating treatment methods have been employed to regenerate the SBE, and the new adsorbents with good adsorption performance has been obtained [318, 319]. Likewise, the salt-activation process was also used to regenerate the SBE [320]. In addition to acid treatment, the regeneration of SBE by a direct pyrolysis method to produce adsorbents has been widely concerned [321, 322]. In comparison with the calcination process, the hydrothermal treatment and SBE has been concerned in recent years, and many carbon/clay composite adsorbents have been prepared [323], and the adsorbent shows the maximum adsorption capacities of t 199.99 mg/g and 166.64 mg/g toward brilliant green and Pb(II), respectively. In order to make the regenerated adsorbent easy to be separated from the solution, the SBE was functionalized with Fe_3O_4 by an in situ hydrothermal process [324]. It has been revealed that the adsorbent can rapidly adsorb methylene blue and Pb(II) with the capacities of 254.83 mg/g and 312.73 mg/g, respectively. In order to further improve the adsorption performance, the calcined SBE was usually activated with zinc chloride [325] and surfactant [326]. Besides, the oil in SBE can also be extracted [327] or reused to produce biodiesel [328, 329], lubricating grease [330], and bricks [331].

However, the clay mineral adsorbents become solid waste after adsorption of dyes, not only by polluting the environment but also by causing a huge waste of resources. In order to take full advantage of these waste dye adsorbents, the spent dye-loaded palygorskite was further treated by a hydrothermal process in the presence of Ag^+ ion to prepare a multifunctional nanocomposite [332]. In this process, the dye adsorbed on palygorskite was oxidized as carbon species, and simultaneously Ag^+ was reduced as Ag^0 nanoparticles. The presence of carbon makes the nanocomposite having very good adsorption properties, and the presence

of Ag^0 nanoparticles makes the complex having catalytic activity. The adsorbent can remove 99.2% of methylene blue (MB), 86.9% of methyl violet (MV), 68.7% of chlortetracycline hydrochloride (CTC), and 46.2% of tetracyclines (TC) from 100 mg/L of the aqueous solution at the adsorbent dosage of 0.5 g/L. The nanocomposites could rapidly catalyze the conversion of 4-nitrophenol (4-NP) to 4-aminophenol (4-AP) within 6.5 min with a catalytic rate constant of 0.0120 s^{-1}. This opens a new avenue for the highly efficient utilization of dye-loaded adsorbent.

Three-Dimensional Network Adsorbents

In recent years, the design and development of adsorbents with three-dimensional network structure have become the subject of great interest in both academic and industry because such adsorbents have better adsorption capacity and faster adsorption rate than the conventional adsorbents, such as clay minerals and activated carbon [333–335]. The special three-dimensional polymer network could slightly swell and expand the network size, which reduces the mass transfer resistance during adsorption process and enhances the adsorption rate. In addition, large number of functional groups in the network enables the adsorbent to adsorb pollutants with high capacity [336]. More importantly, the type and number of functional groups could be controlled by altering the monomers or polymerization condition, so that through the molecular design, different functional groups can be introduced in the hydrogel, and the use of hydrogel with the intelligent response could achieve the selective adsorption of pollutants in water. Compared with other adsorbents, hydrogel adsorbents have the advantages of fast adsorption speed, high adsorption capacity, easy separation, and regeneration. It is a kind of new adsorbent material which is environment friendly and sustainably developed. It is divided into three categories: natural polymer hydrogel, synthetic polymer hydrogel, and composite hydrogel. Natural polymer hydrogels are mainly formed by graft polymerization of hydrophilic natural polysaccharides. The synthetic hydrogels are formed by copolymerization of hydrophilic monomers, such as acrylic acid, acrylamide, and acrylonitrile; and the composite hydrogels are formed by introducing inorganic components such as clay minerals into the polymer network.

Three-dimensional network adsorbent has higher adsorption capacity, fast adsorption rate, and better regeneration properties. The conventional adsorbent prepared by solution polymerization is a bulk gel product, which requires much energy to be dried or prilled. Wang's groups firstly synthesized granular 3D network adsorbent using solution polymerization [333, 337], which can be directly used in practice with no need of prilling. It has been proved that the disaggregation of palygorskite crystal bundles is extremely important to fabricate a uniform granular 3D network adsorbent. Zheng et al. [338] synthesized a granular chitosan-*g*-poly (acrylic acid-*co*-itaconic acid)/palygorskite adsorbent by one-step solution polymerization at room temperature and air atmosphere. The introduction of palygorskite nanorods may increase the adsorption rate and improve the network strength of the as-prepared adsorbent. The nanocomposite adsorbent shows extremely higher adsorption capacity of the dye malachite green (2433 mg/g) and excellent adsorption selectivity to cationic dyes in the binary mixture solution of dyes. After years of

development, different types of three-dimensional network adsorbents have been developed (Table 1), showing excellent adsorption properties for different types of pollutants, and have shown very good application prospects in wastewater treatment and environmental remediation.

Table 1 Comparison of adsorption capacities of different 3D network adsorbents

Adsorbents	Clay content (%)	Adsorbates	Initial concentration (mg/L)	Adsorption capacities (mg/g)	Ref.
PAM-AA/MMT	50	Fe(III)	1120	159.04	[339]
SA-g-P(AA-co-AMPS)/APT	5	Pb(II)	150	1016.77	[340]
SA-g-P(AA-co-AMPS)/APT	5	Cd(II)	150	79.38	[340]
SA-g-P(AA-co-AMPS)/APT	5	Cu(II)	150	406.71	[340]
SA-g-P(AA-co-AMPS)/APT	5	Zn(II)	150	294.86	[340]
PAA/MMT	9	Pb(II)	100	1666.67	[341]
PAA/MMT	9	Ni(II)	100	270.27	[341]
PAA/MMT	9	Cd(II)	100	416.67	[341]
PAA/MMT	9	Cu(II)	100	222.22	[341]
PAA/TM/PVA	20	Pb(II)	1280	645.84	[342]
PAA/TM/PVA	20	Cu(II)	4140	190.72	[342]
S-g-AA/MMT	5	Cu(II)	512	131.84	[343]
S-g-AA/MMT	5	Pb(II)	1656	346.02	[343]
OB-Fe_3O_4 PSA	30	Th(IV)	–	1519.84	[344]
AAm-AMPS/MMT	10	Cu(II)	256	68.48	[345]
AAm-AMPS/MMT	10	Cd(II)	449.64	143.89	[345]
AAm-AMPS/MMT	10	Pb(II)	828.48	213.42	[345]
PAM/PA	76.9	Hg(II)	350	135.5	[346]
PAM/APT	30	Cu(II)	453.12	115.85	[347]
CTS-g-PAA/SH/APT	21.71	Pb(II)	1500	718.5	[348]
PE-g-PAA-co-starch/ OMMT	5.8	Pb(II)	500	430	[349]
CTS-*g*-PAA/APT	10	Cu(II)	1220	241.33	[337]
CTS-g-PMAA/Bent	10	U(VI)	100	117.2	[350]
PMAA-g-Cell/Bent	12	Th(IV)	100	45.75	[351]
CMC-g-PAA/APT	5	Pb(II)	4500	941.28	[352]
CMC-g-PAA/APT	30	Pb(II)	4500	737.15	[352]
ATP/PAA	14.28	Pb(II)	104.22	38.95	[353]
ATP/P(AA-co-AM)	14.28	Cu(II)	200	69.75	[354]
Org-ATP/PAA	25	Pb(II)	100	42.32	[355]
PAA/BT	30	NH_4^+-N	100	32.87	[356]
CTS-g-PAA/APT	20	NH_4^+-N	100	21	[357]
CTS-g-PAA/REC	10	NH_4^+-N	100	40.61	[358]
CTS-g-PAA/UVMT	40	NH_4^+-N	100	21.7	[359]
PAAM-IANa/MMT	3	BCB	500	457.4	[360]
PAAm/Lap	30	CV	30	40	[361]

(*continued*)

Table 1 (continued)

Adsorbents	Clay content (%)	Adsorbates	Initial concentration (mg/L)	Adsorption capacities (mg/g)	Ref.
PAA-co-2-DRAEMA/MMT	5	Indigo carmine	–	319.34	[362]
Poly(AA-co-AM)/APT	10	MV	1000	1194	[363]
PAM/SH/Lap	2	MB	–	800	[364]
PAA-co-VP/Lap	2	CV	4	0.2953	[365]
CTS-g-PAA/VMT	10	MB	1000	1612.32	[366]
NaAlg-g-p(AA-co-St)/ organo-I/S	2.5	MB	1000	1843.46	[170]
SA/Na^{+}REC	2	Basic Blue 9	500	493	[367]
CTS-*g*-PAA/BT	10	MB	1150	2125.70	[368]
CTS-g-AA–IA/APT	5	MG	1000	2433	[338]
LCL-g-PAA/MMT	20	MB	2500	1994.38	[369]

Superabsorbent Composites

Superabsorbent is a new type of functional polymer material with a special three-dimensional network structure, excellent water absorption, and water retention capability [370]. It can quickly absorb water with hundreds of times or even thousands of times its weight. Compared with traditional absorbent materials such as sponge, paper, cotton, towels, and silica gel, the superabsorbent resin exhibited more excellent performance and wider application prospects. It has become an indispensable product in human daily life and national economy. The application of superabsorbent resins in physical hygiene and agroforestry is the main research areas. With the global climate is warming, the drought caused by regional vegetation damage and lack of water caused desertification of land. So, to develop a new type of water-saving materials with high water absorption and retention, salt tolerance, low cost, and environment-friendly superabsorbent have become particularly important and increasingly urgent. However, the currently used superabsorbent resin is mainly neat organic synthetic polymer, which is costly, poor in salt tolerance, and environmental unfavorable. In order to improve the environmental friendliness of the superabsorbent, natural macromolecules, cellulose, and chitosan have been introduced into the superabsorbent resin as a matrix, but natural polymers have little contribution to improve the salt-resistant properties.

The introduction of inorganic materials into the organic superabsorbent network to form organic-inorganic superabsorbent composite has become an ideal strategy and preferred method because such materials exhibited better water-absorbing capability and rate, salt-resistance, and gel strength than the pristine organic superabsorbent [371]. Meanwhile, the production cost can also be reduced due to the addition of cheap inorganic materials, which are favorable to the industrialization of superabsorbent. The inorganic matters that can compound with SAM can be divided

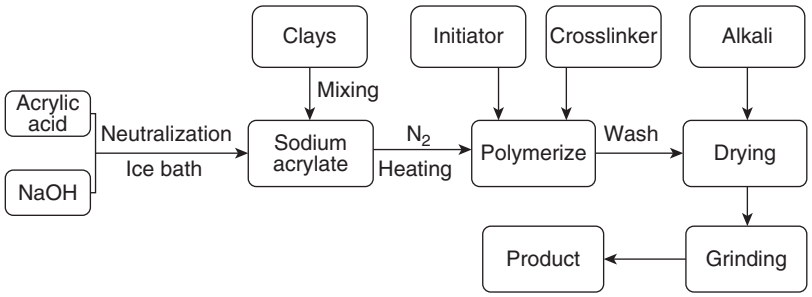

Fig. 24 Preparation flowchart of poly(sodium acrylate)/clay superabsorbent composites

into two classes: (1) inorganic hydrogels such as aluminium, iron, tin, titanium, silicon, and chromium gel; (2) inorganic clay minerals such as kaolin, bentonite, sericite, attapulgite, rectorite, vermiculite, and diatomite. Usually, the inorganic hydrogels or minerals have good salt-resistant properties and the introduction of inorganic matter can improve the salt-resistant property of the organic superabsorbents [372, 373]. Because inorganic minerals are low cost, easy to be deep-processed and compounded with organic monomers or polymer, a superabsorbent composite based on organic minerals has been extensively studied throughout the world in recent years.

Synthetic Polymers/Clay Minerals Superabsorbent Composites

A superabsorbent is a polymer material that can absorb and reserve large volumes of aqueous fluids owing to its unique 3D hydrophilic network, even under pressure. Since the first superabsorbent material has been reported by the US Department of Agriculture [374], the research and development of superabsorbent material has caused great global concerns, and the products were widely used in many fields, such as disposable diapers, agriculture, food packaging, artificial snow, biomedicines, healthcare, and agriculture [375]. The most commonly used method for preparing organic-inorganic superabsorbent composite is solution polymerization. Figure 24 depicted the production process of the popular poly(sodium acrylate)/clay superabsorbent composites. By using the similar procedure, a lot of superabsorbent composites derived from various organic polymers and inorganic minerals have been prepared and evaluated. The comparison of the water absorbency of different superabsorbent composites are listed in Table 2, which comprehensively summarized the synthetic polymers/clay minerals superabsorbent composites reported in literature.

Natural Polymer-Based Superabsorbent Composites

Because of the advantages over conventional absorbents (e.g., sponge, cotton, towel, and colloidal silica), superabsorbents have attracted unwavering attention and found extensive application in various fields, such as agriculture, hygienic products, wastewater treatment, catalyst supports, and drug delivery systems. With the

Table 2 Comparison of the water absorbency of different superabsorbent composites

Superabsorbent	Clay content (%)	Swelling medium	Water absorbency (g/g)	Ref.
PAA/APT	5	Distiled water	1325	[376]
PAA/APT	5	0.9% NaCl solution	117	[376]
PAA/APT	10	Distiled water	1017	[376]
PAA/APT	10	0.9% NaCl solution	77	[376]
PAA/DTM	10	0.9% NaCl solution	99	[377]
PNaA/MMT	2	Distiled water	452	[378]
PSSNa/MMT	2.5	Distiled water	178	[379]
PAM/HAPT	10	Distiled water	1964	[380]
PAM/AAPT	10	Distiled water	1469	[380]
PAA/IMMT	5	Distiled water	198	[381]
PAA/ST	5	Distiled water	1419	[382]
PAA-MAA/MMT	4.76	Distiled water	532	[383]
Poly(AA-co-AM)/HNTs	10	Distiled water	1276	[384]
PAA-AAm–HNT–GO	0.1	Distiled water	743.9	[385]
PAA-co-AM/KAO	10	Distiled water	433	[386]
PAA-co-AM/KAO	10	0.9% NaCl solution	108	[386]
PAA-co-PAM/CloisiteVR 30B	2	Distiled water	80	[387]
Poly(AA–AM)/ DMAEA–DB–MMT	10	Distiled water	1100	[388]
Poly(AA–AM/ CTAB–MMT)	10	Distiled water	875	[388]
PAA-AM/BT	4	Distiled water	1246	[389]
PAA-AM-IA/MT	15	Distiled water	1218	[390]
PAA-Am/EVMT	50	Distiled water	850	[391]
PAM-PVA/Cloisite	2	Distiled water	56.25	[392]
PAM-IA/Mica	5	Distiled water	748	[393]
P(AA-co-AMPS)/APT	8.76	0.9% NaCl solution	47 g/g	[394]
PE-g-PAA/KAO	5	Distiled water	760	[395]

increasing importance of resource and environment issues, new types of natural superabsorbents have attracted considerable attention owing to their renewability, nontoxicity, biocompatibility, and biodegradability; the organic-inorganic superabsorbent composites, derived from a natural polysaccharide and inorganic clay minerals, are representative families of natural superabsorbents. Many natural superabsorbent composites based on starch, cellulose, chitosan, gelatin, dextrin, and alginate have been developed, and the resultant materials exhibited satisfactory properties and environmental-friendly characteristics. Aqueous solution

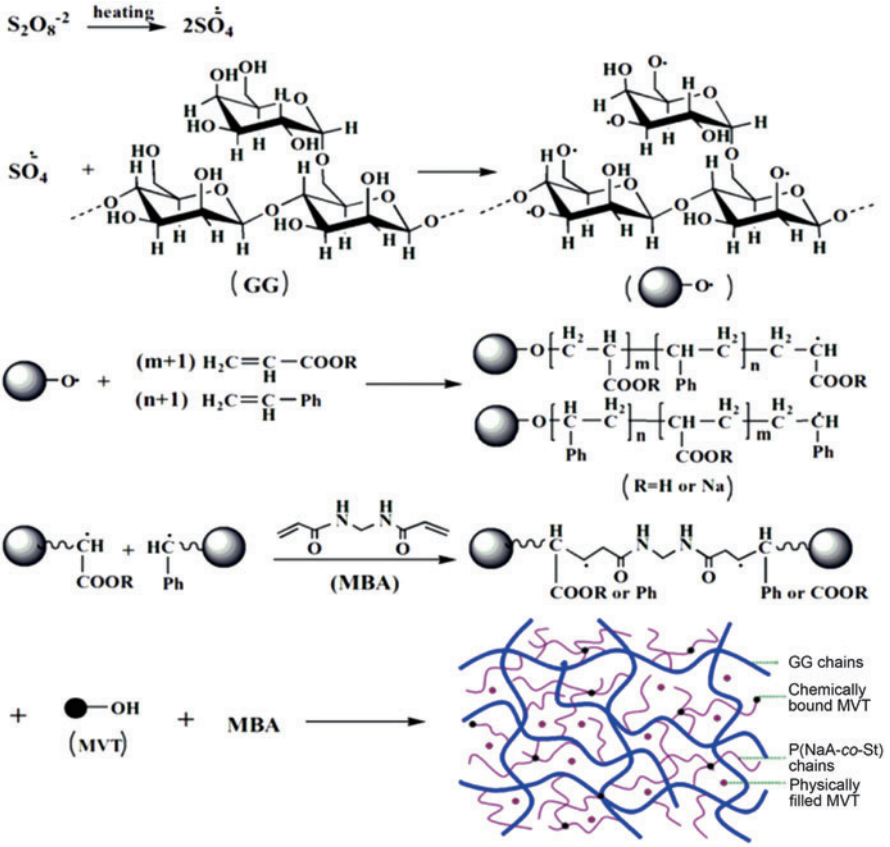

Fig. 25 Proposed grafting and composite mechanism of guar gum-*g*-poly(sodium acrylate-*co*-styrene)/muscovite superabsorbent [396]

polymerization as a commonly recognized green polymerization method has been frequently used to prepare superabsorbent composites based on natural polymer and clay minerals. Figure 25 shows the typical preparation procedure of a guar gum-g-poly(sodium acrylate-co-styrene)/muscovite superabsorbent composite by grafting polymerization reaction. At the initial step, the initiator ammonium persulfide was decomposed under heating to generate a high concentration of sulfate anion radicals. Subsequently, these radicals stripped down the hydrogen from the –OH groups of guar gum and formed macroradicals. These macroradicals can act as the active sites during the reaction and can initiate vinyl groups of monomers to process chain propagation. During the chain propagation, the crosslinker N,N′-methylene-bisacrylamide with double vinyl groups takes part in the polymerization reaction, whereas muscovite combined with a polymeric network through its reactive silanol groups makes the copolymer to form a crosslinked network structure.

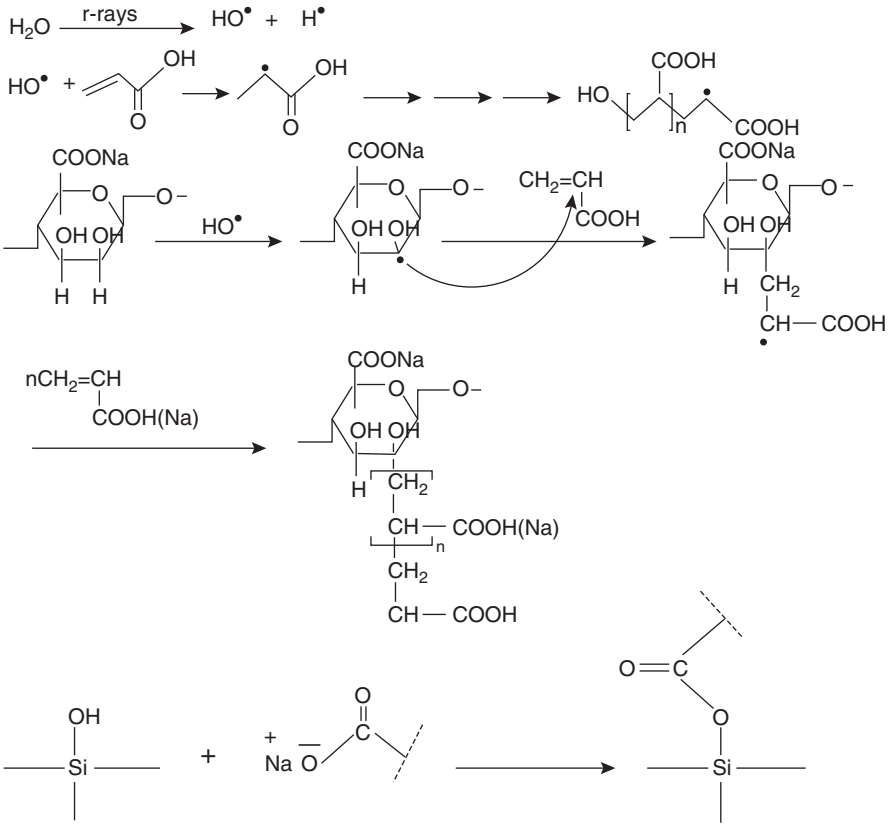

Fig. 26 Scheme of graft-copolymerization of sodium alginate, acrylic acid and Na^+-rectorite [397]

Graft copolymerization of polyacrylic acid (PAA) onto the backbone of natural polymers can also be achieved via ^{60}Co γ-radiation. The mechanism for polymerization process is showed in Fig. 26. First, most of the irradiation energy is absorbed by the water to produce hydroxyl radicals. Initiation occurs mainly by an indirect effect. Second, hydroxyl radical was added to one side of the acrylic acid double bond leading to the formation of an unpaired spin on the other side of a vinyl bond, then homopolymerization of acrylic acid started. At the same time, the hydroxyl radical attacks sodium alginate leading to the breakage of C–H bond to form alginate-based radical, then it will react with an acrylic acid molecule, followed by propagation leading to the growth of a branched chain, following the network was formed via crosslinking. In addition, the carboxylate groups of the grafted poly (acrylic acid) can react with the –OH groups on the Na^+-rectorite surface to produce ester. These reactions should lead to the formation of polyacrylic acid grafted onto sodium alginate and Na^+-rectorite.

Intercalation polymerization has also been widely used for the preparation of chitosan (CTS)-based superabsorbent nanocomposite. In this process, a part of

protonated CTS chains containing the radicals, generated on CTS under the existence of initiator, intercalate into MMT layers and lead to an increase in the *d*-spacing. Subsequently, these radicals initiate the graft copolymerization of the adsorbed AAm molecules into the clay interlayer spaces, where the growth of PAAm chains provokes the exfoliation of MMT sheets [398]. The most probable formation process of CTS-g-PAAm/MMT superabsorbent composite was illustrated in Fig. 27.

In recent years, a large number of environmental friendly superabsorbent resin was developed through the use of different natural polymers, different clay minerals, or different polymerization methods, which show a better water absorption and environmental friendliness. Table 3 listed the water absorption capacities of different types of superabsorbent composites.

Among numerous natural polymers, chitosan is the only cationic polysaccharide with amine groups, so it can form stronger hydrogen-bonding interaction with the in situ formed poly(acrylic acid) chains. In the presence of crosslinker, the chitosan-g-poly(acrylic acid) polymer may entangle together to form a granular product, and the introduction of attapulgite makes the granular product easy to be formed (Fig. 28) [419]. This is the first report about the preparation of granular superabsorbent materials by aqueous solution polymerization reaction, which opens a new avenue to prepare new granular superabsorbent by one-step reaction.

Multifunctional Superabsorbent Composites

As a water-saving and water-retention materials for agroforestry application, it has been expected that the materials can also slowly release functional components such as fertilizer or pesticides. Among numerous organic-organic superabsorbent polymers, the superabsorbent containing sodium humate is an important family. Sodium humate is composed of multifunctional aliphatic and aromatic components and contains large numbers of functional hydrophilic groups such as carboxylates and phenolic hydroxyls [438]. Sodium humate can regulate plant growth, accelerate root development, improve soil cluster structures, and improve the absorption of nutrient elements. It can participate in polymerization with superabsorbent polymer network through its active –OH or –COOH groups. The simultaneous introduction of sodium humate and clay minerals can improve the water absorbency, reduce the production cost, and make the superabsorbent having fertilizer-release function. The preparation procedure is very simple and is similar that of clay-based superabsorbent, and the sodium humate powder can be directly added to the reaction system without further treatment. So far, several research were carried out for preparing superabsorbent containing sodium humate (Table 4). With the increasing attention to the utilization of naturally occurred resource as a substitute for the petroleum-based polymer, the composite of superabsorbent network with other fillers, including clay and sodium humate, will be a promising research field.

The SH in the superabsorbent can be slowly released when the superabsorbent composite was contacted with water. As shown in Fig. 29, the external solution became brown-black, and became more and more opaque with prolonging the contact time, which confirmed the release of SH from superabsorbent into the

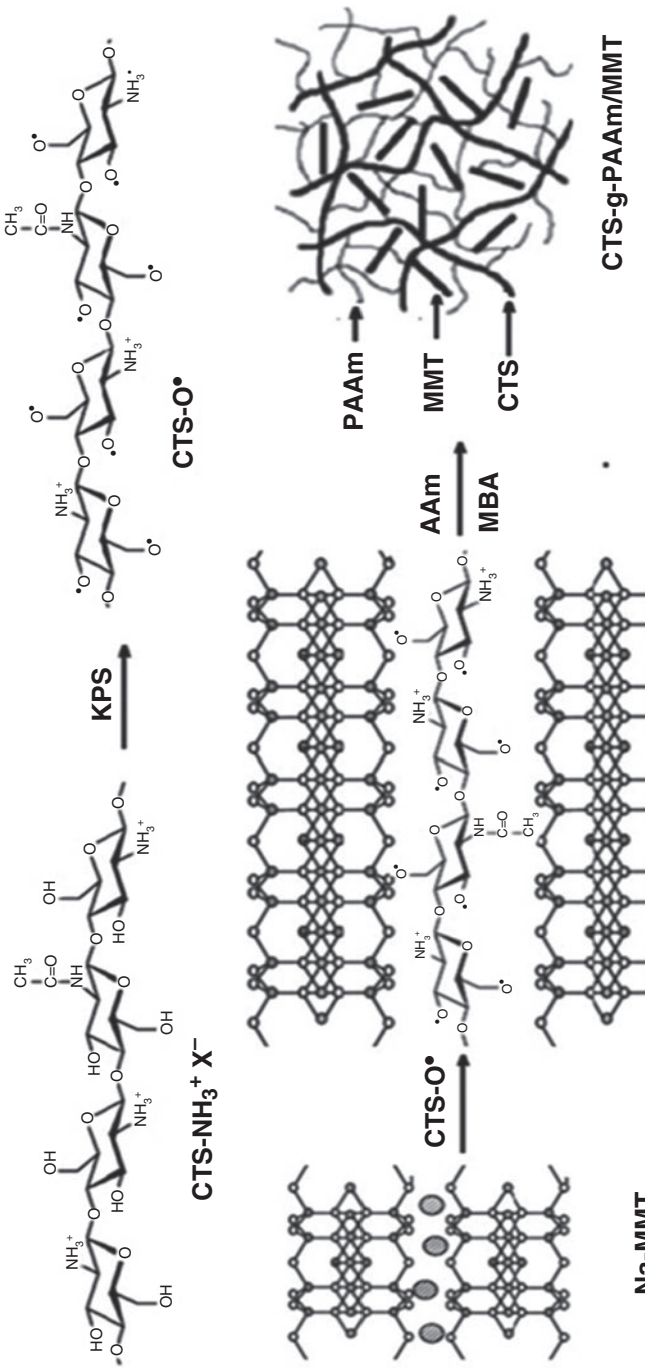

Fig. 27 Formation mechanism of CTS-g-PAAm/MMT superabsorbent composite [398]

Table 3 Comparison of the water absorbency of different natural polymer-based superabsorbents

Superabsorbents	Clay content (%)	Swelling medium	Water absorbency (g/g)	Ref.
St-g-PAA/zeolite	10	Distilled water	410	[399]
St-g-PAA/O-zeolite	10	0.12 mol/L of urea solution	530.3	[400]
St-g-PAM/KAO	13	Distilled water	4000	[401]
St-g-PAM/APT	10	Distilled water	1317	[402]
St-g-PAM/APT	10	0.9% NaCl solution	68	[402]
St-g-PAM-AA/MMT	8	Distilled water	1120	[403]
St-g-PAM-AA/MMT	8	0.9% NaCl solution	128	[403]
P-St-AM/APT	10	Distilled water	1268	[404]
GG-g-PAA/cloisite	10	Distilled water	134.81	[405]
GG-g-P(NaA-co-St)/APT	10	Distilled water	530	[406]
GG-g-P(NaA-co-St)/APT	10	0.9% NaCl solution	65	[406]
GG-g-P(NaA-co-St)/MVT	5	Distilled water	598	[396]
GG-g-P(NaA-co-St)/MVT	5	0.9% NaCl solution	59	[396]
GG-g-PNaA/CTA^{+}-REC	10	Distilled water	601	[203]
GG-g-PAA/MS	10	Distilled water	632	[407]
Alginate-g-PAMPS/MMT	–	Distilled water	3465	[408]
NaAlg-g-PNaA/APT	20	Distilled water	685	[409]
NaAlg-g-poly(NaA-co-NaSS)/APT	10	Distilled water	532	[410]
NaAlg-g-PAA/KAO	–	Distilled water	308	[411]
St-g-PAM/KAO	20	Distilled water	4000	[412]
SA-g-AA/Na^{+}REC	–	Distilled water	641	[413]
NaAlg-g-poly(NaA-co-St)/APT	10	Distilled water	587	[414]
NaAlg-g-poly(NaA-co-St)/APT	10	0.9% NaCl solution	73	[414]
NaAlg-g-p(AA-co-St)/I/S	2.5	Distilled water	810	[415]
NaAlg-g-PAA/O-loess	10	Distilled water	656	[416]
NaAlg-g-PAA/O-loess	10	0.9% NaCl solution	69	[416]
Dextrin-graft-AA/Na-MMT	5	Distilled water	1241.1	[417]
COL-g-PAA-co-AM/MMT	6.97	Distilled water	952.2	[418]
CTS-g-PAA/APT	2.5	Distilled water	159.6	[419]
CTS-g-PAA/APT	2.5	0.9% NaCl solution	42.3	[419]
CTS-g-PAA/kaolin	2	Distilled water	385	[420]
CTS-g-PAA/NONT	10	Distilled water	433	[421]
CTS-g-PAA/MMT	11.04	Distilled water	160.1	[422]
CTS-g-PAA/MMT	11.04	0.9% NaCl solution	46.6	[422]
CTS-g-PAA/OREC	10	Distilled water	265.2	[423]
CTS-g-PAAm /MMT	5	Distilled water	450	[424]
CTS-g-PAA/VMT	5	Distilled water	223.3	[425]
CTS-g-PAA/VMT	5	0.9% NaCl solution	51	[425]

(*continued*)

Table 3 (continued)

Superabsorbents	Clay content (%)	Swelling medium	Water absorbency (g/g)	Ref.
PSY-g-PAA/APT	10	Distilled water	568	[426]
PSY-g-PAA/APT	10	0.9% NaCl solution	64	[426]
HEC-g-PAA/VMT	10	Distilled water	575	[427]
HEC-g-PAA/diatomite	6	Distilled water	1174.85	[428]
HEC-g-PAA/diatomite	6	0.9% NaCl solution	99.55	[428]
SS-g-PAA/APT	12	Distilled water	1236	[429]
SS-g-PAA/APT	12	0.9% NaCl solution	108	[429]
PAA/CMC-mMMT	3	Distilled water	844	[430]
PL-g-P(AA-AM)/OMMT	5	Distilled water	773	[431]
PL-g-P(AA-AM)/OMMT	5	0.9% NaCl solution	68	[431]
PULL/PVA/MMT	5	Distilled water	143.42	[432]
PULL/PVA/MMT	5	0.9% NaCl solution	39.75	[432]
CMC-g-poly(AA-co-AM-co-AMPS)/MMT	–	Distilled water	680.2	[433]
CMC-g-poly(AA-co-AM-co-AMPS)/MMT	–	0.6% NaCl solution	193.4	[433]
CMC-*g*–PNaA/APT	10	Distilledd water	614	[434]
CMC-g-PAA/MS	20	Distilled water	634	[435]
CMC-g-PAA/REC	5	Distilled water	599	[436]
HEC-g-PAA/MS	10	Distilled water	810	[437]

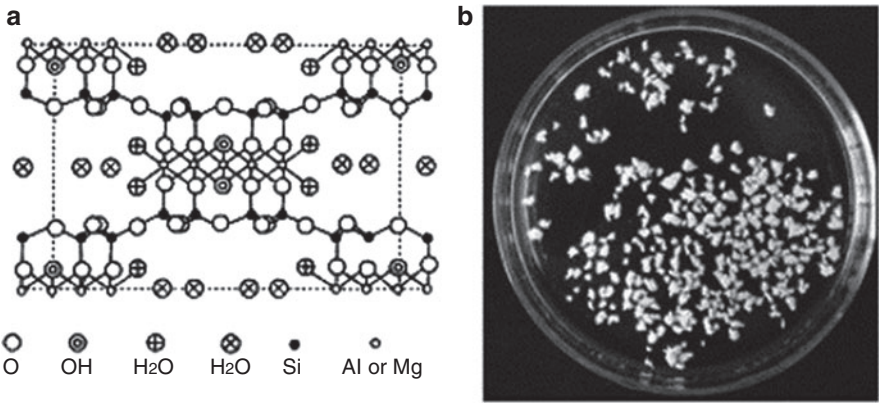

Fig. 28 Structure of attapulgite and the granular shape of chitosan-g-poly(acrylic acid)/attapulgite [419]

external solution. The variation of carbon content in solution was determined to study the slow-release character of SH (Fig. 29d). It is obvious that the carbon content increased with increasing swelling time at initial stage and tends to be

Table 4 Comparison of the water absorbent of the multifunctional superabsorbent composites

Superabsorbent	Clay content (%)	Swelling Medium	Water absorbency (g/g)	Ref.
PAA/APT/SH	20	Distilled water	583	[438]
PAA/APT/SH	20	0.9% NaCl solution	63	[438]
PAA-AM/O-MMT/SH	20	Distilled water	591	[439]
PAM/Lap/SH	1.95	Distilled water	600	[440]
PAA-AM/SH/APT	10	Distilled water	996	[441]
PAA-AM/SH/APT	10	0.9% NaCl solution	63	[441]
PAA-AM/O-APT/SH	10	Distilled water	1282	[442]
PAA-AM/O-APT/SH	10	0.9% NaCl solution	68	[442]
PAA-AM/Ca-MMT/SH	20	Distilled water	641	[443]
PAA-AM/Li-MMT/SH	20	Distilled water	723	[444]
PAA-AM/Na-MMT/SH	20	Distilled water	638	[444]
PAA-AM/Al-MMT/SH	20	Distilled water	363	[444]
PAM/SH/LAP	2	Distilled water	600	[445]
NaAlg-g-poly(AA-co-AAm)/MMT	15	Distilled water	460.02	[446]
kC-g-PAA/Celite	2.5	Distilled water	344	[447]
CMWS-g-PAA/APT	14	Distilled water	186	[448]

constant after 50 days, indicating the release of SH reached equilibrium. In this process, the physical filled SH can be rapidly released, while the chemically bonded SH slowly released with prolonging the swelling time [449]. This observation indicated that the introduction of SH endowed the superabsorbent composite with the slow-release function of fertilizers.

The superabsorbent composite with fertilizer-release function also shows better practical water retention capability in sand soil [439]. The water content in sand soil decreased as prolonged time, and the addition of PAA-AM/O-MMT/SH superabsorbent composite obviously improved the water retention capacity of sand soil. After 20 days, the water content in the blank sample was only 0.4 wt %, whereas the water content in sand soil still reach 3.8, 21.7, or 35.2 wt% after adding 0.1, 0.5, or 1.0 wt% of PAA-AM/O-MMT/SH composite, respectively. Even after 30 days, 24.4 wt% of the water was still retained in the sand soil after adding 1.0 wt % of superabsorbent composite, indicating that the superabsorbent composite can enhance the water retention capacity of sand soil greatly.

Ni et al. [450] developed multifunctional slow-release organic − inorganic compound fertilizer (MSOF) and evaluated its water-holding capacity of soil. It was concluded that the water-holding capacity of soil is 43.5, 47.5, 50.1, and 53.7% for MSOF application rate of 0, 1, 2, and 3%, respectively. The water-holding capacity of the soil increases with increasing the dosage of MSOF. In soil, the MSOF granules were surrounded by soil particles and subjected to a confining pressure by these

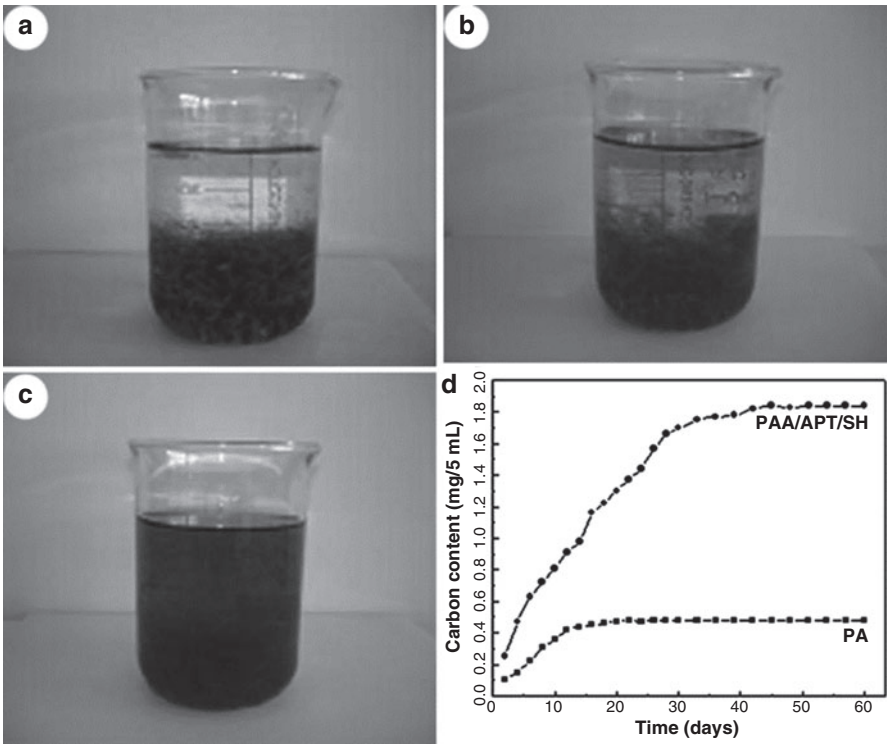

Fig. 29 (**a**-**c**) Digital photos of the superabsorbent composite after slow release and (**d**) the variation of carbon content as a function of swelling time (Redrawn according to [438])

particles [451], which limited the swelling degree of the superabsorbents in soil, but the MSOF still effectively improve the water-holding capacity of soil, even though at low application rate. In addition, the MSOF can slowly release nitrogen (total content of 11.7%), potassium (total content of K_2O is 8.7%), and phosphorus (total P_2O_5 content of 10.3%) to provide nutrient for plant growth, which would be the future development in agricultural fields.

Environment-Friendly Catalytic Materials

Nanoclays with different morphology, composition, and surface activity can serve as the carrier of active species to fabricate functional nanocomposite, which opens a new avenue to fabricate new type of ecofriendly catalysts. The nanorod-like, fibrous, or sheet-like carriers may restrain the aggregation of active particles and allow the small-size nanoparticles to be formed on the carrier, which greatly increased the contact area of catalyst with the reactants and promoted to the proceeding of catalysis reaction. Many active components, e.g., noble metals, transition metals, semiconductor, and solid acid, have been loaded on palygorskite, sepiolite, or other layered clay minerals to prepare a variety of catalysts [452, 453]. The disaggregated palygorskite was

adopted to prepare the Pal/Fe_3O_4/AuNPs catalyst [454] and Pal/AgNPs [455] nanocomposite catalyst by a facile in situ reaction approach. The nanocomposite shows higher catalytic activity for decoloration of Congo red. The palygorskite shows better dispersion and the AgNPs have a uniform distribution on the surface of palygorskite. Mu and Wang [456] prepared the Pal/Fe_3O_4/polyaniline nanocomposite using high-pressure homogenized Pal and used as a carrier to fabricate Pal/Fe_3O_4/polyaniline/AuNPs nanocomposite catalyst, and the desirable catalytic activity for reduction of 4-nitrophenol was obtained. With the increasing industrial requirement to highly active and ecofriendly catalyst, the nanoscale palygorskite will show a great prospect to fabricate new-type nanocomposite catalysts.

Ecofriendly Hybrid Pigments

Pigments provide a colorful world for mankind and are indispensable materials for promosiing social development. However, the organic pigment is not stable enough, and the inorganic pigment is not bright in color. In addition, most of chemical pigments are toxic and hazardous to environment and health. So, the development of ecofriendly pigments with excellent stability and bright color become the hot topic in recent years. Maya blue, an organic-inorganic hybrid pigment, has bright color and superior stability, which does not fade even though it was exposed to the external environment for more than thousands of years [457]. Numerous research confirm that palygorskite is the irreplaceable carrier to prepare a stable Maya blue hybrid pigment. In the preparation procedure, the grinding process is fundamental to achieve a uniform dispersion of dye and better stability [458–460]. The grinding process may disperse the crystal bundles, release more pores, and intensify the interaction between dye and palygorskite, which may promote dye molecules to enter the tunnel, and thus the dispersion of the hybrid materials was improved. The contribution of grinding to the dispersion of crystal bundles causes the increase of specific surface area and the change of surface activity, which are all favorable to the loading of dyes. We have studied the effect of grinding time and the water content during grinding on the stability of the methylene blue/palygorskite hybrid [461]. It was confirmed that grinding time plays a key role in the formation of a stable hybrid structure, because it greatly influenced the dispersion of palygorskite crystal bundles and the interaction between MB molecules and palygorskite. The aggregates of palygorskite rods were highly dispersed as individual nanorods after being ground for 30 min, and the MB molecules are more easily to be adsorbed on the palygorskite nanorod or encapsulated in its tunnels, so the thermal stability, acidity, and UV-light resistance of the nanocomposites were enhanced, which are consistent with previous report [462]. The optimal water content during grinding is 36.9%. These researches confirm that the nanoscale dispersion of palygorskite will be helpful to fabricate a stable inorganic "host" framework that is suitable for holding a "guest" molecule into the channels.

Inorganic pigments have recently received more and more attention because of their excellent heat-resistant properties and stability. The utilization of clay minerals for the fabrication of inorganic–inorganic composite pigments can not only reduce the

production cost greatly but also improve the color performance of pigment. The series of cobalt blue/clays hybrid pigments have been developed by Wang's groups [463, 464] by in situ precipitation and crystallization process. It was found that the composite pigment can still show good blue color and excellent stability even the content of clay minerals are higher than 50%, which greatly reduce the production cost and improve the ecofriendly properties. The pigments can be dispersed and suspended in aqueous solution well, which makes it available for aqueous coatings. The iron red/clays hybrid pigments were also prepared by a one-step hydrothermal process using sepiolite [87], halloysite [87], and attapulgite [66] as the green inorganic precipitant. The pigment shows the red color that is superior to commercial iron red pigment and is highly stable in resisting acid, alkaline, heat, solvents, and UV lights. These research pave a solid foundation to develop new types of ecofriendly hybrid pigments for the applications in coating, paints, ink, plastic, and others.

Packing Materials

With the development and progress of society, the protection of human survival environment has received more and more attention, so that the development of ecofriendly materials and their replacement for traditional plastic products become an inevitable trend. In the daily use of polymer materials, packaging materials accounted for a considerable proportion, and much effort has been made to design and develop new types of packaging materials with good mechanical strength, water permeability, light transmittance, and safety [465]. The synthetic nanomaterials such as carbon nanotubes, graphenee, and metal oxides have been widely applied in the packing membrane material to improve the mechanical properties, but these synthetic nanomaterials are expensive, and the film's light transmittance and safety were limited. Comparatively, natural nanomaterials such as silicate clay minerals are not only nontoxic and low cost, but also can improve the mechanical properties of films. So far, many nanoclays such as attapulgite [466], sepiolite [467–469], halloysite [470], montmorillonite [471, 472], laponite [473], and talc [474] have been used for preparing polymer composites. After the introduction of attapulgite nanorods, the elongation at break of the membrane was obviously increased, and the water resistance of the membrane was obviously improved. The mechanical properties of the film depend on the dispersion degree of attapulgite nanorods. The better the rods dispersion is, the better the reinforcing properties of the films are, and the optimum dosage of attapulgite is usually 1–3% [191]. The well-dispersed attapulgite rods can increase the mechanical properties of films with no expense of light transparency. Different form one-dimensional nanoclay, the two-dimensional nanoclay with sandwhich-type structure could form intercalation or exfoliation nanocomposite with a polymer, which leads to a nanoscale dispersion of clay nanosheets in the polymer matrix, and thereby increase the mechanical parameters, such as modulus and tensile strength [475]. The silicate nanosheets can form a barrier layer within the polymer matrix to improve its water resistance or gas barrier performance, and can also improve the heat and flame retardant properties of films [476, 477]. The highly

dispersed nanofiber, nanorods, nanotubes, or nanosheets in the polymer matrix can serve as "rebar" to reinforce the "concret" (polymer matrix), and nanoclays are nontoxic, safe, and cost-efficient, which is potential nanofiller to be used to prepare new types of eco-friendly food packing materials.

Sand-Fixing Materials

Desertification is the most serious local and global environmental problem, which has become a major obstacle to many countries. Sand fixation measurements are indispensable to solve the problem. Engineering sand fixation, chemical sand fixation, and biological sand fixation are generally in use nowadays. Targeting the problem of available water conservation in sand fixation, clay-based sand-fixing, and grass-planting material was proposed. Zhang and Wang [478] have developed the sand-fixing and grass-planting materials with clay modified by emulsifying vegetable waxes and octylphenol polyoxyethylene ether (OP4). It was shown that the materials are excellent for water retention and sand-fixing, and the vegetable waxes made the clay pores changing from hydrophilic to hydrophobic, which effectively inhibited the water evaporation. Grass-planting experiment showed that, with a reasonable mass ratio of clay, vegetable waxes, and surfactants, the materials not only inhibited water evaporation but also maintained sound air permeability so that the germination rate and survival rate of grass were significantly improved. Qu et al. [479] prepared the water retention materials with montmorillonite (MMT) modified by castor oil polyoxyethylene ether (10) (EL-10) emulsifying vegetable waxes. It was shown that the original big hydrophilic pores between the clay particles turned into capillary hydrophobic pores. So the clay particles formed a bonding layer which could inhibit water evaporation. Grass-planting experiment showed that reasonable mass ratio of vegetable waxes and EL-10 was 1:18. The materials not only had great water retention property but also maintained sound air permeability so that the germination rate of grass seed significantly increased from 8% to 52%.

Conclusions and Further Outlook

Nanoclays have long been used in several applications and their uses are based on their structural and physical characteristics that are discussed in detail in this chapter. The latest progress on the nanoclays and derived ecomaterials has been concluded and discussed based on reviewing a comprehensive literature combined with our group's relevant research achievements. It can be concluded that the nanocrystallization and surface functional modification of clay minerals is a necessary prerequisite for the development of ecological functional materials, and the nanometer fraction of clay minerals can produce composite materials with better performance than primary mineral. The applications of the nanoscale clay minerals are mainly focused on the adsorption materials for the removal of pollutants from

wastewater, the superabsorbent materials for water-saving and water retention, the carrier of catalyst or pigments, the polymer composites, and so on. Beyond all question, it is also the main approach to realize the reasonable application of nanoscale clay minerals in the future. Although clay minerals have been proved to be extremely successful in preparation of many ecomaterials with different distinctive structures and functional groups, there are still many aspects to need study, especially the practical application.

The synthesis of clay mineral needs to pay more attention in the future. Natural clay minerals are rich in nature, but there are obvious differences in the structure and physicochemical properties of clay minerals in different mines or different areas due to the complex geology mineralization environment and the existence of isotopic substitution in the process of minerals. For most minerals, it is difficult to find pure products in nature, often associated with a variety of minerals. It is also difficult to get a purer single mineral using the traditional purification methods, which restrict the industrial applications of clay minerals in many fields, especially in the polymer materials. In recent years, the synthesis or modification of clay minerals has made great progress, and many minerals such as zeolite, laponite, and mica have been synthesized on a large scale. These synthetic minerals show more stable structure and performance than natural mineral, so they have gained large-scale application in the industry. With the development of mineral synthesis technology, a variety of different forms of clay minerals will be synthesized. Their introduction as fillers or additives in polymers for various desired effects has been of enormous interest for research and development studies. These minerals that are similar to carbon nanotubes, graphene, and other carbon nanomaterials in functional aspects will be widely used in the field of polymer composites. In addition, finding new applications of such synthetic clay minerals, including pillared clay minerals, porous clay hetero-structures, and nanocomposites, will be another promising work.

Apart from the synthesis methods existed and proposed during the review process, there are other potential methods which are suitable for the dispersion, modification, and nanocomposite of clay minerals. It is essential to develop novel and environment-friendly technologies for producing clay minerals-based materials with suitable properties in a cost-effective way in the future. For instance, the physical process such as high-pressure homogenization can effectively disaggregate attapulgite crystal bundles into single nanorods, and this process can promote the interaction of organic molecules with clay minerals and then improve the modification efficiency. The traditional modification methods such as mechanical grinding, acid treatment, and heat activation have proven to be effective to enhance the adsorption properties of clay minerals, but these methods have a certain limit on improving the performance of clay minerals. The development of modern ray physics and instrumentation technology makes it possible to modify clay minerals using a simple physical ray. The surface properties of clay minerals could be changed by only a short-time ray treatment, but the adsorption performance could be improved greatly.

With the continuous progress of the research on dispersion, modification, and composite technology of clay minerals, it is becoming more and more important to

study its related mechanism. The traditional structure characterization methods such as X-ray diffraction, scanning electron microscope, transmittance electron microscope, and others played an important role in revealing the structure of clay minerals and the derived materials, but these traditional methods are limited in revealing the fine structure, change of crystalline structure, the interface properties, and the change of chemical bonds during modification, and so on. The advanced analysis techniques that are used to characterize nanoclays or their nanocomposites need to be paid more attention. However, little information is available about the study on mechanism and principle, which are needed to be systematically studied in the future. The breakthrough of advanced analysis technology will lead to the rapid development of clay minerals and their derived ecological materials.

Acknowledgments The authors would like to thank National Natural Science Foundation of China (NO. 51403221, 21377135 and 41601303), the Key Research & Development Project of Gansu Provincial Sci. & Tech. Department, China (17YF1WA167) and the Youth Innovation Promotion Association CAS (2016370) for the financial support.

References

1. Thorkelsson K, Bai P, Xu T (2015) Self-assembly and applications of anisotropic nanomaterials: a review. Nano Today 10(1):48–66
2. Smith SC, Rodrigues DF (2015) Carbon-based nanomaterials for removal of chemical and biological contaminants from water: a review of mechanisms and applications. Carbon 91:122–143
3. Taka AL, Pillay K, Mbianda XY (2017) Nanosponge cyclodextrin polyurethanes and their modification with nanomaterials for the removal of pollutants from waste water: a review. Carbohyd Polym 159:94–107
4. Tian R, Liu H, Jiang Y, Chen J, Tan X, Liu G, Zhang L, Gu X, Guo Y, Wang H, Sun L, Chu W (2015) Drastically enhanced high-rate performance of carbon-coated LiFePO4 nanorods using a green chemical vapor deposition (CVD) method for lithium ion battery: a selective carbon coating process. ACS Appl Mater Interf 7(21):11377–11386
5. Tian J, Zhao Z, Kumar A, Boughton RI, Liu H (2014) Recent progress in design, synthesis, and applications of one-dimensional TiO_2 nanostructured surface heterostructures: a review. Chem Soc Rev 43(20):6920–6937
6. Rao CNR, Müller A, Cheetham AK (2006) The chemistry of nanomaterials: synthesis, properties and applications. Wiley, Weinheim
7. Halada K, Yamamoto R (2001) The current status of research and development on ecomaterials around the world. MRS Bull 26(11):871–879
8. Nie Z (2015) Eco-materials and life-cycle assessment. In: Green and sustainable manufacturing of advanced material. Elsevier, Amsterdam, p 31
9. Moon RJ, Martini A, Nairn J, Simonsen J, Youngblood J (2011) Cellulose nanomaterials review: structure, properties and nanocomposites. Chem Soc Rev 40(7):3941–3994
10. Ruiz-Hitzky E, Darder M, Fernandes FM, Wicklein B, Alcântara AC, Aranda P (2013) Fibrous clays based bionanocomposites. Prog Polym Sci 38(10):1392–1414
11. Kiliaris P, Papaspyrides CD (2010) Polymer/layered silicate (clay) nanocomposites: an overview of flame retardancy. Prog Polym Sci 35(7):902–958
12. Lvov Y, Abdullayev E (2013) Functional polymer–clay nanotube composites with sustained release of chemical agents. Prog Polym Sci 38(10):1690–1719

13. Bergaya F, Lagaly G (2006) General introduction: clays, clay minerals, and clay science. In: Handbook of clay science fundamentals, Developments in clay science, vol 1. Elsevier, Amsterdam, pp 1–18
14. Liu P (2007) Polymer modified clay minerals: a review. Appl Clay Sci 38(1):64–76
15. Kotal M, Bhowmick AK (2015) Polymer nanocomposites from modified clays: recent advances and challenges. Prog Polym Sci 51:127–187
16. Zhou CH, Zhao LZ, Wang AQ, Chen TH, He HP (2016) Current fundamental and applied research into clay minerals in China. Appl Clay Sci 119:3–7
17. Joussein E, Petit S, Churchman J, Theng B, Righi D, Delvaux B (2005) Halloysite clay minerals–a review. Clay Miner 40(4):383–426
18. Jones BF, Galan E (1988) Sepiolite and palygorskite. Rev Mineral Geochem 19(1):631–674
19. Yuan P, Tan DY, Annabi-Bergayac F (2015) Properties and applications of halloysite nanotubes: recent research advances and future prospects. Appl Clay Sci 112–113:75–93
20. Edelman CT, Favejee JCL (1940) On the crystal structure of montmorillonite and halloysite. Zeitschrift für Kristallographie-Crystalline Materials 102(1–6):417–431
21. Wang WB, Wang AQ (2016) Recent progress in dispersion of palygorskite crystal bundles for nanocomposites. Appl Clay Sci 119:18–30
22. Ray SS, Bousmina M (2005) Biodegradable polymers and their layered silicate nanocomposites: in greening the 21st century materials world. Prog Mater Sci 50(8):962–1079
23. Huang DJ, Wang WB, Xu JX, Wang AQ (2012) Mechanical and water resistance properties of chitosan/poly (vinyl alcohol) films reinforced with attapulgite dispersed by high-pressure homogenization. Chem Eng J 210:166–172
24. Ma J, Liu Q, Zhu L, Zou J, Wang K, Yang M, Komarneni S (2016) Visible light photocatalytic activity enhancement of Ag_3PO_4 dispersed on exfoliated bentonite for degradation of rhodamine B. Appl Catal B Environ 182:26–32
25. Sonawane S, Chaudhari P, Ghodke S, Ambade S, Gulig S, Mirikar A, Bane A (2008) Combined effect of ultrasound and nanoclay on adsorption of phenol. Ultrason Sonochem 15(6):1033–1037
26. Hassani A, Khataee A, Karaca S, Karaca M, Kıranşan M (2015) Adsorption of two cationic textile dyes from water with modified nanoclay: a comparative study by using central composite design. J Environ Chem Eng 3(4:2738–2749
27. Meira SMM, Jardim AI, Brandelli A (2015) Adsorption of nisin and pediocin on nanoclays. Food Chem 188:161–169
28. Liang X, Xu Y, Tan X, Wang L, Sun Y, Lin D, Wang Q (2013) Heavy metal adsorbents mercapto and amino functionalized palygorskite: preparation and characterization. Colloid Surface A 426:98–105
29. Zhou CH (2011) An overview on strategies towards clay-based designer catalysts for green and sustainable catalysis. Appl Clay Sci 53(2):87–96
30. Iman M, Maji TK (2012) Effect of crosslinker and nanoclay on starch and jute fabric based green nanocomposites. Carbohyd polym 89(1):290–297
31. Drits VA, Sokolova GV (1971) Structure of palygorskite. Soviet Physics Crystallography 16:183–185
32. Bradley WF (1940) The structure scheme of attapulgite. Am Mineral 25:405–410
33. Galán E (1996) Properties and applications of palygorskite-sepiolite. Clay Clay Miner 31:443–454
34. Giustetto R, Chiari G (2004) Crystal structure refinements of palygorskite and Maya blue from molecular modeling and powder synchrotron diffraction. Eur J Miner 16:521–532
35. Bergaya F, Lagaly G (2013) Handbook of clay science, Developments in clay science, vol 5, 2nd edn. Elsevier, Amsterdam
36. Rhouta B, Zatile E, Bouna L, Lakbita O, Maury F, Daoudi L, Lafont MC, Amjoud M, Senocq F, Jada A (2013) Comprehensive physicochemical study of dioctahedral palygorskite-rich clay from Marrakech high atlas (Morocco). Phys Chem Miner 40(5):411–424

37. Suárez M, García-Romero E (2006) FTIR spectroscopic study of palygorskite:influence of the composition of the octahedral sheet. Appl Clay Sci 31:154–163
38. Mckeown DA, Post JE, Etz ES (2002) Vibrational analysis of palygorskite and sepiolite. Clay Clay Miner 50:667–680
39. Chisholm JE (1990) An X-ray diffraction study of Palygorskite. Can Mineral 28:329–339
40. Chisholm JE (1992) Powder diffraction patterns and structural models of Palygorskite. Can Mineral 30:61–73
41. Galán E, Carretero MI (1999) A new approach to compositional limits for sepiolite and palygorskite. Clay Clay Miner 47:399–409
42. Suárez M, García-Romero E, del Río MS, Martinetto P, Dooryhée E (2007) The effect of octahedral cations on the dimensions of the palygorskite cell. Clay Miner 42:287–297
43. Chryssikos GD, Gionis V, Kacandes GH, Stathopoulou ET, Suarez M, Garcia-Romero E, del Rio MS (2009) Octahedral cation distribution in palygorskite. Am Mineral 94:200–203
44. Krekeler MPS, Guggenheim S (2008) Defects in microstructure in palygorskite–sepiolite minerals: a transmission electron microscopy (TEM) study. Appl Clay Sci 39:98–105
45. García-Romero E, Suárez M (2013) Sepiolite–palygorskite: textural study and genetic considerations. Appl Clay Sci 86:129–144
46. García-Romero E, Suárez M (2014) Sepiolite-palygorskite polysomatic series: oriented aggregation as a crystal growth mechanism in natural environments. Am Mineral 99:1653–1661
47. Corma A, Mifsud A, Sanz E (1987) Influence of the chemical composition and textural characteristics of palygorskite on the acid leaching of octahedral cations. Clay Miner 22:225–232
48. Barrios MS, Gonzhlez LVF, Rodriguez MAV, Pozas JMM (1995) Acid activation of a palygorskite with HCl: development of physico-chemical, textural and surface properties. Appl Clay Sci 10:247–258
49. Baltar CAM, Benvindo da Luz A, Baltar LM, de Oliveira CH, Bezerra FJ (2009) Influence of morphology and surface charge on the suitability of palygorskite as drilling fluid. Appl Clay Sci 42:597–600
50. Boudriche L, Chamayou A, Calvet R, Hamdi B, Balard H (2014) Influence of different dry milling processes on the properties of an attapulgite clay, contribution of inverse gas chromatography. Powder Technol 254:352–363
51. Chen L, Liu K, Jin TX, Chen F, Fu Q (2012) Rod like attapulgite/poly(ethylene terephthalate) nanocomposites with chemical bonding between the polymer chain and the filler. Express Polym Lett 6:629–638
52. Liu P, Zhu LX, Guo JS, Wang AQ, Zhao Y, Wang ZR (2014) Palygorskite/polystyrene nanocomposites via facile in-situ bulk polymerization: gelation and thermal properties. Appl Clay Sci 100:95–101
53. Xu JX, Wang WB, Wang AQ (2014) Enhanced microscopic structure and properties of palygorskite by associated extrusion and high-pressure homogenization process. Appl Clay Sci 95:365–370
54. Haden JWL (1963) Palygorskite: properties and uses. Clay Clay Miner 284–290
55. Gonzalez F, Pesquera C, Blanco C, Benito I, Mendioroz S, Pajares JA (1989) Structural and textural evolution of Al- and Mg-rich palygorskites, I. Under acid treatment. Appl Clay Sci 4:373–388
56. Windsor SA, Tinker MH (1999) Electro-fluorescence polarization studies of the interaction of fluorescent dyes with clay minerals in suspensions. Colloid Surface A 148:61–73
57. Abdo J, Haneef MD (2013) Clay nanoparticles modified drilling fluids for drilling of deep hydrocarbon wells. Appl Clay Sci 86:76–82
58. Chemeda YC, Christidis GE, Khan NMT, Koutsopoulou E, Hatzistamou V, Kelessidis VC (2014) Rheological properties of palygorskite–bentonite and sepiolite–bentonite mixed clay suspensions. Appl Clay Sci 90:165–174
59. Han J, YM X, Liang XF, YJ X (2014) Sorption stability and mechanism exploration of palygorskite as immobilization agent for cd in polluted soil. Water Air Soil Poll 225:2160

60. Tian GY, Wang WB, Zong L, Wang AQ (2017) MgO/palygorskite adsorbent derived from natural mg-rich brine and palygorskite for high-efficient removal of cd (II) and Zn (II) ions. J Environ Chem Eng 5(1):1027–1036
61. Papoulis D, Komarneni S, Panagiotaras D, Nikolopoulou A, Li HH, Shu Y, Tsugio S, Katsuki H (2013) Palygorskite–TiO_2 nanocomposites: part 1. Synthesis and characterization. Appl Clay Sci 83–84:191–197
62. Huo CL, Yang HM (2013) Preparation and enhanced photocatalytic activity of Pd–CuO/palygorskite nanocomposites. Appl Clay Sci 74:87–94
63. Tan L, Tang A, Zou Y, Long M, Zhang Y, Ouyang J, Chen J (2017) Sb_2Se_3 assembling Sb_2O_3@ attapulgite as an emerging composites for catalytic hydrogenation of p-nitrophenol. Sci Rep 7:3281
64. Ruiz-Hitzky E, Darder M, Fernandes FM, Wicklein B, Alcântara ACS, Aranda P (2013) Fibrous clays based bionanocomposites. Prog Polym Sci 38:1392–1414
65. Tang QG, Wang F, Guo H, Yang Y, YL D, Liang JS, Zhang FQ (2015) Effect of coupling agent on surface free energy of organic modified attapulgite (OAT) powders and tensile strength of OAT/ethylene-propylene-diene monomer rubber nanocomposites. Powder Technol 270:92–97
66. Tian GY, Wang WB, Wang DD, Wang Q, Wang AQ (2017) Novel environment friendly inorganic red pigments based on attapulgite. Powder Technol 315:60–67
67. Wang Q, Zhang JP, Wang AQ (2014) Freeze-drying: a versatile method to overcome re-aggregation and improve dispersion stability of palygorskite for sustained release of ofloxacin. Appl Clay Sci 87:7–13
68. Luo SP, Chen Y, Zhou M, Yao C, Xi HT, Kong Y, Deng LH (2013) Palygorskite-poly(o-phenylenediamine) nanocomposite: an enhanced electrochemical platform for glucose biosensing. Appl Clay Sci 86:59–63
69. Lei H, Wei Q, Wang Q, Su A, Xue M, Liu Q, Hu Q (2017) Characterization of ginger essential oil/palygorskite composite (GEO-PGS) and its anti-bacteria activity. Mater Sci Eng C 73:381–387
70. Viseras C, Aguzzi C, Cerezo P, Lopez-Galindo A (2007) Uses of clay minerals in semisolid health care and therapeutic products. Appl Clay Sci 36:37–50
71. Lopez-Galindo A, Viseras C, Cerezo P (2007) Compositional, technical and safety specifications of clays to be used as pharmaceutical and cosmetic products. Appl Clay Sci 36:51–63
72. Li ZH, Liu FH, GJ X, Zhang JL, Chu CY (2014) A kinetics-controlled coating method to construct 1D attapulgite @ amorphous titanium oxide nanocomposite with high electro-rheological activity. Colloid Polym Sci 292:3327–3335
73. Galán E, Aparicio P, Miras A (2011) Chapter 16: Sepiolite and palygorskite as sealing materials for the geological storage of carbon dioxide. In: Galán E, Singer A (eds) Developments in Palygorskite-Sepiolite research. Elsevier, Amsterdam, pp 375–392
74. Zeng HF, Lin LJ, Xi YM, Han ZY (2017) Effects of raw and heated palygorskite on rumen fermentation in vitro. Appl Clay Sci 138:125–130
75. Guggenheim S, Krekeler MP (2011) The structures and microtextures of the palygorskite-sepiolite group minerals. Developments in Palygorskite-Sepiolite research (Galan E. & Singer A., editors). Developments in cay science 3: 3–32 Elsevier, Amsterdam
76. Guggenheim S, Eggleton RA (1988) Crystal chemistry, classification and identification of modulated layer silicates. Rev Mineral 19:675–725
77. Ferraris G, Makovicky E, Merlino S (2008) Crystallography of modular materials. IUCr. Oxford University Press, Oxford
78. Fernández-Saavedra R, Aranda P, Ruiz-Hitzky E (2004) Templated synthesis of carbon nanofibers from polyacrylonitrile using sepiolite. Adv Funct Mater 14(1):77–82
79. Bailey SW, Alietti A, Brindley GW, Formosa MLL, Jasmund K, Konta J, Mackenzie RC, Nagasawa K, Rausell-Colom RA, Zvyagin BB (1980) Summary of recommendations of AIPEA nomenclature committee. Clay Clay Miner 28(1):73–78
80. de Lima JA, Camilo FF, Faez R, Cruz SA (2017) A new approch to sepiolite dispersion by treatment with ionic liquids. Appl Clay Sci 143:234–240

81. Alkan M, Doğan M, Turhan Y, Demirbaş Ö, Turan P (2008) Adsorption kinetics and mechanism of maxilon blue 5G dye on sepiolite from aqueous solutions. Chem Eng J 139(2):213–223
82. Tian GY, Wang WB, Kang YR, Wang AQ (2014) Study on thermal activated sepiolite for enhancing decoloration of crude palm oil. J Therm Anal Calorim 117(3):1211–1219
83. Zhou F, Yan C, Wang H, Zhou S, Komarneni S (2017) Sepiolite-TiO_2 nanocomposites for photocatalysis: synthesis by microwave hydrothermal treatment versus calcination. Appl Clay Sci 146:246–253
84. Darder M, Matos CRS, Aranda P, Gouveia RF, Ruiz-Hitzky E (2017) Bionanocomposite foams based on the assembly of starch and alginate with sepiolite fibrous clay. Carbohyd Polym 157:1933–1939
85. Gao Y, Gan H, Zhang G, Guo Y (2013) Visible light assisted Fenton-like degradation of rhodamine B and 4-nitrophenol solutions with a stable poly-hydroxyl-iron/sepiolite catalyst. Chem Eng J 217:221–230
86. Degirmenbasi N, Boz N, Kalyon DM (2014) Biofuel production via transesterification using sepiolite-supported alkaline catalysts. Appl Catal B Environ 150:147–156
87. Ma Y, Zhang G (2016) Sepiolite nanofiber-supported platinum nanoparticle catalysts toward the catalytic oxidation of formaldehyde at ambient temperature: efficient and stable performance and mechanism. Chem Eng J 288:70–78
88. Benli B, Yalın C (2017) The influence of silver and copper ions on the antibacterial activity and local electrical properties of single sepiolite fiber: a conductive atomic force microscopy (C-AFM) study. Appl Clay Sci 146:449–456
89. Tian GY, Wang WB, Mu B, Wang Q, Wang AQ (2017) Cost-efficient, vivid and stable red hybrid pigments derived from naturally available sepiolite and halloysite. Ceram Int 43(2):1862–1869
90. Pappalardo S, Russo P, Acierno D, Rabe S, Schartel B (2016) The synergistic effect of organically modified sepiolite in intumescent flame retardant polypropylene. Eur Polym J 76:196–207
91. Mahdavinia GR, Hosseini R, Darvishi F, Sabzi M (2016) The release of cefazolin from chitosan/polyvinyl alcohol/sepiolite nanocomposite hydrogel films. Iran Polym J 25(11): 933–943
92. Xie YT, Wang AQ, Liu G (2010) Superabsorbent composite XXII: effects of modified sepiolite on water absorbency and swelling behavior of chitosan-g-poly (acrylic acid)/sepiolite superabsorbent composite. Polym Compos 31(1):89–96
93. Kara A, Tekin N, Alan A, Şafaklı A (2016) Physicochemical parameters of Hg (II) ions adsorption from aqueous solution by sepiolite/poly (vinylimidazole). J Environ Chem Eng 4(2):1642–1652
94. Liu Y, Zhao J, Deng CL, Chen L, Wang DY, Wang YZ (2011) Flame-retardant effect of sepiolite on an intumescent flame-retardant polypropylene system. Ind Eng Chem Res 50(4):2047–2054
95. Yuan P, Thill A, Bergaya F (2016) Nanosized tubular clay minerals: Halloysite and Imogolite, vol 7. Elsevier, Amsterdam
96. Yuan P, Southon PD, Liu Z, Green ME, Hook JM, Antill SJ, Kepert CJ (2008) Functionalization of halloysite clay nanotubes by grafting with γ-aminopropyltriethoxysilane. J Phys Chem C 112(40):15742–15751
97. Du M, Guo B, Jia D (2010) Newly emerging applications of halloysite nanotubes: a review. Polym Int 59:574–582
98. Yuan P, Tan D, Annabi-Bergaya F (2015) Properties and applications of halloysite nanotubes: recent research advances and future prospects. Appl Clay Sci 112:75–93
99. Liu M, Jia Z, Jia D, Zhou C (2014) Recent advance in research on halloysite nanotubes-polymer nanocomposite. Prog Polym Sci 39:1498–1525
100. Mitra GB (2013) Spiral structure of 7 Å halloysite: mathematical models. Clay Clay Miner 61:499–507

101. Keeling JL (2015) The mineralogy, geology and occurrences of halloysite. In: Pasbakhsh P, Churchman GJ (eds) Natural mineral nanotubes. Apple Academic Press, Oakville, pp 95–115
102. Dong Y, Marshall J, Haroosh HJ, Mohammadzadehmoghadam S, Liu D, Qi X, Lau KT (2015) Polylactic acid (PLA)/halloysite nanotube (HNT) composite mats: influence of HNT content and modification. Compos A: Appl Sci Manufact 76:28–36
103. Ghanbari M, Emadzadeh D, Lau WJ, Lai SO, Matsuura T, Ismail AF (2015) Synthesis and characterization of novel thin film nanocomposite (TFN) membranes embedded with halloysite nanotubes (HNTs) for water desalination. Desalination 358:33–41
104. Zhu K, Duan Y, Wang F, Gao P, Jia H, Ma C, Wang C (2017) Silane-modified halloysite/Fe_3O_4 nanocomposites: simultaneous removal of Cr(VI) and Sb(V) and positive effects of Cr(VI) on Sb(V) adsorption. Chem Eng J 311:236–246
105. Carrillo AM, Carriazo JG (2015) Cu and co oxides supported on halloysite for the total oxidation of toluene. Appl Catal B Environ 164:443–452
106. Lvov Y, Wang W, Zhang L, Fakhrullin R (2016) Halloysite clay nanotubes for loading and sustained release of functional compounds. Adv Mater 28(6):1227–1250
107. Bonifacio MA, Gentile P, Ferreira AM, Cometa S, De Giglio E (2017) Insight into halloysite nanotubes-loaded gellan gum hydrogels for soft tissue engineering applications. Carbohyd Polym 163:280–291
108. Smith RJ, Holder KM, Ruiz S, Hahn W, Song Y, Lvov YM, Grunlan JC (2017) Environmentally benign Halloysite nanotube multilayer assembly significantly reduces polyurethane flammability. Adv Funct Mater. https://doi.org/10.1002/adfm.201703289
109. Jin J, Fu L, Yang H, Ouyang J (2015) Carbon hybridized halloysite nanotubes for high-performance hydrogen storage capacities. Sci Rep 5:12429
110. Liang J, Tan H, Xiao C, Zhou G, Guo S, Ding S (2015) Hydroxyl-riched halloysite clay nanotubes serving as substrate of NiO nanosheets for high-performance supercapacitor. J Power Sources 285:210–216
111. Ganganboina AB, Chowdhury AD, Doong RA (2017) Nano assembly of N-doped graphene quantum dots anchored Fe_3O_4/halloysite nanotubes for high performance supercapacitor. Electrochim Acta 245:912–923
112. Lvov Y, Abdullayev E (2013) Functional polymer–clay nanotube composites with sustained release of chemical agents. Prog Polym Sci 38:1690–1719
113. Pasbakhsh P, Churchman GJ, Keeling JL (2013) Characterisation of properties of various halloysites relevant to their use as nanotubes and microfibre fillers. Appl Clay Sci 74:47–57
114. Liu QF, Li XG, Cheng HF (2016) Insight into the self-adaptive deformation of kaolinite layers into nanoscrolls. Appl Clay Sci 124-125:175–182
115. Yamamoto K, Otsuka H, Wada SI, Sohn D, Takahara A (2005) Transparent polymer nanohybrid prepared by in situ synthesis of aluminosilicate nanofibers in poly (vinyl alcohol) solution. Soft Matter 1(5):372–377
116. Yang H, Wang C, Su Z (2008) Growth mechanism of synthetic imogolite nanotubes. Chem Mater 20(13):4484–4488
117. Lourenco MP, Guimaraes L, da Silva MC, de Oliveira C, Heine T, Duarte HA (2014) Nanotubes with well-defined structure: single-and double-walled imogolites. J Phys Chem C 118(11):5945–5953
118. Ackerman WC, Smith DM, Huling JC, Kim YW, Bailey JK, Brinker CJ (1993) Gas/vapor adsorption in imogolite: a microporous tubular aluminosilicate. Langmuir 9(4):1051–1057
119. Imamura S, Hayashi Y, Kajiwara K, Hoshino H, Kaito C (1993) Imogolite: a possible new type of shape-selective catalyst. Ind Eng Chem Res 32(4):600–603
120. Yah WO, Yamamoto K, Jiravanichanun N, Otsuka H, Takahara A (2010) Imogolite reinforced nanocomposites: multifaceted green materials. Materials 3(3):1709–1745
121. Lee H, Ryu J, Kim D, Joo Y, Lee SU, Sohn D (2013) Preparation of an imogolite/poly (acrylic acid) hybrid gel. J Colloid Interf Sci 406:165–171

122. Bottero I, Bonelli B, Ashbrook SE, Wright PA, Zhou W, Tagliabue M, Armandi M, Garrone E (2011) Synthesis and characterization of hybrid organic/inorganic nanotubes of the imogolite type and their behaviour towards methane adsorption. Phys Chem Chem Phys 13(2):744–750
123. Zanzottera C, Armandi M, Esposito S, Garrone E, Bonelli B (2012) CO_2 adsorption on aluminosilicate single-walled nanotubes of imogolite type. J Phys Chem C 116 (38):20417–20425
124. Ma W, Yah WO, Otsuka H, Takahara A (2012) Application of imogolite clay nanotubes in organic–inorganic nanohybrid materials. J Mater Chem 22(24):11887–11892
125. Ma W, Otsuka H, Takahara A (2011) Preparation and properties of PVC/PMMA-g-imogolite nanohybrid via surface-initiated radical polymerization. Polymer 52(24):5543–5550
126. Avellan A, Levard C, Chaneac C, Borschneck D, Onofri FR, Rose J, Masion A (2016) Accelerated microwave assisted synthesis of alumino-germanate imogolite nanotubes. RSC Adv 6(109):108146–108150
127. Thomas B, Coradin T, Laurent G, Valentin R, Mouloungui Z, Babonneau F, Baccile N (2012) Biosurfactant-mediated one-step synthesis of hydrophobic functional imogolite nanotubes. RSC Adv 2:426–435
128. Chemmi A, Brendlé J, Marichal C, Lebeau B (2013) A novel fluoride route for the synthesis of aluminosilicate nanotubes. Nano 3(1):117–125
129. Avellan A, Levard C, Chaneac C, Borschneck D, Onofri FR, Rose J, Masion A (2016) Accelerated microwave assisted synthesis of alumino-germanate imogolite nanotubes. RSC Adv 6(109):108146–108150
130. Amara MS, Paineau E, Bacia-Verloop M, Krapf MEM, Davidson P, Belloni L, Levard C, Rose J, Launois P, Thill A (2013) Single-step formation of micron long $(OH)_3Al_2O_3Ge(OH)$ imogolite-like nanotubes. Chem Commun 49(96):11284–11286
131. Avellan A, Levard C, Kumar N, Rose J, Olivi L, Thill A, Chaurand P, Borschneck D, Masion A (2014) Structural incorporation of iron into Ge–imogolite nanotubes: a promising step for innovative nanomaterials. RSC Adv 4(91):49827–49830
132. Shafia E, Esposito S, Manzoli M, Chiesa M, Tiberto P, Barrera G, Menard G, Allia P, Freyria FS, Garrone E, Bonelli B (2015) Al/Fe isomorphic substitution versus Fe_2O_3 clusters formation in Fe-doped aluminosilicate nanotubes (imogolite). J Nanopart Res 17(8):336
133. Murray HH (2007) Applied clay mineralogy: occurrences, processing and application of Kaolins, Bentonites, Palygorskite-Sepiolite, and common clays. Elsevier, Amsterdam
134. Bhattacharyya KG, Gupta SS (2008) Adsorption of a few heavy metals on natural and modified kaolinite and montmorillonite: a review. Adv Colloid Interf Sci 140(2):114–131
135. Deer WA, Howie RA, Zussman J (1985) An introduction to the rock-forming minerals. Longman, Harlow, pp 260–263
136. Arora A, Padua G (2010) Review: nanocomposites in food packaging. J Food Sci 75:43–49
137. Azeredo HMCD (2009) Nanocomposites for food packaging applications. Food Res Int 42:1240–1253
138. Paul DR, Robeson LM (2008) Polymer nanotechnology: nanocomposites. Polymer 49(15): 3187–3204
139. Bhattacharyya KG, Gupta SS (2008) Adsorption of a few heavy metals on natural and modified kaolinite and montmorillonite: a review. Adv Colloid Interf Sci 140(2):114–131
140. Bordes P, Pollet E, Avérous L (2009) Nano-biocomposites: biodegradable polyester/nanoclay systems. Prog Polym Sci 34:125–155
141. Murray HH (2000) Traditional and new applications for kaolin, smectite, and palygorskite: a general overview. Appl Clay Sci 17:207–221
142. Alexandre M, Dubois P (2000) Polymer-layered silicate nanocomposites: preparation, properties and uses of a new class of materials. Mat Sci Eng R 28:1–63
143. Zhang K, Xu J, Wang KY, Cheng L, Wang J, Liu B (2009) Preparation and characterization of chitosan nanocomposites with vermiculite of different modification. Polym Degrad Stab 94(12):2121–2127

144. Dorado AD, Lafuente FJ, Gabriel D, Gamisans X (2010) A comparative study based on physical characteristics of suitable packing materials in biofiltration. Environ Technol 31(2):193–204
145. Priolo MA, Holder KM, Greenlee SM, Grunlan JC (2012) Transparency, gas barrier, and moisture resistance of large-aspect-ratio vermiculite nanobrick wall thin films. ACS Appl Mater Interf 4(10):5529–5533
146. Dultz S, An JH, Riebe B (2012) Organic cation exchanged montmorillonite and vermiculite as adsorbents for Cr (VI): effect of layer charge on adsorption properties. Appl Clay Sci 67:125–133
147. Wang WB, Zhai NH, Wang AQ (2011) Preparation and swelling characteristics of a super-absorbent nanocomposite based on natural guar gum and cation-modified vermiculite. J Appl Polym Sci 119(6):3675–3686
148. Liu Y, He Z, Zhou L, Hou Z, Eli W (2013) Simultaneous oxidative conversion and CO_2 reforming of methane to syngas over Ni/vermiculite catalysts. Catal Commun 42:40–44
149. Qian Y, Lindsay CI, Macosko C, Stein A (2011) Synthesis and properties of vermiculite-reinforced polyurethane nanocomposites. ACS Appl Mater Interf 3(9):3709–3717
150. Dorel S (2000) Nanostructuration de la muscovite. Ph.D. Thesis, Lab. d'Orsay, Université de Paris, France
151. Sivakumar T, Krithiga T, Shanthi K, Mori T, Kubo J, Morikawa Y (2004) Noble metals intercalated/supported mica catalyst–synthesis and characterization. J Mol Catal A Chem 223(1):185–194
152. De CP, Hutcheon I, Walshe JL (1993) Chlorite geothermometry: a review. Clay Clay Miner 41(2):219–239
153. Dowey PJ, Hodgson DM, Worden RH (2012) Pre-requisites, processes, and prediction of chlorite grain coatings in petroleum reservoirs: a review of subsurface examples. Mar Petrol Geol 32(1):63–75
154. Worden RH, Morad S (2003) Clay minerals in sandstones: controls on formation, distribution and evolution. Blackwell, Oxford, UK, pp 1–41
155. Bethke CM, Reynolds RC (1986) Recursive method for determining frequency factors in interstratified clay diffraction calculations. Clay Clay Miner 34:224–226
156. Drits VA, Dainyak LG, Muller F, Besson G, Manceau A (1997) Isomorphous cation distribution in celadonites, glauconites and Fe-illites determined by infrared, Mossbauer and EXAFS spectroscopies. Clay Miner 32:153–179
157. Drits VA, Lindgreen H, Salyn AL (1997) Determination by XRD of content and distribution of fixed ammonium in illite-smectite. Application to North Sea illite-smectite. Am Mineral 82:80–88
158. Reynolds RC (1980) Crystal structures of clay minerals and their X-ray identification. Mineralogical Society, London, pp 249–303
159. Wang X, Du Y, Luo J, Lin B, Kennedy JF (2007) Chitosan/organic rectorite nanocomposite films: structure, characteristic and drug delivery behaviour. Carbohyd Polym 69(1):41–49
160. Wang X, Du Y, Luo J, Yang J, Wang W, Kennedy JF (2009) A novel biopolymer/rectorite nanocomposite with antimicrobial activity. Carbohyd Polym 77(3):449–456
161. Huang Y, Ma X, Liang G, Yan H (2008) Adsorption of phenol with modified rectorite from aqueous solution. Chem Eng J 141:1): 1–1): 8
162. Wang N, Feng Z, Ma X, Zheng P (2017) The modification of rectorite with carbon layers and trisodium trimetaphosphate for the removal of Pb^{2+}. Appl Clay Sci 146:115–121
163. Chen Y, Fang J, Lu S, Wu Y, Chen D, Huan L, Zhu XM, Ren L, Cheng C, Fang Z (2015) Plasmonic ag-pillared rectorite as catalyst for degradation of 2, 4-DCP in the H_2O_2-containing system under visible light irradiation. J Hazard Mater 297:278–285
164. Jin J, Tu H, Chen J, Cheng G, Shi X, Deng H, Li Z, Du Y (2017) Rectorite-intercalated nanoparticles for improving controlled release of doxorubicin hydrochloride. Int J Biol Macromol 101:815–822

165. Wang Y, Zhang H, Wu Y, Yang J, Zhang L (2005) Preparation, structure, and properties of a novel rectorite/styrene–butadiene copolymer nanocomposite. J Appl Polym Sci 96(2): 324–328
166. Altaner SP, Weiss CA, Kirkpatrick RJ (1988) Evidence from ^{29}Si NMR for the structure of mixed-layer illite/smectite clay minerals. Nature 331:699–702
167. Altaner SP, Ylagan RF (1997) Comparison of structural models of mixed-layer illite/smectite and reaction mechanisms of smectite illitization. Clay Clay Miner 45(4):517–533
168. Missana T, Garcia-Gutierrez M, Alonso U (2008) Sorption of strontium onto illite/smectite mixed clays. Phys Chem Earth Parts A/B/C 33:S156–S162
169. Buchwald A, Hohmann M, Posern K, Brendler E (2009) The suitability of thermally activated illite/smectite clay as raw material for geopolymer binders. Appl Clay Sci 46(3):300–304
170. Wang YZ, Wang WB, Wang AQ (2013) Efficient adsorption of methylene blue on an alginate-based nanocomposite hydrogel enhanced by organo-illite/smectite clay. Chem Eng J 228:132–139
171. Huertas FJ, Huertas F, Linares J (1993) Hydrothermal synthesis of kaolinite: method and characterization of synthetic materials. Appl Clay Sci 7(5):345–356
172. Zhang D, Zhou CH, Lin CX, Tong DS, WH Y (2010) Synthesis of clay minerals. Appl Clay Sci 50(1):1–11
173. Vicente I, Salagre P, Cesteros Y, Medina F, Sueiras JE (2010) Microwave-assisted synthesis of saponite. Appl Clay Sci 48(1):26–31
174. Torii K, Iwasaki T (1987) Synthesis of hectorite. Clay Sci 7(1):1–16
175. Kloprogge JT, Komarneni S, Amonette JE (1999) Synthesis of smectite clay minerals: a critical review. Clay Clay Miner 47(5):529–554
176. Lantenois S, Champallier R, Bény JM, Muller F (2008) Hydrothermal synthesis and characterization of dioctahedral smectites: a montmorillonites series. Appl Clay Sci 38(3):165–178
177. Levinson AA, Day JJ (1968) Low temperature hydrothermal synthesis of montmorillonite. Ammonium-micas and ammonium-zeolites. Earth Planet Sci Lett 5:52–54
178. Reichle WT (1986) Synthesis of anionic clay minerals (mixed metal hydroxides, hydrotalcite). Solid State Ionics 22(1):135–141
179. Golden DC, Dixon JB, Shadfan H, Kippenberger LA (1985) Palygorskite and sepiolite alteration to smectite under alkaline conditions. Clay Clay Miner 33(1):44–50
180. Wang WB, Zhang ZF, Tian GY, Wang AQ (2015) From nanorods of palygorskite to nanosheets of smectite via a one-step hydrothermal process. RSC Adv 5(72):58107–58115
181. Liu Y, Wang WB, Wang AQ (2012) Effect of dry grinding on the microstructure of palygorskite and adsorption efficiency for methylene blue. Powder Technol 225:124–129
182. Darvishi Z, Morsali A (2011) Sonochemical preparation of palygorskite nanoparticles. Appl Clay Sci 51:51–53
183. Boudriche L, Calvet R, Hamdi B, Balard H (2012) Surface properties evolution of attapulgite by IGC analysis as a function of thermal treatment. Colloid Surface A 399:1–10
184. Xu JX, Zhang JP, Wang Q, Wang AQ (2011) Disaggregation of palygorskite crystal bundles via high-pressure homogenization. Appl Clay Sci 54(1):118–123
185. Xu JX, Wang WB, Wang AQ (2013) A novel approach for dispersion palygorskite aggregates into nanorods via adding freezing process into extrusion and homogenization treatment. Powder Technol 249:157–162
186. Xu JX, Wang WB, Wang AQ (2014) Effect of squeeze, homogenization, and freezing treatments on particle diameter and rheological properties of palygorskite. Adv Powder Technol 25(3):968–977
187. Wang WB, Wang FF, Kang YR, Wang AQ (2015) Nanoscale dispersion crystal bundles of palygorskite by associated modification with phytic acid and high-pressure homogenization for enhanced colloidal properties. Powder Technol 269:85–92
188. Xu JX, Wang WB, Wang AQ (2013) Effects of solvent treatment and high-pressure homogenization process on dispersion properties of palygorskite. Powder Technol 235:652–660

189. Xu JX, Wang WB, Wang AQ (2014) Dispersion of palygorskite in ethanol–water mixtures via high-pressure homogenization: microstructure and colloidal properties. Powder Technol 261:98–104
190. Xu JX, Wang WB, Wang AQ (2013) Superior dispersion properties of palygorskite in dimethyl sulfoxide via high-pressure homogenization process. Appl Clay Sci 86:174–178
191. Zhou F, Yan C, Zhang Y, Tan J, Wang H, Zhou S, Pu S (2016) Purification and defibering of a Chinese sepiolite. Appl Clay Sci 124:119–126
192. de Lima JA, Camilo FF, Faez R, Cruz SA (2017) A new approch to sepiolite dispersion by treatment with ionic liquids. Appl Clay Sci 143:234–240
193. Liu J, Boo WJ, Clearfield A, Sue HJ (2006) Intercalation and exfoliation: a review on morphology of polymer nanocomposites reinforced by inorganic layer structures. Mater Manuf Process 21(2):143–151
194. Deng H, Lin P, Xin S, Huang R, Li W, Du Y, Zhou X, Yang J (2012) Quaternized chitosan-layered silicate intercalated composites based nanofibrous mats and their antibacterial activity. Carbohyd Polym 89(2):307–313
195. Li Z, Jiang WT, Chen CJ, Hong H (2010) Influence of chain lengths and loading levels on interlayer configurations of intercalated alkylammonium and their transitions in rectorite. Langmuir 26(11):8289–8294
196. De Cristofaro A, Violante A (2001) Effect of hydroxy-aluminium species on the sorption and interlayering of albumin onto montmorillonite. Appl Clay Sci 19(1):59–67
197. Xu S, Zhang S, Yang J (2008) An amphoteric semi-IPN nanocomposite hydrogels based on intercalation of cationic polyacrylamide into bentonite. Mater Lett 62(24):3999–4002
198. Huang X, Xu S, Zhong M, Wang J, Feng S, Shi R (2009) Modification of Na-bentonite by polycations for fabrication of amphoteric semi-IPN nanocomposite hydrogels. Appl Clay Sci 42(3):455–459
199. Chiu CW, Huang TK, Wang YC, Alamani BG, Lin JJ (2014) Intercalation strategies in clay/polymer hybrids. Prog Polym Sci 39(3):443–485
200. Monvisade P, Siriphannon P (2009) Chitosan intercalated montmorillonite: preparation, characterization and cationic dye adsorption. Appl Clay Sci 42(3):427–431
201. Huskić M, Žigon M (2007) PMMA/MMT nanocomposites prepared by one-step in situ intercalative solution polymerization. Eur Polym J 43(12):4891–4897
202. Du X, Xiao M, Meng Y, Hay AS (2004) Synthesis of poly (arylene disulfide)–vermiculite nanocomposites via in situ ring-opening polymerization of macrocyclic oligomers. Polym Int 53(6):789–793
203. Wang WB, Wang AQ (2009) Preparation, characterization and properties of superabsorbent nanocomposites based on natural guar gum and modified rectorite. Carbohyd Polym 77(4):891–897
204. Frost RL, Mako E, Kristóf J, Kloprogge JT (2002) Modification of kaolinite surfaces through mechanochemical treatment—a mid-IR and near-IR spectroscopic study. Spectrochim Acta A 58(13):2849–2859
205. Pérez-Maqueda LA, De Haro MCJ, Poyato J, Pérez-Rodríguez JL (2004) Comparative study of ground and sonicated vermiculite. J Mater Sci 39(16):5347–5351
206. Djukić A, Jovanović U, Tuvić T, Andrić V, Novaković JG, Ivanović N, Matović L (2013) The potential of ball-milled Serbian natural clay for removal of heavy metal contaminants from wastewaters: simultaneous sorption of Ni, Cr, cd and Pb ions. Ceram Int 39(6):7173–7178
207. Maleki S, Karimi-Jashni A (2017) Effect of ball milling process on the structure of local clay and its adsorption performance for Ni (II) removal. Appl Clay Sci 137:213–224
208. Yoshimoto S, Ohashi F, Ohnishi Y, Nonami T (2004) Synthesis of polyaniline–montmorillonite nanocomposites by the mechanochemical intercalation method. Syn Met 145(2):265–270
209. Polette-Niewold LA, Manciu FS, Torres B, Alvarado M, Chianelli RR (2007) Organic/inorganic complex pigments: ancient colors Maya blue. J Inorg Biochem 101(11):1958–1973

210. Wu W, SC L (2003) Mechano-chemical surface modification of calcium carbonate particles by polymer grafting. Powder Technol 137(1):41–48
211. Voronov A, Kohut A, Synytska A, Peukert W (2007) Mechanochemical modification of silica with poly (1-vinyl-2-pyrrolidone) by grinding in a stirred media mill. J Appl Polym Sci 104(6):3708–3714
212. Al-Futaisi A, Jamrah A, Al-Hanai R (2007) Aspects of cationic dye molecule adsorption to palygorskite. Desalination 214:327–342
213. Louati S, Hajjaji W, Baklouti S, Samet B (2014) Structure and properties of new eco-material obtained by phosphoric acid attack of natural Tunisian clay. Appl Clay Sci 101:60–67
214. Temuujin J, Senna M, Jadambaa T, Burmaa D, Erdenechimeg S, MacKenzie KJD (2006) Characterization and bleaching properties of acid-leached montmorillonite. J Chem Technol Biotechnol 81:688–693
215. Temuujin J, Senna M, Jadambaa T, Burmaa D, Erdenechimeg S, MacKenzie KJD (2006) Characterization and bleaching properties of acid-leached montmorillonite. J Chem Technol Biotechnol 81:688–693
216. Kilislioglu A, Aras G (2010) Adsorption of uranium from aqueous solution on heat and acid treated sepiolites. Appl Radiat Isot 68:2016–2019
217. Chaari I, Fakhfakh E, Chakroun S, Bouzid J, Boujelben N, Feki M, Rocha F, Jamoussi F (2008) Lead removal from aqueous solutions by a Tunisian smectitic clay. J Hazard Mater 156:545–551
218. Panda AK, Mishra BG, Mishra DK, Singh RK (2010) Effect of sulphuric acid treatment on the physico-chemical characteristics of kaolin clay. Colloid Surf A 363:98–104
219. Alkan M, Kalay B, Dogan M, Demirbas O (2008) Removal of copper ions from aqueous solutions by kaolinite and batch design. J Hazard Mater 153:867–876
220. Sennour R, Mimane G, Benghalem A, Taleb S (2009) Removal of the persistent pollutant chlorobenzene by adsorption onto activated montmorillonite. Appl Clay Sci 43:503–506
221. Toor M, Jin B (2012) Adsorption characteristics, isotherm, kinetics, and diffusion of modified natural bentonite for removing diazo dye. Chem Eng J 187:79–88
222. Mana M, Ouali MS, Lindheimer M, de Menorval LC (2008) Removal of lead from aqueous solutions with a treated spent bleaching earth. J Hazard Mater 159:358–364
223. Owabor CN, Ono UM, Isuekevbo A (2012) Enhanced sorption of naphthalene onto a modified clay adsorbent: effect of acid, base and salt modifications of clay on sorption kinetics. Adv Chem Eng Sci 2:330–335
224. Owabor CN, Ono UM, Isuekevbo A (2012) Enhanced sorption of naphthalene onto a modified clay adsorbent: effect of acid, base and salt modifications of clay on sorption kinetics. Adv Chem Eng Sci 2:330–335
225. Lakevičs V, Stepanova V, Skuja L, Dušenkova I, Ruplis A (2014) Influence of alkali and acidic treatment on sorption properties of Latvian illite clays. Key Eng Mater 604:71–74
226. Wang WB, Wang FF, Kang YR, Wang AQ (2015) Enhanced adsorptive removal of methylene blue from aqueous solution by alkali-activated palygorskite. Water Air Soil Pollut 226(3):83
227. Akpomie KG, Dawodu FA (2014) Efficient abstraction of nickel (II) and manganese (II) ions from solution onto an alkaline-modified montmorillonite. J Taibah Univ Sci 8(4):343–356
228. Öztop B, Shahwan T (2006) Modification of a montmorillonite–illite clay using alkaline hydrothermal treatment and its application for the removal of aqueous Cs^{+} ions. J Colloid Interface Sci 295(2):303–309
229. Lihareva N, Dimova L, Petrov O, Tzvetanova Y (2010) Ag^{+} sorption on natural and Na-exchanged clinoptilolite from eastern Rhodopes, Bulgaria. Microporous Mesoporous Mater 130:32–37
230. Coruh S (2008) The removal of zinc ions by natural and conditioned clinoptilolites. Desalination 225:41–57
231. Ma YL, ZR X, Guo T, You P (2004) Adsorption of methylene blue on cu (II)-exchanged montmorillonite. J Colloid Interf Sci 280(2):283–288

232. Huang FC, Lee JF, Lee CK, Tseng WN, Juang LC (2002) Effects of exchange titanium cations on the pore structure and adsorption characteristics of montmorillonite. J Colloid Interf Sci 256(2):360–366
233. Wang CC, Juang LC, Hsu TC, Lee CK, Lee JF, Huang FC (2004) Adsorption of basic dyes onto montmorillonite. J Colloid Interf Sci 273(1):80–86
234. Ye H, Chen F, Sheng Y, Sheng G, Fu J (2006) Adsorption of phosphate from aqueous solution onto modified palygorskites. Sep Purif Technol 50:283–290
235. Gan F, Zhou J, Wang H, Du C, Chen X (2009) Removal of phosphate from aqueous solution by thermally treated natural palygorskite. Water Res 43:2907–2915
236. Kuang W, Facey GA, Detellier C (2004) Dehydration and rehydration of palygorskite and the influence of water on the nanopores. Clay Clay Miner 52:635–642
237. Chen T, Liu H, Li J, Chen D, Chang D, Kong D, Frost RL (2011) Effect of thermal treatment on adsorption–desorption of ammonia and sulfur dioxide on palygorskite: change of surface acid-alkali properties. Chem Eng J 166:1017–1021
238. Chen H, Zhao J, Zhong A, Jin Y (2011) Removal capacity and adsorption mechanism of heat-treated palygorskite clay for methylene blue. Chem Eng J 174(1):143–150
239. Shariatmadari H, Mermut AR, Benke MB (1999) Sorption of selected cationic and neutral organic molecules on palygorskite and sepiolite. Clay Clay Miner 47:44–53
240. Sabah E, Turan M, Celik MS (2002) Adsorption mechanism of cationic surfactants onto acid- and heat-activated sepiolites. Water Res 36(16):3957–3964
241. Koswojo R, Utomo RP, Ju YH, Ayucitra A, Soetaredjo FE, Sunarso J, Ismadji S (2010) Acid green 25 removal from wastewater by organo-bentonite from Pacitan. Appl Clay Sci 48:81–86
242. Chen J, Li G, He Z, An T (2011) Adsorption and degradation of model volatile organic compounds by a combined titania–montmorillonite–silica photocatalyst. J Hazard Mater 190:416–423
243. Huang J, Wang X, Jin Q, Liu Y, Wang Y (2007) Removal of phenol from aqueous solution by adsorption onto OTMAC-modified attapulgite. J Environ Manag 84:229–236
244. Yilmaz N, Yapar S (2004) Adsorption properties of tetradecyl and hexadecyl trimethylammonium bentonites. Appl Clay Sci 27:223–228
245. Singla P, Mehta R, Upadhyay SN (2012) Clay modification by the use of organic cations. Green Sustain Chem 2:21–25
246. Anirudhan TS, Ramachandran M (2007) Surfactant-modified bentonite as adsorbent for the removal of humic acid from wastewaters. Appl Clay Sci 35:276–281
247. Hedley CB, Yuan G, Theng BKG (2007) Thermal analysis of montmorillonites modified with quaternary phosphonium and ammonium surfactants. Appl Clay Sci 35:180–188
248. Kan T, Jiang X, Zhou L, Yang M, Duan M, Liu P, Jiang X (2011) Removal of methyl orange from aqueous solutions using a bentonite modified with a new Gemini surfactant. Appl Clay Sci 54:184–187
249. Zhu J, Wang T, Zhu R, Ge F, Wei J, Yuan P, He H (2011) Novel polymer/surfactant modified montmorillonite hybrids and the implications for the treatment of hydrophobic organic compounds in wastewaters. Appl Clay Sci 51:317–322
250. Shah KJ, Mishra MK, Shukla AD, Imae T, Shah DO (2013) Controlling wettability and hydrophobicity of organoclays modified with quaternary ammonium surfactants. J Colloid Interface Sci 407:493–499
251. Tunc S, Duman O, Kanci B (2012) Rheological measurements of Na-bentonite and sepiolite particles in the presence of tetradecyltrimethylammonium bromide, sodium tetradecyl sulfonate and Brij 30 surfactants. Colloid Surf A 398:37–47
252. Gunawan NS, Indraswati N, YH J, Soetaredjo FE, Ayucitra A, Ismadji S (2010) Bentonites modified with anionic and cationic surfactants for bleaching of crude palm oil. Appl Clay Sci 47:462–464
253. Nathaniel E, Kurniawan A, Soetaredjo FE, Ismadji S (2011) Organo-bentonite for the adsorption of Pb(II) from aqueous solution: temperature dependent parameters of several adsorption equations. Desalin Water Treat 36:280–288

254. Sandy MV, Kurniawan A, Ayucitra A, Sunarso J, Ismadji S (2012) Removal of copper ions from aqueous solution by adsorption using LABORATORIES-modified bentonite (organo-bentonite). Front Chem Sci Eng 6:58–66
255. Kirby AJ, Camilleri P, Engberts JBN, Feiters MC, Nolte RJM, Soderman O, Bergsma M, Bell PC, Fielden ML, Garcia-Rodriguez CL, Guedat P, Kremer A, McGregor C, Perrin C, Ronsin G, Van Eijk MCP (2003) Gemini surfactants: new synthetic vectors for gene transfection. Angew Chem Int Ed 42:1448–1457
256. Liu Y, Gao M, Gu Z, Luo Z, Ye Y, Lu L (2014) Comparison between the removal of phenol and catechol by modified montmorillonite with two novel hydroxyl-containing Gemini surfactants. J Hazard Mater 267:71–80
257. Yang S, Gao M, Luo Z (2014) Adsorption of 2-Naphthol on the organo-montmorillonites modified by Gemini surfactants with different spacers. Chem Eng J 256:39–50
258. Suwandi AC, Indraswati N, Ismadji S (2012) Adsorption of N-methylated diaminotriphenilmethane dye (malachite green) on natural rarasaponin modified kaolin. Desalin Water Treat 41(1–3):342–355
259. Chandra IK, YH J, Ayucitra A, Ismadji S (2013) Evans blue removal from wastewater by rarasaponin–bentonite. Int J Environ Sci Technol 10(2):359–370
260. Kurniawan A, Sutiono H, YH J, Soetaredjo FE, Ayucitra A, Yudha A, Ismadji S (2011) Utilization of rarasaponin natural surfactant for organo-bentonite preparation: application for methylene blue removal from aqueous effluent. Microporous Mesoporous Mater 142(1): 184–193
261. Cui H, Qian Y, Li Q, Wei Z, Zhai J (2013) Fast removal of hg (II) ions from aqueous solution by amine-modified attapulgite. Appl Clay Sci 72:84–90
262. Mu B, Kang YR, Wang AQ (2013) Preparation of a polyelectrolyte-coated magnetic attapulgite composite for the adsorption of precious metals. J Mater Chem A1:4804–4811
263. Chakraborty U, Singha T, Chianelli RR, Hansda C, Paul PK (2017) Organic-inorganic hybrid layer-by-layer electrostatic self-assembled film of cationic dye methylene blue and a clay mineral: spectroscopic and atomic force microscopic investigations. J Lumin 187:322–332
264. Mu B, Wang AQ (2015) One-pot fabrication of multifunctional superparamagnetic attapulgite/Fe3O4/polyaniline nanocomposites served as adsorbent and catalyst support. J Mater Chem A3:281–289
265. Peng Y, Chen D, Ji J, Kong Y, Wan H, Yao C (2013) Chitosan-modified palygorskite: preparation, characterization and reactive dye removal. Appl Clay Sci 74:81–86
266. Gecol H, Ergican E, Miakatsindila P (2005) Biosorbent for tungsten species removal from water: effects of co-occurring inorganic species. J Colloid Interface Sci 292:344–353
267. Meenakshi A, Natalia KE, Kathryn AM, Yoshinari B, Jilska MP, Stevens GW (2010) Surface modification of natural zeolite by chitosan and its use for nitrate removal in cold regions. Cold Reg Sci Technol 62:92–97
268. Futalan CM, Kan CC, Dalida ML (2011) Comparative and competitive adsorption of copper, lead, and nickel using chitosan immobilized on bentonite. Carbohyd Polym 83:528–536
269. Zhai R, Zhang B, Wan Y, Li C, Wang J, Liu J (2013) Chitosan–halloysite hybrid-nanotubes: horseradish peroxidase immobilization and applications in phenol removal. Chem Eng J 214:304–309
270. Marrakchi F, Khanday WA, Asif M, Hameed BH (2016) Cross-linked chitosan/sepiolite composite for the adsorption of methylene blue and reactive orange 16. Int J Biol Macromol 93:1231–1239
271. He H, Tao Q, Zhu J, Yuan P, Shen W, Yang S (2013) Silylation of clay mineral surfaces. Appl Clay Sci 71:15–20
272. De Paiva LB, Morales AR, Díaz FRV (2008) Organoclays: properties, preparation and applications. Appl Clay Sci 42(1):8–24
273. Celis R, Hermosin MC, Cornejo J (2000) Heavy metal adsorption by functionalized clays. Environ Sci Technol 34(21):4593–4599

274. Mercier L, Detellier C (1995) Preparation, characterization, and applications as heavy metals sorbents of covalently grafted thiol functionalities on the interlamellar surface of montmorillonite. Environ Sci Technol 29(5):1318–1323
275. Xue A, Zhou S, Zhao Y, Lu X, Han P (2011) Effective NH 2-grafting on attapulgite surfaces for adsorption of reactive dyes. J Hazard Mater 194:7–14
276. Guimarães ADMF, Ciminelli VST, Vasconcelos WL (2009) Smectite organofunctionalized with thiol groups for adsorption of heavy metal ions. Appl Clay Sci 42(3):410–414
277. Mercier L, Pinnavaia TJ (1998) A functionalized porous clay heterostructure for heavy metal ion (Hg^{2+}) trapping. Microporous Mesoporous Mater 20(1–3):101–106
278. Liu P, Wang TM (2007) Adsorption properties of hyperbranched aliphatic polyester grafted attapulgite towards heavy metal ions. J Hazard Mater 149(1):75–79
279. MacEwan DM, Wilson MJ (1980) Interlayer and intercalation complexes of clay minerals. In: Crystal structures of clay minerals and their X-ray identification, vol 5. Mineralogical Society, London, pp 197–248
280. Wang L, Wang AQ (2008) Adsorption properties of Congo red from aqueous solution onto surfactant-modified montmorillonite. J Hazard Mater 160(1):173–180
281. Fan H, Zhou L, Jiang X, Huang Q, Lang W (2014) Adsorption of Cu^{2+} and methylene blue on dodecyl sulfobetaine surfactant-modified montmorillonite. Appl Clay Sci 95:150–158
282. Anirudhan TS, Ramachandran M (2015) Adsorptive removal of basic dyes from aqueous solutions by surfactant modified bentonite clay (organoclay): kinetic and competitive adsorption isotherm. Process Saf Environ 95:215–225
283. Huang Y, Ma X, Liang G, Yan H (2008) Adsorption of phenol with modified rectorite from aqueous solution. Chem Eng J 141:1): 1–1): 8
284. Liu Y, Wang WB, Wang AQ (2010) Removal of congo red from aqueous solution by sorption on organified rectorite. Clean–Soil Air Water 38(7):670–677
285. Sánchez-Martín MJ, Dorado MC, Del Hoyo C, Rodríguez-Cruz MS (2008) Influence of clay mineral structure and surfactant nature on the adsorption capacity of surfactants by clays. J Hazard Mater 150(1):115–123
286. Sanchez-Martin MJ, Rodriguez-Cruz MS, Andrades MS, Sanchez-Camazano M (2006) Efficiency of different clay minerals modified with a cationic surfactant in the adsorption of pesticides: influence of clay type and pesticide hydrophobicity. Appl Clay Sci 31(3):216–228
287. Alkaram UF, Mukhlis AA, Al-Dujaili AH (2009) The removal of phenol from aqueous solutions by adsorption using surfactant-modified bentonite and kaolinite. J Hazard Mater 169(1):324–332
288. Darder M, Colilla M, Ruiz-Hitzky E (2003) Biopolymer− clay nanocomposites based on chitosan intercalated in montmorillonite. Chem Mater 15(20):3774–3780
289. Lu Y, Chang PR, Zheng P, Ma X (2015) Porous 3D network rectorite/chitosan gels: preparation and adsorption properties. Appl Clay Sci 107:21–27
290. Dalida MLP, Mariano AFV, Futalan CM, Kan CC, Tsai WC, Wan MW (2011) Adsorptive removal of cu (II) from aqueous solutions using non-crosslinked and crosslinked chitosan-coated bentonite beads. Desalination 275(1):154–159
291. Vanamudan A, Pamidimukkala P (2015) Chitosan, nanoclay and chitosan–nanoclay composite as adsorbents for rhodamine-6G and the resulting optical properties. Int J Biol Macromol 74:127–135
292. Bleiman N, Mishael YG (2010) Selenium removal from drinking water by adsorption to chitosan–clay composites and oxides: batch and columns tests. J Hazard Mater 183(1):590–595
293. Pereira FAR, Sousa KS, Cavalcanti GRS, Fonseca MG, de Souza AG, Alves APM (2013) Chitosan-montmorillonite biocomposite as an adsorbent for copper (II) cations from aqueous solutions. Int J Biol Macromol 61:471–478
294. Zhang D, Zhou CH, Lin CX, Tong DS, Yu WH (2010) Synthesis of clay minerals. Appl Clay Sci 50(1):1–11

295. Zhang ZF, Wang WB, Wang AQ (2015) Effects of solvothermal process on the physicochemical and adsorption characteristics of palygorskite. Appl Clay Sci 107:230–237
296. Wang WB, Tian GY, Zhang ZF, Wang AQ (2015) A simple hydrothermal approach to modify palygorskite for high-efficient adsorption of methylene blue and cu (II) ions. Chem Eng J 265:228–238
297. Tian GY, Wang WB, Kang YR, Wang AQ (2016) Palygorskite in sodium sulphide solution via hydrothermal process for enhanced methylene blue adsorption. J Taiwan Inst Chem E 58:417–423
298. Tian GY, Wang WB, Kang YR, Wang AQ (2016) Ammonium sulfide-assisted hydrothermal activation of palygorskite for enhanced adsorption of methyl violet. J Environ Sci 41:33–43
299. Zhang ZF, Wang WB, Wang AQ (2015) High-pressure homogenization associated hydrothermal process of palygorskite for enhanced adsorption of methylene blue. Appl Surf Sci 329:306–314
300. Wang WB, Tian GY, Zhang ZF, Wang AQ (2016) From naturally low-grade palygorskite to hybrid silicate adsorbent for efficient capture of cu (II) ions. Appl Clay Sci 132:438–448
301. Zhang ZF, Wang WB, Wang AQ (2015) Highly effective removal of methylene blue using functionalized attapulgite via hydrothermal process. J Environ Sci 33:106–115
302. Zhang ZF, Wang WB, Kang YR, Zong L, Wang AQ (2016) Tailoring the properties of palygorskite by various organic acids via a one-pot hydrothermal process: a comparative study for removal of toxic dyes. Appl Clay Sci 120:28–39
303. Zhang ZF, Wang WB, Kang YR, Zong L, Wang AQ (2015) Glycine-assisted evolution of palygorskite via a one-step hydrothermal process to give an efficient adsorbent for capturing Pb (II) ions. RSC Adv 5(117):96829–96839
304. Zhang Y, Wang WB, Zhang JP, Liu P, Wang AQ (2015) A comparative study about adsorption of natural palygorskite for methylene blue. Chem Eng J 262:390–398
305. Wang WB, Tian GY, Zong L, Wang Q, Zhou YM, Wang AQ (2016) Mesoporous hybrid Zn-silicate derived from red palygorskite clay as a high-efficient adsorbent for antibiotics. Microporous Mesoporous Mater 234:317–325
306. Wang WB, Tian GY, Wang DD, Zhang ZF, Kang YR, Zong L, Wang AQ (2016) All-into-one strategy to synthesize mesoporous hybrid silicate microspheres from naturally rich red palygorskite clay as high-efficient adsorbents. Sci Rep 6:39599
307. Wang WB, Tian GY, Zong L, Zhou YM, Kang YR, Wang Q, Wang AQ (2017) From illite/smectite clay to mesoporous silicate adsorbent for efficient removal of chlortetracycline from water. J Environ Sci 51:31–43
308. Tian GY, Wang WB, Zong L, Kang YR, Wang AQ (2016) A functionalized hybrid silicate adsorbent derived from naturally abundant low-grade palygorskite clay for highly efficient removal of hazardous antibiotics. Chem Eng J 293:376–385
309. Bakandritsos A, Steriotis T, Petridis D (2004) High surface area montmorillonite−carbon composites and derived carbons. Chem Mater 16(8):1551–1559
310. XP W, Zhu WY, Zhang XL, Chen TH, Frost RL (2011) Catalytic deposition of nanocarbon onto palygorskite and its adsorption of phenol. Appl Clay Sci 52:400–406
311. Chen LF, Liang HW, Lu Y, Cui CH, SH Y (2011) Synthesis of an attapulgite clay@ carbon nanocomposite adsorbent by a hydrothermal carbonization process and their application in the removal of toxic metal ions from water. Langmuir 27(14):8998–9004
312. Wu X, Gao P, Zhang X, Jin G, Xu Y, Wu Y (2014) Synthesis of clay/carbon adsorbent through hydrothermal carbonization of cellulose on palygorskite. Appl Clay Sci 95:60–66
313. Liu W, Yao C, Wang M, Ji J, Ying L, Fu C (2013) Kinetics and thermodynamics characteristics of cationic yellow X-GL adsorption on attapulgite/rice hull-based activated carbon nanocomposites. Environ Prog Sustain 32(3):655–662
314. Ai L, Li L (2013) Efficient removal of organic dyes from aqueous solution with ecofriendly biomass-derived carbon@ montmorillonite nanocomposites by one-step hydrothermal process. Chem Eng J 223:688–695

315. Zhang R, Chen C, Li J, Wang X (2015) Preparation of montmorillonite@ carbon composite and its application for U (VI) removal from aqueous solution. Appl Surf Sci 349:129–137
316. Wu LM, Tong DS, Li CS, Ji SF, Lin CX, Yang HM, Zhong ZK, CY X, Zhou CH (2016) Insight into formation of montmorillonite-hydrochar nanocomposite under hydrothermal conditions. Appl Clay Sci 119:116–125
317. Tian GY, Wang WB, Mu B, Kang YR, Wang AQ (2015) Facile fabrication of carbon/attapulgite composite for bleaching of palm oil. J Taiwan Inst Chem E 50:252–258
318. Mahramanlioglu M, Güçlü K (2004) Equilibrium, kinetic and mass transfer studies and column operations for the removal of arsenic (III) from aqueous solutions using acid treated spent bleaching earth. Environ Technol 25(9):1067–1076
319. Wambu EW, Muthakia GK, Shiundu PM (2009) Regeneration of spent bleaching earth and its adsorption of copper (II) ions from aqueous solutions. Appl Clay Sci 46(2):176–180
320. Tsai WT, Chen HP, Hsieh MF, Sun HF, Lai CW (2003) Regeneration of bleaching clay waste by chemical activation with chloride salts. J Environ Sci Heal A 38(4):685–696
321. Tsai WT, Lai CW (2006) Adsorption of herbicide paraquat by clay mineral regenerated from spent bleaching earth. J Hazard Mater 134(1):144–148
322. Tang J, Mu B, Zong L, Zheng M, Wang A (2015) Fabrication of attapulgite/carbon composites from spent bleaching earth for the efficient adsorption of methylene blue. RSC Adv 5(48): 38443–38451
323. Tang J, Mu B, Wang WB, Zheng MS, Wang AQ (2016) Fabrication of manganese dioxide/carbon/attapulgite composites derived from spent bleaching earth for adsorption of Pb (II) and brilliant green. RSC Adv 6(43):36534–36543
324. Tang J, Mu B, Zong L, Zheng M, Wang A (2017) Facile and green fabrication of magnetically recyclable carboxyl-functionalized attapulgite/carbon nanocomposites derived from spent bleaching earth for wastewater treatment. Chem Eng J 322:102–114
325. Tsai WT, Chen HP, Hsien WY, Lai CW, Lee MS (2003) Thermochemical regeneration of bleaching earth waste with zinc chloride. Resour Conserv Recy 39(1):65–77
326. Mana M, Ouali MS, De Menorval LC, Zajac JJ, Charnay C (2011) Regeneration of spent bleaching earth by treatment with cethyltrimethylammonium bromide for application in elimination of acid dye. Chem Eng J 174(1):275–280
327. Chang JI, Tai HS, Huang TH (2006) Regeneration of spent bleaching earth by lye-extraction. Environ Prog Sustain 25(4):373–378
328. Pourvosoghi N, Nikbakht AM, Jafarmadar S (2013) An optimized process for biodiesel production from high FFA spent bleaching earth. Int J Eng Trans C Aspects 26(12):1545–1550
329. Sahafi SM, Goli SAH, Tabatabaei M, Nikbakht A, Pourvosoghi N (2016) The reuse of waste cooking oil and spent bleaching earth to produce biodiesel. Energ Source Part A 38(7): 942–950
330. Abdulbari HA, Rosli MY, Abdurrahman HN, Nizam MK (2011) Lubricating grease from spent bleaching earth and waste cooking oil: tribology properties. Int J Phys Sci 6(20):4695–4699
331. Eliche-Quesada D, Corpas-Iglesias FA (2014) Utilisation of spent filtration earth or spent bleaching earth from the oil refinery industry in clay products. Ceram Int 40(10):16677–16687
332. Tian GY, Wang WB, Zong L, Kang YR, Wang AQ (2016) From spent dye-loaded palygorskite to a multifunctional palygorskite/carbon/ag nanocomposite. RSC Adv 6(48):41696–41706
333. Wang WB, Huang DJ, Kang YR, Wang AQ (2013b) One-step in-situ fabrication of a granular semi-IPN hydrogel based on chitosan and gelatin for fast and efficient adsorption of Cu^{2+} ion. Colloid Surface B 106:51–59
334. Wang WB, Kang YR, Wang AQ (2013c) One-step fabrication in aqueous solution of a granular alginate-based hydrogel for fast and efficient removal of heavy metal ions. J Polym Res 20:101. (10pp)
335. Zhu YF, Wang WB, Zheng YA, Wang F, Wang AQ (2016) Rapid enrichment of rare-earth metals by carboxymethyl cellulose-based open-cellular hydrogel adsorbent from HIPEs template. Carbohyd Polym 140:51–58

336. Zhu YF, Wang WB, Zhang HF, Ye XS, Wu Z, Wang AQ (2017) Fast and high-capacity adsorption of Rb^{+} and Cs^{+} onto recyclable magnetic porous spheres. Chem Eng J 327:982–991
337. Wang X, Zheng Y, Wang A (2009) Fast removal of copper ions from aqueous solution by chitosan-g-poly (acrylic acid)/attapulgite composites. J Hazard Mater 168(2):970–977
338. Zheng Y, Zhu Y, Wang A (2014) Highly efficient and selective adsorption of malachite green onto granular composite hydrogel. Chem Eng J 257:66–73
339. Natkański P, Kuśtrowski P, Białas A, Piwowarska Z, Michalik M (2013) Thermal stability of montmorillonite polyacrylamide and polyacrylate nanocomposites and adsorption of Fe (III) ions. Appl Clay Sci 75:153–157
340. Zhu L, Zhang L, Tang Y, Kou X (2014) Synthesis of sodium alginate graft poly (acrylic acid-co-2-acrylamido-2-methyl-1-propane sulfonic acid)/attapulgite hydrogel composite and the study of its adsorption. Polym-Plast Technol 53(1):74–79
341. Bulut Y, Akçay G, Elma D, Serhatlı IE (2009) Synthesis of clay-based superabsorbent composite and its sorption capability. J Hazard Mater 171(1):717–723
342. Zheng YA, Wang AQ (2010) Removal of heavy metals using polyvinyl alcohol semi-IPN poly (acrylic acid)/tourmaline composite optimized with response surface methodology. Chem Eng J 162(1):186–193
343. Güçlü G, Al E, Emik S, İyim TB, Özgümüş S, Özyürek M (2010) Removal of Cu^{2+} and Pb^{2+} ions from aqueous solutions by starch-graft-acrylic acid/montmorillonite superabsorbent nanocomposite hydrogels. Polym Bull 65(4):333–346
344. Wu L, Ye Y, Liu F, Tan C, Liu H, Wang S, Wu W (2013) Organo-bentonite-Fe_3O_4 poly (sodium acrylate) magnetic superabsorbent nanocomposite: synthesis, characterization, and thorium (IV) adsorption. Appl Clay Sci 83:405–414
345. Kaşgöz H, Durmuş A, Kaşgöz A (2008) Enhanced swelling and adsorption properties of AAm-AMPSNa/clay hydrogel nanocomposites for heavy metal ion removal. Polym Adv Technol 19(3):213–220
346. Chen Y, Zhao Y, Zhou S, Chu X, Yang L, Xing W (2009) Preparation and characterization of polyacrylamide/palygorskite. Appl Clay Sci 46(2):148–152
347. Chen H, Wang AQ (2009) Adsorption characteristics of cu (II) from aqueous solution onto poly (acrylamide)/attapulgite composite. J Hazard Mater 165(1):223–231
348. Zhang JP, Wang AQ (2010) Adsorption of Pb(II) from aqueous solution by chitosan-g-poly (acrylic acid)/attapulgite/sodium humate composite hydrogels. J Chem Eng Data 55:2379–2384
349. Irani M, Ismail H, Ahmad Z, Fan M (2015) Synthesis of linear low-density polyethylene-g-poly (acrylic acid)-co-starch/organo-montmorillonite hydrogel composite as an adsorbent for removal of Pb (II) from aqueous solutions. J Environ Sci 27:9–20
350. Anirudhan TS, Rijith S (2012) Synthesis and characterization of carboxyl terminated poly (methacrylic acid) grafted chitosan/bentonite composite and its application for the recovery of uranium (VI) from aqueous media. J Environ Radioactiv 106:8–19
351. Anirudhan TS, Suchithra PS, Senan P, Tharun AR (2012) Kinetic and equilibrium profiles of adsorptive recovery of thorium (IV) from aqueous solutions using poly (methacrylic acid) grafted cellulose/bentonite superabsorbent composite. Ind Eng Chem Res 51(13):4825–4836
352. Liu Y, Wang WB, Wang AQ (2010) Adsorption of lead ions from aqueous solution by using carboxymethyl cellulose-g-poly (acrylic acid)/attapulgite hydrogel composites. Desalination 259(1):258–264
353. Liu P, Jiang L, Zhu L, Wang AQ (2014) Novel approach for attapulgite/poly (acrylic acid) (ATP/PAA) nanocomposite microgels as selective adsorbent for Pb (II) ion. React Funct Polym 74:72–80
354. Liu P, Jiang L, Zhu L, Guo J, Wang AQ (2015) Synthesis of covalently crosslinked attapulgite/poly (acrylic acid-co-acrylamide) nanocomposite hydrogels and their evaluation as adsorbent for heavy metal ions. J Ind Eng Chem 23:188–193
355. Liu P, Jiang L, Zhu L, Wang AQ (2013) Attapulgite/poly (acrylic acid) nanocomposite (ATP/PAA) hydrogels with multifunctionalized attapulgite (org-ATP) nanorods as unique cross-

linker: preparation optimization and selective adsorption of Pb (II) ion. ACS Sus Chem Eng 2 (4):643–651
356. Zheng YA, Wang AQ (2010) Preparation and ammonium adsorption properties of biotite-based hydrogel composites. Ind Eng Chem Res 49(13):6034–6041
357. Zheng Y, Zhang J, Wang A (2009) Fast removal of ammonium nitrogen from aqueous solution using chitosan-g-poly (acrylic acid)/attapulgite composite. Chem Eng J 155(1):215–222
358. Zheng Y, Wang A (2009) Evaluation of ammonium removal using a chitosan-g-poly (acrylic acid)/rectorite hydrogel composite. J Hazard Mater 171(1):671–677
359. Zheng Y, Xie Y, Wang A (2012) Rapid and wide pH-independent ammonium-nitrogen removal using a composite hydrogel with three-dimensional networks. Chem Eng J 179:90–98
360. Kaplan M, Kasgoz H (2011) Hydrogel nanocomposite sorbents for removal of basic dyes. Polym Bull 67(7):1153–1168
361. Li P, Kim NH, Heo SB, Lee JH (2008) Novel PAAm/Laponite clay nanocomposite hydrogels with improved cationic dye adsorption behavior. Compos Part B Eng 39(5):756–763
362. Dalaran M, Emik S, Güçlü G, İyim TB, Özgümüş S (2011) Study on a novel polyampholyte nanocomposite superabsorbent hydrogels: synthesis, characterization and investigation of removal of indigo carmine from aqueous solution. Desalination 279(1):170–182
363. Wang Y, Zeng L, Ren X, Song H, Wang A (2010) Removal of methyl violet from aqueous solutions using poly (acrylic acid-co-acrylamide)/attapulgite composite. J Environ Sci 22(1): 7–14
364. Yi JZ, Zhang LM (2008) Removal of methylene blue dye from aqueous solution by adsorption onto sodium humate/polyacrylamide/clay hybrid hydrogels. Bioresour Technol 99(7): 2182–2186
365. Zhang LM, Zhou YJ, Wang Y (2006) Novel hydrogel composite for the removal of water-soluble cationic dye. J Chem Technol Biotechnol 81(5):799–804
366. Liu Y, Zheng Y, Wang A (2010) Enhanced adsorption of methylene blue from aqueous solution by chitosan-g-poly (acrylic acid)/vermiculite hydrogel composites. J Environ Sci 22(4):486–493
367. Yang L, Ma X, Guo N (2012) Sodium alginate/Na^+-rectorite composite microspheres: preparation, characterization, and dye adsorption. Carbohyd Polym 90(2):853–858
368. Liu Y, Zheng YA, Wang AQ (2011) Effect of biotite content of hydrogels on enhanced removal of methylene blue from aqueous solution. Ionics 17(6):535–543
369. Shi Y, Xue Z, Wang X, Wang L, Wang A (2013) Removal of methylene blue from aqueous solution by sorption on lignocellulose-g-poly (acrylic acid)/montmorillonite three-dimensional cross-linked polymeric network hydrogels. Polym Bull 70(4):1163–1179
370. Wang AQ, Wang WB (2009) Superabsorbent materials. Kirk-Othmer Encycl Chem Technol. https://doi.org/10.1002/0471238961.supewang.a01
371. Kabiri K, Omidian H, Zohuriaan-Mehr MJ, Doroudiani S (2011) Superabsorbent hydrogel composites and nanocomposites: a review. Polym Compos 32(2):277–289
372. Bao Y, Ma J, Sun Y (2012) Swelling behaviors of organic/inorganic composites based on various cellulose derivatives and inorganic particles. Carbohyd Polym 88(2):589–595
373. Olad A, Gharekhani H, Mirmohseni A, Bybordi A (2017) Synthesis, characterization, and fertilizer release study of the salt and pH-sensitive NaAlg-g-poly (AA-co-AAm)/RHA superabsorbent nanocomposite. Polym Bull 74(8):3353–3377
374. Fanta GF, Burr RC, Russell CR, Rist CE (1966) Graft copolymers of starch. I. Copolymerization of gelatinized wheat starch with acrylonitrile. Fractionation of copolymer and effect of solvent on copolymer composition. J Appl Polym Sci 10(6):929–937
375. Bajpai AK, Giri A (2002) Swelling dynamics of a macromolecular hydrophilic network and evaluation of its potential for controlled release of agrochemicals. React Funct Polym 53(2): 125–141
376. Li A, Wang A, Chen J (2004) Studies on poly (acrylic acid)/attapulgite superabsorbent composite. I. Synthesis and characterization. J Appl Polym Sci 92(3):1596–1603

377. Qi X, Liu M, Chen Z, Liang R (2007) Preparation and properties of diatomite composite superabsorbent. Polym Adv Technol 18(3):184–193
378. Lee WF, Yang LG (2004) Superabsorbent polymeric materials. XII. Effect of montmorillonite on water absorbency for poly (sodium acrylate) and montmorillonite nanocomposite superabsorbents. J Appl Polym Sci 92(5):3422–3429
379. Urbano B, Rivas BL (2011) Poly (sodium 4-styrene sulfonate) and poly (2-acrylamidoglycolic acid) nanocomposite hydrogels: montmorillonite effect on water absorption, thermal, and rheological properties. Polym Bull 67(9):1823–1836
380. Wang WB, Zhang JP, Chen H, Wang AQ (2007) Study on superabsorbent composite. VIII. Effects of acid-and heat-activated attapulgite on water absorbency of polyacrylamide/attapulgite. J Appl Polym Sci 103(4):2419–2424
381. Lee WF, Chen YC (2005) Preparation of reactive mineral powders used for poly (sodium acrylate) composite superabsorbents. J Appl Polym Sci 97(3):855–861
382. Santiago F, Mucientes AE, Osorio M, Poblete FJ (2006) Synthesis and swelling behaviour of poly (sodium acrylate)/sepiolite superabsorbent composites and nanocomposites. Polym Int 55(8):843–848
383. Mu Y, Du D, Yang R, Xu Z (2015) Preparation and performance of poly (acrylic acid–methacrylic acid)/montmorillonite microporous superabsorbent nanocomposite. Mater Lett 142:94–96
384. Wang Y, Zhang X, Wei H, Zhang B, Xiang X, Chen R (2015) Synthesis of poly (AA-co-AM) superabsorbent composites by reinforcement of halloysite nanotubes. Polym Compos 36(2):229–236
385. Liu C, Yu L, Zhang Y, Zhang B, Liu J, Zhang H (2013) Preparation of poly (sodium acrylate-acrylamide) superabsorbent nanocomposites incorporating graphene oxide and halloysite nanotubes. RSC Adv 3(33):13756–13763
386. Wan T, Wang X, Yuan Y, He W (2006) Preparation of a kaolinite–poly (acrylic acid acrylamide) water superabsorbent by photopolymerization. J Appl Polym Sci 102(3):2875–2881
387. Patra SK, Swain SK (2011) Swelling study of superabsorbent PAA-co-PAM/clay nanohydrogel. J Appl Polym Sci 120(3):1533–1538
388. Zhang Y, Gu Q, Yin J, Wang Z, He P (2014) Effect of organic montmorillonite type on the swelling behavior of superabsorbent nanocomposites. Adv Polym Technol 33(2):21400
389. Kalaleh HA, Tally M, Atassi Y (2015) Preparation of bentonite-g-poly (acrylate-co-acrylamide) superabsorbent polymer composite for agricultural applications: optimization and characterization. Polym Sci Series B 57(6):750–758
390. Wan T, Zhou Z, Huang R, Zou C, Xu M, Cheng W, Li R (2014) Synthesis and swelling properties of microcrystal muscovite composite superabsorbent. Appl Clay Sci 101:199–204
391. Tang Q, Lin J, Wu J, Xu Y, Zhang C (2007) Preparation and water absorbency of a novel poly (acrylate-co-acrylamide)/vermiculite superabsorbent composite. J Appl Polym Sci 104(2): 735–739
392. Swain SK, Shur B, Patra SK (2013) Poly (acrylamide-co-vinyl alcohol)—superabsorbent materials reinforced by modified clay. Polym Compos 34(11):1794–1800
393. Foungfung D, Phattanarudee S, Seetapan N, Kiatkamjornwong S (2011) Acrylamide–itaconic acid superabsorbent polymers and superabsorbent polymer/mica nanocomposites. Polym for Adv Technol 22(5):635–647
394. Qi X, Liu M, Chen Z (2015) Study on swelling behavior of poly (sodium acrylate-co-2-acryloylamino-2-methyl-1-propanesulfonic acid)/attapulgite macroporous superabsorbent composite. Polym Eng Sci 55(3):681–687
395. Irani M, Ismail H, Ahmad Z (2014) Hydrogel composites based on linear low-density polyethylene-g-poly (acrylic acid)/kaolin or halloysite nanotubes. J Appl Polym Sci 131(8): 40101
396. Wang WB, Kang YR, Wang AQ (2010) Synthesis, characterization and swelling properties of guar gum-g-poly (sodium acrylate-co-styrene)/muscovite superabsorbent composites. Sci Technol Adv Mater 11(2):025006

397. Yang L, Ma X, Guo N (2011) Synthesis and properties of sodium alginate/Na^+ rectorite grafted acrylic acid composite superabsorbent via ^{60}Co γ irradiation. Carbohyd Polym 85(2):413–418
398. Ferfera-Harrar H, Aiouaz N, Dairi N, Hadj-Hamou AS (2014) Preparation of chitosan-g-poly (acrylamide)/montmorillonite superabsorbent polymer composites: studies on swelling, thermal, and antibacterial properties. J Appl Polym Sci 131(1):39747
399. Yan Z, Lin Z, Kai M, Guozhu M (2014) The surface modification of zeolite 4a and its effect on the water-absorption capability of starch-g-poly (acrylic acid) composite. Clay Clay Miner 62(3):211–223
400. Zhang Y, Zhao L, Chen Y (2015) Synthesis and characterization of starch-g-poly (acrylic acid)/Organo-zeolite 4A superabsorbent composites with respect to their water-holding capacities and nutrient-release behavior. Polym Compos 38:1838–1848
401. Wu J, Wei Y, Lin J, Lin S (2003) Preparation of a starch-graft-acrylamide/kaolinite superabsorbent composite and the influence of the hydrophilic group on its water absorbency. Polym Int 52(12):1909–1912
402. Li A, Liu R, Wang A (2005) Preparation of starch-graft-poly (acrylamide)/attapulgite superabsorbent composite. J Appl Polym Sci 98(3):1351–1357
403. Zhou M, Zhao J, Zhou L (2011) Utilization of starch and montmorrilonite for the preparation of superabsorbent nanocomposite. J Appl Polym Sci 121(4):2406–2412
404. Zhang JP, Li A, Wang AQ (2006) Study on superabsorbent composite. VI. Preparation, characterization and swelling behaviors of starch phosphate-graft-acrylamide/attapulgite superabsorbent composite. Carbohyd Polym 65(2):150–158
405. Likhitha M, Sailaja RRN, Priyambika VS, Ravibabu MV (2014) Microwave assisted synthesis of guar gum grafted sodium acrylate/cloisite superabsorbent nanocomposites: reaction parameters and swelling characteristics. Int J Biol Macromol 65:500–508
406. Shi XN, Wang WB, Wang AQ (2011) Synthesis and enhanced swelling properties of a guar gum-based superabsorbent composite by the simultaneous introduction of styrene and attapulgite. J Polym Res 18(6):1705–1713
407. Zhai NH, Wang WB, Wang AQ (2011) Synthesis and swelling characteristics of a pH-responsive guar gum-g-poly (sodium acrylate)/medicinal stone superabsorbent composite. Polym Compos 32(2):210–218
408. Yadav M, Rhee KY (2012) Superabsorbent nanocomposite (alginate-g-PAMPS/MMT): synthesis, characterization and swelling behavior. Carbohyd Polym 90(1):165–173
409. Yang HX, Wang WB, Wang AQ (2012) A pH-sensitive biopolymer-based superabsorbent nanocomposite from sodium alginate and attapulgite: synthesis, characterization, and swelling behaviors. J Disper Sci Technol 33(8):1154–1162
410. Wang YZ, Wang WB, Shi XN, Wang AQ (2013) Enhanced swelling and responsive properties of an alginate-based superabsorbent hydrogel by sodium p-styrenesulfonate and attapulgite nanorods. Polym Bull 70(4):1181–1193
411. Pourjavadi A, Ghasemzadeh H, Soleyman R (2007) Synthesis, characterization, and swelling behavior of alginate-g-poly (sodium acrylate)/kaolin superabsorbent hydrogel composites. J Appl Polym Sci 105(5):2631–2639
412. Wu J, Lin J, Zhou M, Wei C (2000) Synthesis and properties of starch-graft-polyacrylamide/clay superabsorbent composite. Macromol Rapid Commun 21(15):1032–1034
413. Deng J, Yang L, Liang G, He S (2013) Preparation, characterization and swelling Behaviors sodium alginate-graft-acrylic acid/Na^+ Rectorite superabsorbent composites. J Inorg Organomet 23(3):525–532
414. Shi XN, Wang WB, Kang YR, Wang AQ (2012) Enhanced swelling properties of a novel sodium alginate-based superabsorbent composites: NaAlg-g-poly (NaA-co-St)/APT. J Appl Polym Sci 125(3):1822–1832
415. Wang YZ, Wang WB, Shi XN, Wang AQ (2013) A superabsorbent nanocomposite based on sodium alginate and illite/smectite mixed-layer clay. J Appl Polym Sci 130(1):161–167

416. Ma G, Ran F, Yang Q, Feng E, Lei Z (2015) Eco-friendly superabsorbent composite based on sodium alginate and organo-loess with high swelling properties. RSC Adv 5(66): 53819–53828
417. Ding X, Li L, Liu PS, Zhang J, Zhou NL, Lu S, Shen J (2009) The preparation and properties of dextrin-graft-acrylic acid/montmorillonite superabsorbent nanocomposite. Polym Compos 30(7):976–981
418. Marandi GB, Mahdavinia GR, Ghafary S (2011) Collagen-g-poly (sodium acrylate-co-acrylamide)/sodium montmorillonite superabsorbent nanocomposites: synthesis and swelling behavior. J Polym Res 18(6):1487–1499
419. Zhang JP, Wang Q, Wang AQ (2007) Synthesis and characterization of chitosan-g-poly (acrylic acid)/attapulgite superabsorbent composites. Carbohyd Polym 68(2):367–374
420. Xie H, Jia Z, Huang J, Zhang C (2011) Study on the preparation of superabsorbent composite of chitosan-g-poly (acrylic acid)/kaolin by in-situ polymerization. Int J Chem 3(3):69
421. Rodrigues FH, Pereira AG, Fajardo AR, Muniz EC (2013) Synthesis and characterization of chitosan-graft-poly (acrylic acid)/nontronite hydrogel composites based on a design of experiments. J Appl Polym Sci 128(5):3480–3489
422. Zhang J, Wang L, Wang A (2007) Preparation and properties of chitosan-g-poly (acrylic acid)/montmorillonite superabsorbent nanocomposite via in situ intercalative polymerization. Ind Eng Chem Res 46(8):2497–2502
423. Liu JH, Wang AQ (2008) Study on superabsorbent composites. XXI. Synthesis, characterization and swelling behaviors of chitosan-g-poly (acrylic acid)/organo-rectorite nanocomposite superabsorbents. J Appl Polym Sci 110(2):678–686
424. Ferfera-Harrar H, Aiouaz N, Dairi N, Hadj-Hamou AS (2014) Preparation of chitosan-g-poly (acrylamide)/montmorillonite superabsorbent polymer composites: studies on swelling, thermal, and antibacterial properties. J Appl Polym Sci 131:39747
425. Xie YT, Wang AQ (2009) Effects of modified vermiculite on water absorbency and swelling behavior of chitosan-g-poly (acrylic acid)/vermiculite superabsorbent composite. J Compos Mater 43(21):2401–2417
426. An JK, Wang WB, Wang AQ (2012) Preparation and swelling behavior of a pH-responsive psyllium-g-poly (acrylic acid)/attapulgite superabsorbent nanocomposite. Int J Polym Mater 61(12):906–918
427. Wang JL, Wang WB, Zheng YA, Wang AQ (2011) Effects of modified vermiculite on the synthesis and swelling behaviors of hydroxyethyl cellulose-g-poly (acrylic acid)/vermiculite superabsorbent nanocomposites. J Polym Res 18(3):401–408
428. Mukerabigwi JF, Lei S, Fan L, Wang H, Luo S, Ma X, Qin J, Huang XY, Cao Y (2016) Eco-friendly nano-hybrid superabsorbent composite from hydroxyethyl cellulose and diatomite. RSC Adv 6(38):31607–31618
429. Hu X, Deng Y (2015) Synthesis and swelling properties of silk sericin-g-poly (acrylic acid/attapulgite) composite superabsorbent. Polym Bull 72(3):487–501
430. Qiu H, Yu J (2008) Polyacrylate/(carboxymethylcellulose modified montmorillonite) superabsorbent nanocomposite: preparation and water absorbency. J Appl Polym Sci 107(1): 118–123
431. Wang YP, Liang Y, Chen JC, Yan XD, Li CL, Wang XP (2009) Utilisation of potato leaves and organophilic montmorillonite for the preparation of superabsorbent composite under microwave irradiation. Polym Polym Compos 17(7):423
432. Islam MS, Rahaman MS, Yeum JH (2015) Electrospun novel super-absorbent based on polysaccharide–polyvinyl alcohol–montmorillonite clay nanocomposites. Carbohyd Polym 115:69–77
433. Bao Y, Ma J, Li N (2011) Synthesis and swelling behaviors of sodium carboxymethyl cellulose-g-poly (AA-co-AM-co-AMPS)/MMT superabsorbent hydrogel. Carbohyd Polym 84(1):76–82

434. Wang WB, Wang AQ (2010) Nanocomposite of carboxymethyl cellulose and attapulgite as a novel pH-sensitive superabsorbent: synthesis, characterization and properties. Carbohyd Polym 82(1):83–91
435. Wang WB, Xu JX, Wang AQ (2011) A pH-, salt-and solvent-responsive carboxymethylcellulose-g-poly (sodium acrylate)/medical stone superabsorbent composite with enhanced swelling and responsive properties. Express Polym Lett 5(5):385–400
436. Wang WB, Wang AQ (2011) Preparation, swelling, and stimuli-responsive characteristics of superabsorbent nanocomposites based on carboxymethyl cellulose and rectorite. Polym Adv Technol 22(12):1602–1611
437. Wang WB, Wang J, Kang YR, Wang AQ (2011) Synthesis, swelling and responsive properties of a new composite hydrogel based on hydroxyethyl cellulose and medicinal stone. Compos Part B Eng 42(4):809–818
438. Li A, Zhang JP, Wang AQ (2007) Preparation and slow-release property of a poly (acrylic acid)/attapulgite/sodium humate superabsorbent composite. J Appl Polym Sci 103(1):37–45
439. Zheng YA, Wang AQ (2008) Study on superabsorbent composites. XVIII. Preparation, characterization, and property evaluation of poly (acrylic acid-co-acrylamide)/organomontmorillonite/sodium humate superabsorbent composites. J Appl Polym Sci 108(1):211–219
440. Yi JZ, Liang ZQ, Zhang LM (2007) Studies on sodium humate/polyacrylamide/clay hybrid hydrogels. Acta Polymerica (Chinese) 6:548–553
441. Zhang JP, Li A, Wang AQ (2005) Study on superabsorbent composite. V. Synthesis,swelling behaviors and application of poly(acrylic acid-co-acrylamide)/sodium humate/attapulgite superabsorbent composite. Polym Adv Technol 16:813–820
442. Zhang JP, Chen H, Wang AQ (2006) Study on superabsorbent composite—VII. Effects of organification of attapulgite on swelling behaviors of poly (acrylic acid-co-acrylamide)/sodium humate/organo-attapulgite composite. Polym Adv Technol 17(5):379–385
443. Zheng YA, Gao TP, Wang AQ (2008) Preparation, swelling, and slow-release characteristics of superabsorbent composite containing sodium humate. Ind Eng Chem Res 47:1766–1773
444. Zheng YA, Wang AQ (2009) Study on superabsorbent composite. XX. Effects of cation-exchanged montmorillonite on swelling properties of superabsorbent composite containing sodium humate. Polym Compos 30(8):1138–1145
445. Yi JZ, Zhang LM (2007) Studies of sodium humate/polyacrylamide/clay hybrid hydrogels. I. Swelling and rheological properties of hydrogels. Eur Polym J 43(8):3215–3221
446. Rashidzadeh A, Olad A (2014) Slow-released NPK fertilizer encapsulated by NaAlg-g-poly (AA-co-AAm)/MMT superabsorbent nanocomposite. Carbohyd Polym 114:269–278
447. Wang Y, Liu M, Ni B, Xie L (2012) κ-carrageenan–sodium alginate beads and superabsorbent coated nitrogen fertilizer with slow-release, water-retention, and anticompaction properties. Ind Eng Chem Res 51(3):1413–1422
448. Xie L, Liu M, Ni B, Zhang X, Wang Y (2011) Slow-release nitrogen and boron fertilizer from a functional superabsorbent formulation based on wheat straw and attapulgite. Chem Eng J 167(1):342–348
449. Zhang JP, Liu RF, Li A, Wang AQ (2006) Preparation, swelling behaviors, and slow-release properties of a poly (acrylic acid-co-acrylamide)/sodium humate superabsorbent composite. Ind Eng Chem Res 45(1):48–53
450. Ni B, Liu M, Lü S, Xie L, Wang Y (2010) Multifunctional slow-release organic− inorganic compound fertilizer. J Agri Food Chem 58(23):12373–12378
451. Bhardwaj AK, Shainberg I, Goldstein D, Warrington DN, Levy GJ (2007) Water retention and hydraulic conductivity of cross-linked polyacrylamides in Sandy soils. Soil Sci Soc Am J 71:406–412
452. He X, Yang HM (2014) A novel strategy to the synthesis of $Na_3YSi_2O_7$ from natural palygorskite. Appl Clay Sci 101:339–344
453. Lin Q, Hao J, Li J, Ma Z, Lin W (2007) Copper-impregnated Al–Ce-pillared clay for selective catalytic reduction of NO by C_3H_6. Catal Today 126(3):351–358; Wang Y, Qu J, Liu H, Hu C

(2007) Adsorption and reduction of nitrate in water on hydrotalcite-supported Pd-cu catalyst. Catal Today 26(3):476–482
454. Wang WB, Wang FF, Kang YR, Wang AQ (2013) Facile self-assembly of au nanoparticles on a magnetic attapulgite/Fe_3O_4 composite for fast catalytic decoloration of dye. RSC Adv 3 (29):11515–11520
455. Wang WB, Kang YR, Wang AQ (2014) In situ fabrication of ag nanoparticles/attapulgite nanocomposites: green synthesis and catalytic application. J Nanopart Res 16(2):2281
456. Mu B, Wang AQ (2015) One-pot fabrication of multifunctional superparamagnetic attapulgite/Fe_3O_4/polyaniline nanocomposites served as an adsorbent and catalyst support. J Mater Chem A 3(1):281–289
457. Sanz E, Arteaga A, García MA, Cámara C, Dietz C (2012) Chromatographic analysis of indigo from Maya blue by LC–DAD–QTOF. J Archaeol Sci 39:3516–3523
458. Doménech A, Doménech-Carbó MT, del Río MS, de Agredos Pascual MLV (2009) Comparative study of different indigo-clay Maya blue-like systems using the voltammetry of microparticles approach. J Solid State Electrochem 13:869–878
459. Giustetto R, Wahyudi O (2011) Sorption of red dyes on palygorskite: synthesis and stability of red/purple Mayan nanocomposites. Microporous Mesoporous Mater 142:221–235
460. Leitão IM, Seixas de Melo JS (2013) Maya blue, an ancient guest–host pigment: synthesis and models. J Chem Edu 90:1493–1497
461. Zhang Y, Wang WB, Mu B, Wang Q, Wang AQ (2015) Effect of grinding time on fabricating a stable methylene blue/palygorskite hybrid nanocomposites. Powder Technol 280:173–179
462. Reinen D, Köhl P, Muller C (2004) Colour centres in 'Maya blue'—the incorporation of organic pigment molecules into the palygorskite lattice. Z Anorg Allg Chem 630:97–103
463. Mu B, Wang Q, Wang AQ (2015) Effect of different clay minerals and calcination temperature on the morphology and color of clay/$CoAl_2O_4$ hybrid pigments. RSC Adv 5(124): 102674–102681
464. Zhang AJ, Mu B, Luo ZH, Wang AQ (2017) Bright blue halloysite/$CoAl_2O_4$ hybrid pigments: preparation, characterization and application in water-based painting. Dyes Pigments 139:473–481
465. Chen GG, Qi XM, Guan Y, Peng F, Yao CL, Sun RC (2016) High strength hemicellulose-based nanocomposite film for food packaging applications. ACS Sus Chem Eng 4(4): 1985–1993
466. Azahari NA, Othman N, Ismail H (2012) Effect of attapulgite clay on biodegradability and tensile properties of polyvinyl alcohol/corn starch blend film. Int J Polym Mater 61(14): 1065–1078
467. Huang D, Mu B, Wang A (2012) Preparation and properties of chitosan/poly (vinyl alcohol) nanocomposite films reinforced with rod-like sepiolite. Mater Lett 86:69–72
468. Samper-Madrigal MD, Fenollar O, Dominici F, Balart R, Kenny JM (2015) The effect of sepiolite on the compatibilization of polyethylene–thermoplastic starch blends for environmentally friendly films. J Mater Sci 50(2):863–872
469. Moazeni N, Mohamad Z, Dehbari N (2015) Study of silane treatment on poly-lactic acid (PLA)/sepiolite nanocomposite thin films. J Appl Polym Sci 132(6):41428
470. Makaremi M, Pasbakhsh P, Cavallaro G, Lazzara G, Aw YK, Lee SM, Milioto S (2017) Effect of morphology and size of halloysite nanotubes on functional pectin bionanocomposites for food packaging applications. ACS Appl Mater Interf 9(20):17476–17488
471. Strawhecker KE, Manias E (2000) Structure and properties of poly (vinyl alcohol)/Na^+ montmorillonite nanocomposites. Chem Mater 12(10):2943–2949
472. Avella M, De Vlieger JJ, Errico ME, Fischer S, Vacca P, Volpe MG (2005) Biodegradable starch/clay nanocomposite films for food packaging applications. Food Chem 93(3):467–474
473. Li X, Liu A, Ye R, Wang Y, Wang W (2015) Fabrication of gelatin–laponite composite films: effect of the concentration of laponite on physical properties and the freshness of meat during storage. Food Hydrocolloid 44:390–398

474. López OV, Castillo LA, García MA, Villar MA, Barbosa SE (2015) Food packaging bags based on thermoplastic corn starch reinforced with talc nanoparticles. Food Hydrocolloid 43:18–24
475. Avella M, De Vlieger JJ, Errico ME, Fischer S, Vacca P, Volpe MG (2005) Biodegradable starch/clay nanocomposite films for food packaging applications. Food Chem 93(3):467–474
476. Carosio F, Colonna S, Fina A, Rydzek G, Hemmerlé J, Jierry L, Schaaf P, Boulmedais F (2014) Efficient gas and water vapor barrier properties of thin poly (lactic acid) packaging films: functionalization with moisture resistant nafion and clay multilayers. Chem Mater 26(19): 5459–5466
477. Laufer G, Kirkland C, Cain AA, Grunlan JC (2012) Clay–chitosan nanobrick walls: completely renewable gas barrier and flame-retardant nanocoatings. ACS Appl Mater Interf 4(3):1643–1649
478. Zhang ZZ, Wang BT (2013) Preparation and water retention properties of clay-based sand-fi xing and grass-planting materials. J Wuhan Univ Technol 28(2):325–328
479. Qu YP, Zhang ZZ, Li CL (2017) Preparation and water retention properties of montmorillonite modified by EL-10 emulsifying agent. J Wuhan Univ Technol 32(4):S06–S11